DEGRADATION OF ELECTRIC VEHICLE LITHIUM-ION BATTERIES IN ELECTRICITY GRID SERVICES

by

Mark Bradford Elliott

Submitted in partial fulfilment of the requirements
for the degree of Master of Applied Science

at

Dalhousie University
Halifax, Nova Scotia
May 2020

Table of Contents

List of Tables

List of Figures

Abstract

It has been proposed to repurpose retired electric vehicle (EV) lithium ion batteries (LIB) into stationary electricity grid services to increase utilization and correspondingly reduce environmental footprint prior to their recycling. This thesis investigates the performance characteristics of two popular leading commercial EV LIB repurposed into two merchant-able electricity grid services. LIBs with different positive electrode are compared: (1) a hybrid of lithium nickel manganese cobalt oxide ($LiNiMnCoO_2$, termed "NMC") and lithium manganese oxide ($LiMn_2O_4$, termed "LMO") which together are called "NMC+LMO"; and (2) lithium iron phosphate ($LiFePO_4$, termed "LFP"). The distinct energy electricity service of energy arbitrage (EA) and power electricity service of frequency regulation (FR) are compared.

LIB performance was compared on the basis of energy capacity degradation throughout cycle life, round trip energy efficiency, and thermal response. Additional diagnostics methods including scanning electron microscope (SEM), energy dispersive spectroscopy (EDS), half-cell testing, impedance growth and differential voltage and capacity analysis were used to determine why each LIB degraded. The results give useful insight into which EV LIB chemistries are most appropriate for repurposing into which electricity grid application.

It was found that EA degrades LIB twice as fast as FR. It is possible that stacking FR service on EA will cause only a minor increase in degradation rate while substantially increasing potential revenue. NMC+LMO degrades twice as fast as LFP but is 1.5% more energy efficient. The choice of LIB type thus depends on the service conducted as some services do not demand long life, and some are insensitive to the cost of energy inefficiencies.

List of Abbreviations and Symbols Used

AC	Alternating Current
Ah	Amp-hour
AhD	Amp-hour Depletion
AM	Active Material
BOL	Beginning of Life
C	Capacitance
CC	Constant Current
CP	Constant Power
CV	Constant Voltage
DCR	Direct Current Resistance
EA	Energy Arbitrage
ECM	Equivalent Circuit Model
EDS	Energy Dispersive X-Ray Spectroscopy
EIS	Electrochemical Impedance Spectroscopy
EOL	End of Life
EV	Electric Vehicle
F	Faradays Constant
f	AC frequency
FR	Frequency Regulation
GHG	Green House Gasses
GIC	Graphite Intercalation Compound
i	Current
ICA	Incremental Capacity Analysis
IR	Internal Resistance
ISO	Independent System Operator
j	Phase Angle
k_B	Boltzmann Constant
L	Inductance Value of Material
LAM	Loss of Active Material
LFP	Lithium Iron Phosphate
LIB	Lithium-ion Battery
LLI	Loss of Lithium Inventory
LMO	Lithium Manganese Oxide
NAM	Negative Active Material
NE	Negative Electrode
NMC	Nickel Manganese Cobalt Oxide
OCV	Open Circuit Voltage
ρ	Specific Electrical Resistance
PAM	Positive Active Material
PE	Positive Electrode
Q	Capacity

R	Resistance
RPT	Reference Performance Test
SEI	Solid Electrolyte Interface
SEM	Scanning Electron Microscopy
SOC	State of Charge
SOE	State of Energy
SOH	State of Health
T	Temperature
t	Time
V	Volts
V2G	Vehicle to Grid
W	Molecular Weight
X_l	Inductance Reactance
XPS	X-ray Photoelectron Spectroscopy
Z	Impedance

Acknowledgements

I thank my supervisor Dr. Lukas Swan whom has made this degree invaluable and his constant push to make me become a more diligent and thoughtful scientist has enhanced many aspects of my life. I commend his exceptional abilities as supervisor and mentor.

I thank my supervisory committee, Drs. Little and Groulx for their work in advising and reviewing this project.

I thank all my colleagues, friends and family, who have helped make my degree a pleasant experience.

And finally, I thank my partner Brittany for her endless patience and support throughout this time.

This work was made possible with funding from the National Science and Engineering Research Council of Canada through support of the Strategic Network of Energy Storage Technology based at Ryerson University, and through Dr. Lukas Swan's Discovery Grant.

Additional support was provided by the Province of Nova Scotia through Graduate Scholarships.

Research equipment support was provided by the Canadian Foundation for Innovation and the Nova Scotia Research Innovation Trust.

Chapter 1 Introduction

The combustion of carbon fuels releases greenhouse gasses (GHG) into our atmosphere that cause climate change. This change in climate has detrimental affects on crop yield, energy security, and water scarcity [1]. Renewable energy is a solution for production of electricity without GHG. Throughout the last few decades Canada has implemented a variety of renewable energy technology such as solar, thermal, and most abundantly wind with over 13,000 MW of installed capacity [2]. Weather and environmental patterns are constantly in flux and this leads to intermittency in electricity generation from wind and solar.

Due to the intermittency of renewables, generation does not always coincide with energy consumption. Thus, with an energy mix heavily favouring renewables there are times when there is a surplus of energy and others when there is not enough to meet the demand. Former Energy Minister of Nova Scotia Geoff Maclellan said “while Canada stands to benefit from improved energy networks and local companies involved in wind farm construction, right now it can't add anymore intermittent energy to the grid” [3]. The simple reason for this is because most places do not have any significant amount of energy storage. Energy storage can store energy during surplus generation and deploy it while generation is low, and demand is high. Having more energy storage presents the opportunity to increase the penetration rate of renewables to the energy mix, thus reducing the amount of GHG emitted and helps to meet the global energy demand in a sustainable way.

Batteries are an energy storage technology that is scalable, energy efficient and distributable. Lithium ion batteries (LIB) for consumer electronics have both increased dramatically since year 2000 [4], but their production for electric vehicles (EV) have seen the largest growth by total energy capacity [5].

1.1 Research Objective

The cumulative sales of EVs has been growing exponentially over the last 10 years, thus being the subject for many research and development projects [6]. After the useful life cycle of the EV (approximately 10-15 years) [7] the LIB may still have substantial energy capacity remaining. It is estimated that EV LIBs can continue to function for an additional 7-10 years after being retired from passenger vehicle use [8]. Retired EV LIBs could be re-purposed to stationary electricity grid services, where energy density and specific energy requirements are less significant. There are 13 different electricity grid services and many research has already been conducted to prove the viability of this EV LIB repurposing concept [6] [9] [10].

The objective of this thesis is experimentally analyzing the degradation characteristics of EV LIBs over their useful cycle-life in two potential grid storage services: Energy arbitrage (EA) and frequency regulation (FR). EA is a deep discharge service used to smooth the effects of intermittent generation and loads by purchasing excess electricity (charge) at low price periods and selling electricity (discharge) at high price periods [11]. FR is a partial state of charge service used to maintain the electricity grid at a desired frequency by continuously modulating power output (including transitioning from charge to discharge) with update intervals of 2 or 4 seconds [12].

Two popular commercial types of EV LIBs with different positive electrodes are compared: (1) a hybrid of lithium nickel manganese cobalt oxide ($LiNiMnCoO_2$, termed “NMC”) and lithium manganese oxide ($LiMn_2O_4$, termed “LMO) which together are called “NMC+LMO”; and (2) lithium iron phosphate ($LiFePO_4$, termed “LFP”). They are similar in format and capacity, and are made by leading manufacturers LG Chem (LGC, NMC+LMO) and A123 Systems (LFP).

For this study it was necessary to set up a test area that could control external factor such as temperature and promote cell uniformity. Using a power cycler, (dis)charging protocol was implemented to imitate either EA or FR services on twelve LIBs.

scanning electron microscope (SEM) and energy dispersive spectroscopy (EDS) were performed at beginning of life (BOL) to understand the composition of the LIB material. LIB degradation under EA and FR services were recorded, compared, and analyzed on the basis of energy capacity degradation throughout cycle life, round trip energy efficiency, and thermal response. Additional diagnostics methods were used to determine why each LIB degraded, and include half-cell testing, impedance growth and differential voltage and capacity analysis [6] .

The research results give useful insights into which EV LIB chemistries are most appropriate to which electricity grid service. Being knowledgeable to, and having the ability to predict future performance of, how different LIBs will degrade under certain grid services is a valuable resource for system designers and modelers (selecting quantities), project term commitments (lasting duration of contract), financiers (risk), and system augmenters (adding capacity at key times). Such knowledge will inform the selection of batteries for grid services based on power capacity, energy efficiency and expected project life. This will increase the economic success of the energy storage system provider while reducing the costs of electricity for the end consumer. Furthermore, it will gain additional utilization of the EV LIB with a correspondingly reduced environmental footprint prior to final recycling.

Chapter 2 Background

2.1 Electricity Grid Services

EA and FR were chosen for this experiment as they are two of the main grid services in North America per total electricity throughput [13]. EA is an energy intense, but only moderate power service. It is characterized by 1+ cycles per day that operate over the majority of the usable capacity of the LIB. FR is a high power, partial state of charge service used to maintain the electricity grid at a desired frequency. It is characterized by rapid variations in power level, including the switching from charge to discharge, typically on 2 or 4 second intervals. Representative power profiles of EA and FR are shown in Figure 1. Note the timescales are drastically different and the shapes of the profiles go from consistent charge or discharge modes (EA) to high fluctuations (FR). It is possible to test LIBs under each of these cycling regimes with a high degree of accuracy using a programmable battery power cycler (charger/discharger) [14].

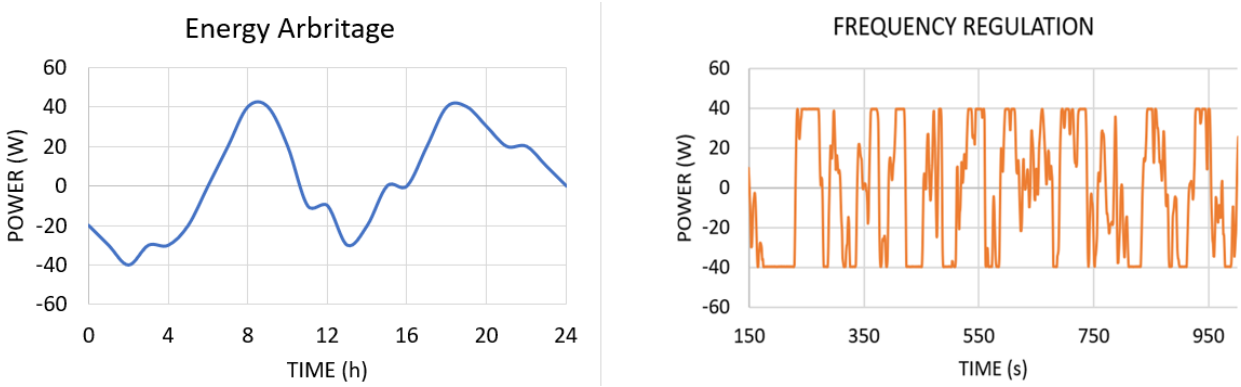

Figure 1 EA and FR Power Profile

2.1.1 Energy Arbitrage

The macro electricity power demand of the consumer fluctuates substantially throughout the day and seasons, leading to peaks and troughs for daily, seasonal and annual energy consumption that the electricity utility must provide to the grid. Ideally the utility would provide constant power to the

consumer as this would make sizing of power-generation simple and efficient, however this is not the case. In most areas of the developed world the grid must be able to generate enough power for the potential highest peak in energy consumption to avoid blackouts [15]. This leads to over sized generation plants and consequently increased capital expenditure and cost for the consumer. A solution to this problem is storing energy when consumption is low and deploying it when the demand rises thus getting closer to a constant power generation.

Depending on local legislation the energy price ($/kWh) can fluctuate throughout the day. Energy can be purchased, charged, and stored when demand and price is low; and can be sold, discharge, and released back to the electricity grid when demand and price rises. This is possible on the both the generation side (day-ahead and real-time markets) and on the load side (time-of-day tariff), both with give potential performing EA.

A generation side study [16] focusing on the New York Independent system operator (ISO) showed the maximum electricity price period has a relatively wide distribution and shows a seasonal shift in the maximum revenue period. The maximum revenue period for 4-hour energy arbitrage is from 12h to 16h in the summer period and shifts to 15h to 19h in the winter period. The study found that average gross profits for a 2 h, 4 h and 10 h EA service were $25/MWh, $26/MWh, and $14/MWh respectively. It should be noted the New York ISO gave credits for an EA service ≥ 4 h making it more profitable per MWh to perform EA for 4 h opposed to 2 h, highlighting how immensely local legislation effects how a storage system performs EA optimally.

A load side study expects that more participation in EA will occur as consumer level energy storage becomes more accessible [15]. It is more likely that an individual will simply store energy when the price is low and use that stored energy when the price is high, which is referred to as “time-shifting”. There are typically two daily peaks in electricity consumption, in the morning before people go to work and, in

the evening, when people get home from work. Ideally energy storage would be used during these two daily peaks. Two cycles per day equates to a potential 730 complete cycles per year. Complete cycles are defined by discharging a LIB from its upper voltage limit (100% state of charge, SOC) to its lower voltage limit (0% SOC), and then fully recharging it, within manufacturer specifications. This type of complete cycle is used for EA and is termed Δ100%SOC.

2.1.2 Frequency Regulation

The electric power grid transmits power from a generator to the end user using alternating current (AC) operating at a specific frequency (60 Hz for North America). If demand attempts to be higher than supply the frequency will fall slightly, and vice versa, require continuous modulation of generation. Lack of precise and fast regulation control would lead to brownouts [17]. Recently, rapid fluctuations in the grid frequency have increased because of the increasing penetration of highly variable renewable resources. FR is the second-by-second adjustment of electrical power generation to maintain grid frequency at 60 Hz to ensure grid stability.

Grid operators (utility companies) use an electronic or mechanical device called a governor which implements FR on a generating facility via a droop parameter. Droop is the variation in real power output due to variations in system frequency and is expressed as a percentage. Droop reflects the amount of frequency change from nominal (e.g. 5 % of 60 Hz is 3 Hz) that is necessary to cause the governor control mechanism of a generating facility to move from fully closed to fully open. A governor also has a deadband parameter which represents a minimum frequency deviation from nominal system frequency that must be exceeded in order for the generating facility to provide FR [12]. The Federal Energy Regulatory Commission regulates the maximum droop and deadband deviation to be 5 % from nominal frequency and ±0.036 Hz, respectively [18].

Today, most governors are natural gas generators that ramp power up or down from a medium

generation level of 50% capacity to support changes in supply and demand. The need for faster responding resources such LIBs has the potential for a pay-for-performance which has economic premium for fast regulation [19].

Payment for FR services vary depending on the contract set by the grid operator, however generally the payment for regulation has two components. First, generators are paid for the capacity that they commit to providing to FR and is paid each time the services is used or it is paid on an annual basis regardless of the number of times the service is provided. This is sometimes called the "capability" price and has units of $ per MW of capacity. Second, when a generator is called on to increase or decrease output in response to a frequency deviation event, it is paid for the energy that is produced or absorbed. This is sometimes called the "performance" payment and is often set equal to the real time price energy with units of $ per MWh [20].

2.2 How Lithium-ion Batteries Work

A battery is a device that charges and discharge electricity, but stores energy electrochemically. This conversion of electrical to chemical energy occurs through the transfer of electrons and ions between the positive active material (PAM) and negative active material (NAM), each located at an electrode [21]. This process is shown in graphically in Figure 2.

When a LIB is completely charged the NAM contains Li^+ which reduces the voltage of the NAM to 0.1-0.3 V vs. Li metal as Li is -3.040 V vs the standard hydrogen electrode. At this time the PAM has no Li and thus at its maximum voltage between 3.7 V - 4.5 V vs. Li metal, depending on the mixed metal oxide composition. As the total cell voltage is the difference between the PAM and NAM this increases the total cell voltage to the maximum. When an external load is applied to the battery the circuit between the positive and negative current collectors and electrodes is completed and it is favourable for the Li valence electron to break its bond and flow through the external circuit and into the PAM towards a

state of lower potential. This separates the reduction and oxidation reactions and leaves Li cations (Li^+) inside the NAM giving it a positive ionic charge. From the 2nd law of thermodynamics, it is known that every system attains to be at a state of equilibrium (charge neutral) which means for every electron that flows into the PAM a Li^+ must also enter to maintain this neutrality. This electromotive force pulls the Li^+ out of the NAM and into the electrolyte. These Li^+ along with the Li^+ from the lithium salt ($LiFP_6$) in the electrolyte begin to move through the electrolyte and intercalate into the PAM. As Li^+ fill the PAM the voltage of the PAM drops, reducing the total cell voltage. The electrons can continue to do useful work in the external circuit until all the Li^+ have been depleted from the NAM or the lower voltage limit is reached in the cell. At this point the battery is considered fully discharged. During charging a higher potential is applied to the external circuit and make it favourable for the Li^+ and electrons to flow in the opposite direction until an upper voltage limit is reached.

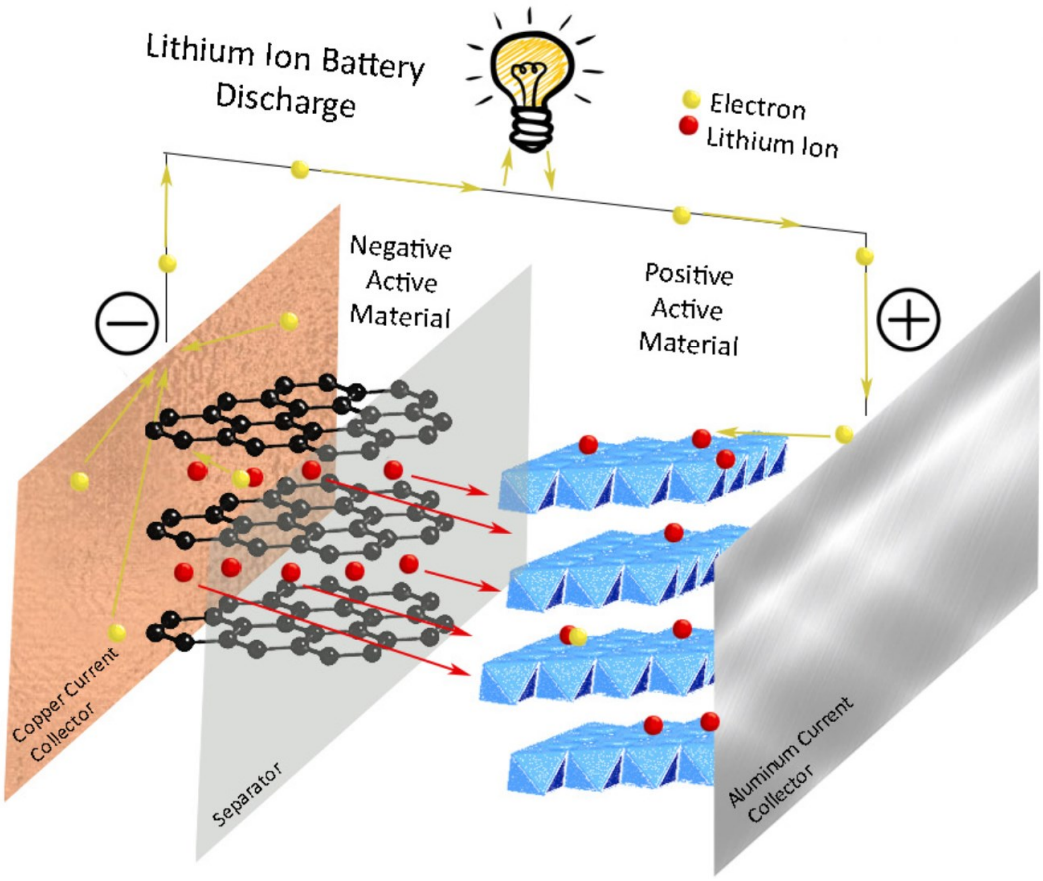

Figure 2 Lithium ion cell

2.3 Lithium Ion Battery Components

A LIB is made up of 5 core components: active material, electrolyte, current collectors, separators, and binders.

2.3.1 Positive Active Material

The main requirements of a PAM as an intercalation compound is to have high specific capacity (mAh/g) and be able to (de)intercalate Li^+ for many cycles without degrading. PAMs are generally oxides or sulfides and usually built up of close packed layers. Usually, PAMs require at least one atom that can

exist in several oxidation states, so transition metal are commonly used. Workable upper voltages against lithium metal of most PAMs in LIBs range from 3.7 V for LFP to 4.3 V for NMC.

With all the different grid services available for a battery to deliver energy, selecting a LIB chemistry for which grid service is an important and difficult task. NMC+LMO and LFP were chosen for many reasons as the chemistry of research, largely since these chemistries are among the most common used today for large scale applications and have reduced Co which is a trend that will continue. Furthermore NMC+LMO is now a common PAM blend, but has not been used in similar experiments [22] [23].

Having these 3 active materials for the experiment is ideal as it covers the 3 types of commercial structures in use for PAMs, layered (NMC), spinel (LMO), and olivine (LFP). Each type of structure preforms differently and degrades in a unique way, making each type of material suited for a unique grid service. An overview of each material is presented in Figure 3 .

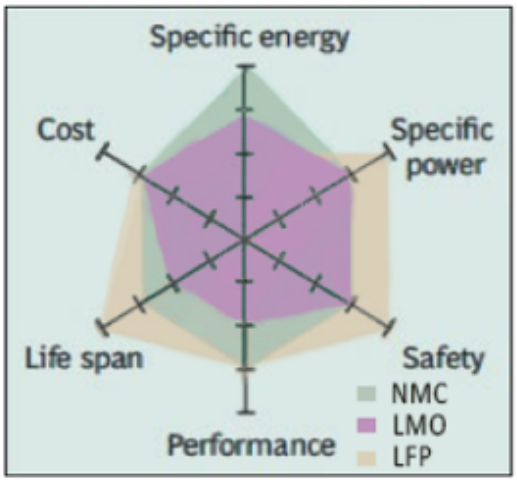

	NMC	LMO	LFP
Structure	Layered	Spinel	Oviline
Specific Energy	150-220 Wh/kg	100-150 Wh/kg	90-120 Wh/kg
Lower Voltage (vs Graphite)	2.5 V	2.5 V	2.0 V
Upper Voltage (vs Graphite)	4.2 V	4.2 V	3.65 V
Approximate Cycle Life	1500-3000	500-1000	1500-3000
Thermal Runaway	210 °C	250 °C	270 °C

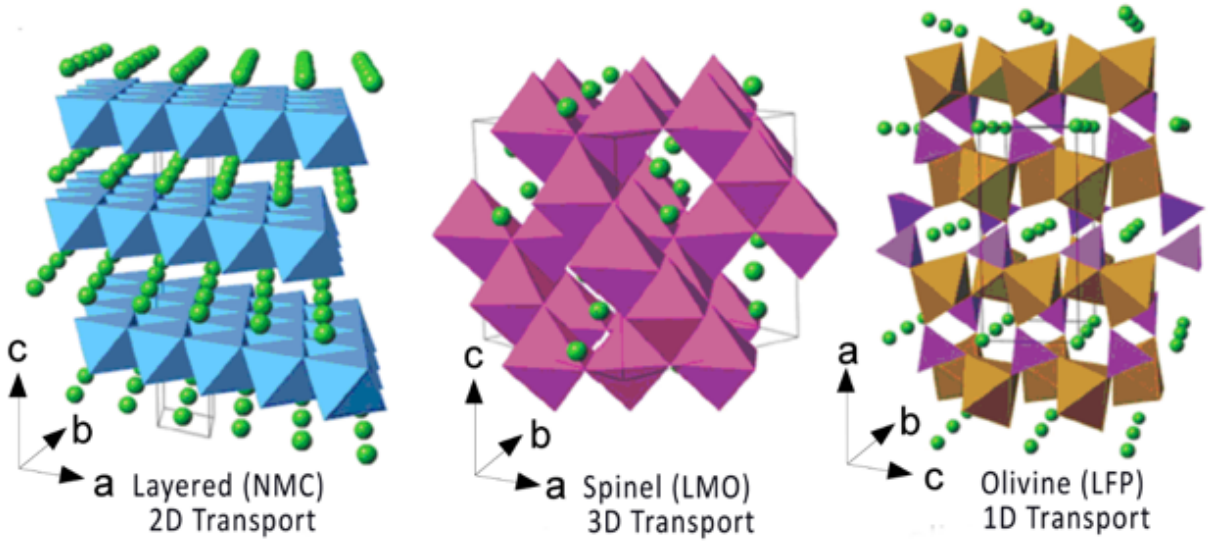

Figure 3 PAM Characteristics "Used with Permission from Author" [24] [25]

2.3.1.1 Nickel Manganese Cobalt Oxide

NMC ($LiNiMnCoO_2$) is a layered structure with high energy density and low self-heating rate (potential for passive cooling) which makes NMC a popular choice for EVs. Due to its wide range of applications and high discharge rate capability NMC cells have potential for re-purposing for grid-storage. Currently NMC is used for EVs, power tools, e-bikes and other electric powertrains [24].

Due to its toxicity and high cost of Co [26] many cell manufactures strive to reduce the amount in LIBs. NMC is gaining favor over the traditional LCO Li^+ cell which contains significantly more Co [8]. Ni based systems have higher energy density, lower cost, and longer cycle life than the Co based cells. They have a slightly lower voltage, although new electrolytes and additives are being developed which enable charging to 4.4 V per cell and higher to boost capacity. Furthermore, LMO is now being added to many NMC cells which further reduces the Co quantity. Studies are now being published which suggest that Co could be taken out of the cell entirely with little effect on performance [27].

NMC cells can be fitted to be a suitable energy cell or power cell depending on customer needs. The high specific energy of Ni and the low internal resistance (IR) of Mn counteract the poor stability of Ni and low specific energy of Mn, making a well-balanced battery chemistry. Depending on the ratio of Ni, Co and Mn the cell will perform differently. To determine the ratios of the NMC, scanning electron microscopy (SEM) was performed on a test cell.

2.3.1.2 Lithium Manganese Oxide

LMO ($LiMn_2O_4$) was created in 1983 and was one of the first commercially available LIB chemistries. LMO benefits from the abundance, cost, and benign qualities of Mn. LMO is unique as it is found as both a layered and spinel structure. Layered structures are less used than the three-dimensional spinel structure as the three dimensional Li^+ transport enhances solid state diffusion into the electrode, leading to low IR, thermal stability and high power capabilities [24].

However, the cycling performance of spinel LMO is not good, as continuous degradation at the PE-electrolyte interface is observed when the average oxidation state of the manganese drops below $Mn^{+3.5}$. At this concentration, irreversible side reactions with electrolyte cause Mn^{3+} ions to undergo a disproportionation reaction to form Mn^{2+} and Mn^{4+} ($2\ Mn^{3+} \rightarrow Mn^{4+} + Mn^{2+}$). Mn^{2+} is soluble in most electrolytes used in LIBs and is composed of nanosized crystals which act as catalysts to drastically increase the rate of solid electrolyte interface (SEI) growth [28] [29]. Mn dissolution causes capacity fade from loss of active material (LAM) and a power fade from an increase in interfacial resistance from a growing SEI layer. Mn dissolution is increased in cells that are charged above 4.0 V and in PEs with excess amount of carbon [28] . To mitigate this phenomenon Mn trapping polymers coated separators, which reduce the amount of Mn migrating to the negative electrode are being developed [30]. In $Li_xMn_2O_4$ a large phase transition occurs at x= 0.5 by formation of an ordered lithium superstructure. In some cases, a change from spinel structure to double hexagonal occurs during this transition which enhances mechanical stress and Mn dissolution in the material.

2.3.1.3 Lithium Iron Phosphate

LFP ($LiFePO_4$) has good electrochemical performance with high specific power and long cycle life. LFP is more tolerant to full charge conditions and is less stressed than other Li^+ systems if held at high voltage for a prolonged time. One of the major drawbacks of LFP is the potential of the Fe^{2+}/Fe^{3+} redox couple (3.45 V vs Li/Li^+) which keeps the workable nominal voltage to 3.2 V vs Li/Li^+. This hinders the specific energy below that of Co-blended Li^+ [31]. LFP was initially disadvantaged with low electrical and ionic conductivity, although nano-scale phosphate PE material has increased power capabilities [25]. Carbon coating and cathodic doping has increased specific power further making LFP now known as the leading power cell. Currently 80% of all LFP production and use occurs in China [32] . China chooses LFP for its low price, and due to its olivine structure, high intrinsic safety performance and high-temperature stability.

2.3.2 Negative Active Material

Although metallic lithium as NAM gives the highest energy dense Li^+ cell, using a low voltage intercalating NAM in Li^+ cells is favourable. Metallic lithium has poor cycle life and the metal forms dendrites which can cause short circuiting and start a thermal run-away reaction and catch fire [33]. As an alternative graphitic NAM is almost exclusively used. Activated carbon has a very low potential (0.9 V vs Li^+/Li) and is made up of very small graphene sheets (4-10 $\AA$ lateral length) that are stacked in a "layered" structure [34]. Li^+ intercalate through this porous material between the graphene layers. Furthermore, activated carbon can be made by heating many common materials such as wood, coal, coconuts etc. between 600 °C and 1300 °C, thus making the material very cost effective. To improve the electron conductivity of graphitic NAM other carbon materials like acetylene black are used as conductive material to facilitate electron flow to the copper current collector.

Li staging has been well documented in graphitic NAMs [33] [34] [35], however recently research shows that Li staging is likely happening at the PAM of some materials as well [36] . Li staging occurs in graphite when Li^+ (de)intercalate in an organized way. As Li^+ intercalate they keep an equal number of graphene layers between each row of Li until too much Li has intercalated and a phase transition occurs, and the Li enters the next stage. Omitting kinetics and considering only thermodynamics there are three prominent structural transitions that occur in graphite as shown in Figure 4. LiC_{24} to LiC_{18} (formation of stage III), LiC_{18} to LiC_{12} (stage III to stage II), and LiC_{12} to LiC_6 (stage II to stage I) [37]. As the lithium transition through stages this causes a large change in voltage with little change in capacity. When Li^+ have more time to diffuse the lithium ordering is more prominent. Alternatively, fast charge causes the Li^+ to place wherever they fit quickly, leading to more randomized intercalation and less prominent shifts in voltage from phase transitions. At very fast rates phase transitions will not happen at all. To identify these transitions a low rate must be used for techniques such as differential voltage or incremental capacity.

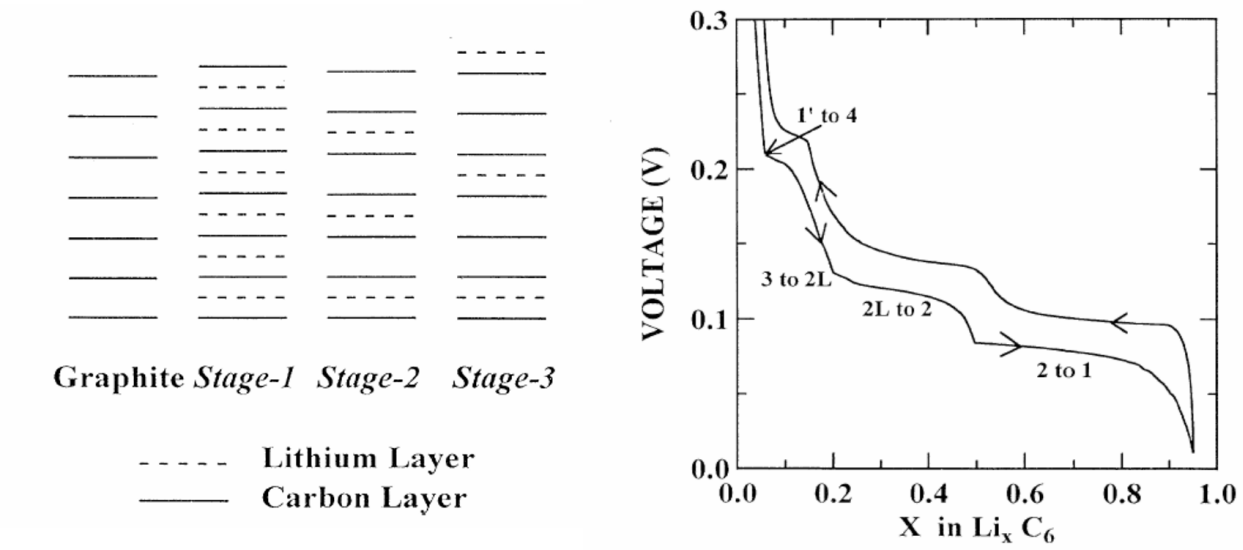

Figure 4 Lithium Ordering in Graphite "Used with Permission From Author" [38]

2.3.3 Electrolyte

Electrolyte transports the positive Li^+ between the positive and the negative active materials. A good electrolyte should non react with the electrode materials, have good electronic insulation, high ionic conductivity, and stability in the electrochemical window and operating temperatures of the cell.
The electrolyte consists of 2 parts, a solvent, usually a mixture of ethylene carbonate (EC), dimethyl carbonate (DMC), diethyl carbonate (DEC), and a salt, typically $LiPF_6$. Small amounts of additives such as vinylene carbonate (VC) are also dissolved in the electrolyte to improve the battery performance [39].

Most commercial LIBs electrolyte have an upper voltage of 4.2 V, which is less than the PAM rating, and limits the cell energy and capacity. At voltages above 4.0 V commercial electrolyte has the potential to break down and adds into the SEI layer this causes a loss of lithium inventory (LLI) (capacity decrease)

and an increase in cell interfacial impendence. Finding a suitable electrolyte that is stable in high voltage (>4.20 V) is a limiting factor to increasing the energy density of LIBs.

2.3.4 Solid Electrolyte Interphase

The SEI is a passivated layer created from decomposed electrolyte that forms mainly on the NAM of LIBs during the initial formation cycle [34]. The SEI is essential to the longevity of a LIB. At the lower voltage limit of most LIBs the electrolyte is not stable at the NAM potential, thus the SEI is created by reduction reactions between the electrolyte salts and solvents at the NAM. The SEI adheres to the NAM and creates an insoluble, quasi electrochemically stable interface. An ideal SEI would be thin to reduce ionic resistance, strong to prevent cracking, have high conductivity to allow Li^+ transport and should block electrons in order to prevent further electrolyte decomposition [40]. The SEI becomes a problem in LIBs when it continues to grow throughout cycle life.

2.3.5 Separator

The separator is a semi permeable membrane which stops short circuits by separating the positive and negative electrodes while permitting the transfer of Li^+ during charge or discharge. Polyethylene or polypropylene microporous membranes are used as separators. The separator is immersed in electrolyte.

To improve energy density battery manufactures, make separators as thin and light as possible. This can lead to favourable conditions for penetration with conductive particles or Li dendrites across the electrodes causing a short circuit and thermal runaway. This was thought to be the cause of the 2017 high profile case of the exploding Samsung Galaxy Note 7 [41].

2.3.6 Binder

The binder is an inert material which can be thought of the glue of the active material. It also provides adhesion of the active material to the current collector. The binder needs to be insoluble in the

electrolyte and able to resist oxidation in the PAM. The binder adds conductivity to the active material which facilitates an easier flow of electrons from the electrode to the current collector and vise versa. A common binder material for the PAM is polyvinylidene fluoride, whereas a common NAM binder material is styrene-butadiene copolymer [42].

2.3.7 Current Collector

The current collector facilitates the flow of electrons through the external circuit and into the other electrode to bond back with a Li^+. LIBs use copper (Cu) and aluminum (Al) foil for the NAM and PAM, respectively. These metals are chosen as they are both electrochemically stable at the operating potential, are highly conductive and relatively inexpensive. Current collectors add cost and take away from energy as they are inert in the system, but still must be thick enough to provide adequate electrical and thermal conductance.

2.4 Impedance in Lithium-ion Batteries

Resistance (*R*) and impedance (*Z*) both measure the ability of a circuit to resist electrical current flow and have units of Ohms, however R is pure resistance and has several simplifying properties:

- It follows Ohm's law at all current and voltage levels.
- Its resistance is independent of frequency.
- AC current and voltage signals though a resistor is in phase with one another. [43]

Impedance does not follow theses simplifying properties and is reactive elements of inductance and capacitance.

The relationship between the different types of impendences is shown in Table 1 [44].

Table 1 Relationship of Current, Voltage and Impedance

Component	Relationship of Current and Voltage	Impedance
Resistor	$V = IR$ (1)	$Z = R$ (2)
Inductor	$V = L\frac{di}{dt}$ (3)	$Z = j2\pi fL$ (4)
Capacitor	$I = C\frac{dV}{dt}$ (5)	$Z = \frac{1}{j2\pi f\ C}$ (6)

where *V* is voltage in volts, *I* is current in amps, *t* is time in seconds, *C* is capacitance in farads, f is the AC frequency of the electrical supply in hertz , *L* is the inductance value of the material in henrys and *j* is the imaginary part of the circuit, which shifts any signal or function by 90 degrees.

Similar to most electrical loads, a battery has resistance, capacitance and inductance, therefore impedance is used to best describe what is happening in the battery [45].

The impedance of the cell changes as the cell ages and there is a strong correlation between a rise in impedance and a loss of capacity in the cell. Monitoring the impedance an important factor in being able to understand how the cell is degrading and to diagnose the SOH of a battery. Figure 5 examines the impacts of impedance in LIBs.

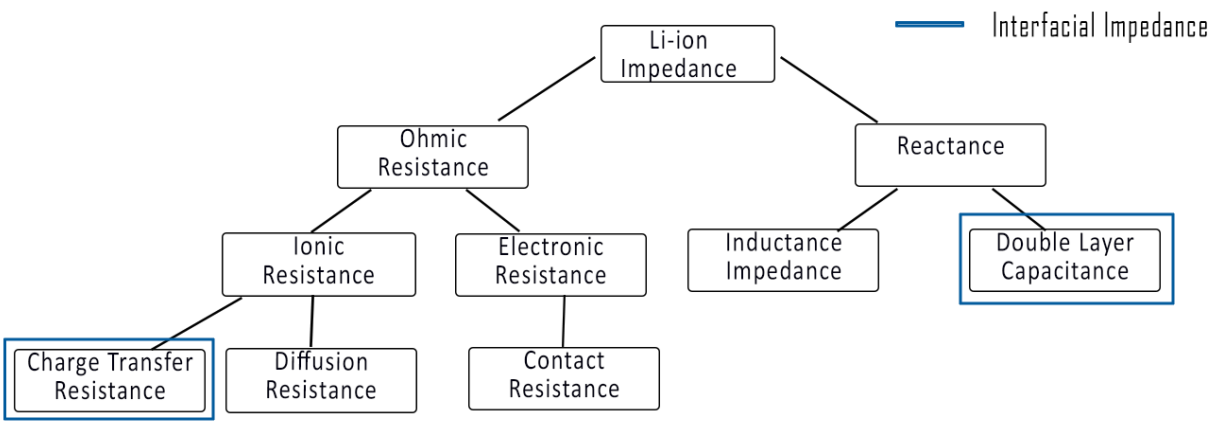

Figure 5 Impedance Pyramid

2.4.1 Ohmic Resistance

Ohmic resistance accounts for the majority of impedance in most LIBs and includes ionic conduction in the electrolyte, electronic conduction in the electrode, and the resistivity of the components of the battery such as the AM, current collectors, and electrolyte [46].

Phenomena such as gas evolution, SEI growth and current collector corrosion can lead to an increase in ohmic resistance in a Li^+ cell.

2.4.1.1 Ionic resistance

The resistance of an ionic solution such as an electrolyte can be estimated from the ionic concentration, type of ions, temperature, and the geometry of the current flow area. The resistance in ohms can be calculated:

$$R = \frac{\rho\, L}{A} \tag{7}$$

where *A* is the bounded area of the solution, *L* is the length of the uniform carrying current and *ρ* is the specific electrical resistance (Ω·m).

Generally, Li^+ cells do not have uniform current distribution through a electrolyte area so even if the electrolyte and cell geometry is known theoretical results tend to be erroneous [44].

2.4.1.1.1 Diffusion resistance

Diffusion resistance is associated with diffusion of Li^+ in the electrolyte and solid active particles. Diffusion resistance depends on the active materials and electrolyte used in the battery but generally it increases with increasing (dis)charge rates and decreasing temperature. Equivalent circuit models (ECMs) and electrochemical impedance spectroscopy is generally used to quantify the diffusion resistance.

2.4.1.1.2 Charge Transfer Resistance

Charge transfer resistance (R_{ct}) is associated with charge transport of Li^+ through the electrolyte, SEI and electrode. In LIBs charge transfer resistance is expected to follow the Arrhenius equation:

$$\frac{1}{R_{ct}} = Ae^{-Ea/K_BT} \quad (8)$$

where R_{ct} is the motion resistance of Li^+ moving through the electrolyte *Ea* is the activation energy associated with Li^+ jumping through sites in the SEI material, k_B is the Boltzmann constant, *T* is the temperature, and A is a proportionality constant [47].

Continuous growth of the SEI causes a thicker SEI layer and Li^+ must move further through this solid which increases R_{ct}.

R_{ct} is largely dependent on the kinetics of the cell, thus it increases proportionally with (dis)charge rate. A classic example of water flowing through a hose and out of a small metal spout. Increasing the (dis)charge rate is analogous to increasing the water flow, the more water you have flowing the higher the pressure (resistance) will be at the hole at the spout opening (the interfacial layer). Taking this analogy further as the spout corrodes overtime (SEI Growth) the water would have to move through and around the corrosion thus increasing further the pressure (resistance) at the spout opening (the interfacial layer).

2.4.1.2 Electronic Resistance

Electronic resistance is associated with the flow of electrons through electronically resistive materials and is quantified by the contact resistance.

2.4.1.2.1 Contact Resistance

Contact resistance ($R_{Contact}$) is pure resistivity so follows ohms law. Contact resistance is associated with the electrical contact between AMs and the current collector. The amount of contact resistance varies by the surface geometry (roughness and out-of-flatness), pressure distribution, and degree of corrosion of the current collector. Rougher surfaces, uneven surfaces, and uneven pressures cause a higher resistance. Higher quality manufacturing and polishing of the current collector could reduce surface geometry resistance and improved cell design could reduce uneven distributions of pressure at the electrode-current collector interface. The latter raises important safety concerns as an uneven electrode–current collector connection leads to heat generation at the interface. At high (dis)charge rates, the rate of heat generation at the electrodes due to high contact resistance could exceed the electrochemical heat generation rate inside the battery. This would initiate a heat flow from the

electrode-current collector interface towards the center of the cell. This would increase the cell temperature and the risk of thermal runaway. Furthermore, prolonged high battery temperature damages battery performance and longevity [48].

2.4.2 Reactance

Reactance in a LIB includes elements of capacitance and inductance.

2.4.2.1 Capacitance

A capacitor is formed when two conducting plates are separated by a non-conducting medium, called a dielectric.

A capacitor's impedance decreases as the frequency is raised (opposite to an inductor). Capacitors have only an imaginary impedance and the current through a capacitor is phase shifted –90° with respect to the voltage [43].

In a LIB an electrical double layer exists at the interfaces between the electrode-SEI-electrolyte and the electrode-current collector. This double layer is formed when Li^+ are stuck at the interfaces. Charges in the electrode are separated from the charges of the Li^+ in the electrolyte forming a capacitor. This effect is enhanced at higher (dis)charge rates and thicker SEIs as more ions get "stuck" at these interfaces waiting for other Li^+ to diffuse into the electrode. On bare Aluminum immersed in an electrolyte, there will be approximately 30 mF of capacitance for every cm^2 of electrode area [49].

The formula for capacitance of parallel plates shown below can roughly model what you find in a LIB:

$$C = \frac{\epsilon \epsilon_0 A}{d} \tag{9}$$

where *C* is capacitance ϵ is the dielectric constant of the material between the plates, ϵ_0 is the permittivity of free space, *A* is the plate area and *d* is the spacing between the plates [50].

The true value of the double-layer capacitance depends on many variables including electrode potential, temperature, ionic concentrations, types of ions, oxide layers, electrode roughness and impurity adsorption [44].

2.4.2.2 Inductance

An inductor can be any conductive material however it is generally thought of as a conductive coil (usually wire). As current passes through this coil a magnetic field is generated. In inductors, voltage leads current by 90 degrees [43]. Inductive reactance (X_I) is the name given to the opposition to a changing AC flow and is an indication of the capability of storing magnetic energy [51] . inductive resistance (R_I) is an indication of dissipated heat and is mostly contributed to the material used to make the inductor. R_I is considered pure resistance and follows Ohms law.

$$R_I = \frac{V}{I} \tag{10}$$

$$X_I = 2\pi f L. \tag{11}$$

$$Z_I = R_I + jX_I \tag{12}$$

where Z_I is inductive impedance. In a LIB, an inductive loop is formed during electrochemical impedance spectroscopy measurements while pulsing at high frequencies. This is easily observed in a Nyquist plots but generally omitted as it is considered irrelevant. It is debated if inductance plays a roll in the degradation of LIBs. In normal operating conditions of the battery, small inductance loops could be formed from SEI growth, corrosion or poor manufacturing [52] however inductance in LIBs was not investigated during this research.

2.5 Degradation of Lithium-ion Batteries

Battery degradation is complicated because a LIB degrades mainly in three different ways: loss of lithium inventory (LLI), loss of active material (LAM), and impedance changes. This can lead to either capacity fade, power fade, or both, and can be caused by a variety of reasons.

Figure 6 is a "web of degradation" showing how one phenomenon can lead to multiple forms of degradation. Green lines indicate the primary form of degradation a phenomenon caused.

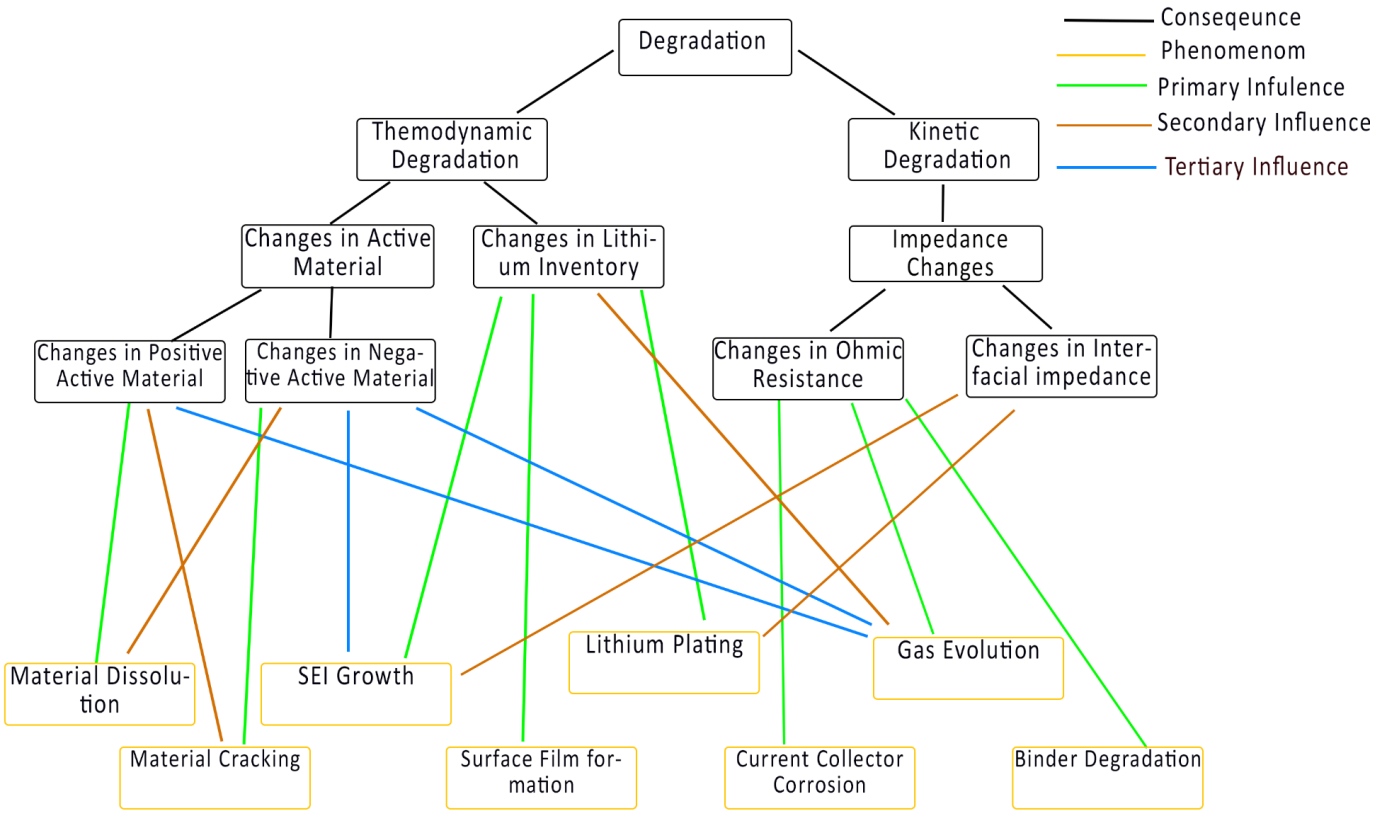

Figure 6 Degradation Web

Differential voltage (dVdQ) and differential capacity (dQdV) are methods used to analyze battery degradation throughout cycle life. The dVdQ and dQdV technique allow for the observation of small changes in voltages and capacities across the operating range of SOC of the battery that would not be observable in a traditional voltage vs. capacity curve. The dVdQ and dQdV curve changes as the cell ages and each change corresponds to one of three degradation pathways mentioned above. The dVdQ and dQdV each have their advantages and can be chosen depending on the situation. Understanding the changes in these curves is the best non-destructive method of understanding how a LIB is behaving in real time.

Alawa is a battery diagnostic tool made by Matthieu Dubarry at the University of Hawaii [53]. Alawa simulates how each of the 3 main degradation mechanisms impact the NE, PE, full cell, dVdQ and dQdV curves of a LIB. Degradation mechanisms will be simulated using the Alawa software from the half cell A123 data. All the graphs shown in the subsections below are purely illustrational to explain the generic changes from degradation on these curves and do not represent actual results from the A123 cell.

2.5.1 Loss of Lithium Inventory

LLI causes a capacity fade in the battery as less Li is available to (de)intercalate into the electrode.

2.5.1.1 Lithium Plating

Li plating is the formation of metallic Li on the NAM and occurs under two conditions, kinetic plating can happen if the polarization of the NE during charging makes the NAM potential ≤ 0 V vs Li metal. Thermodynamic plating occurs when the loss of active material (LAM) in the NAM is significantly larger than the LLI to reach a condition where overcharging in NAM happens [53]. Kinetic plating can be avoided by reducing polarization by either lowering current, increasing temperature, or lowering cut off voltage. Thermodynamic plating cannot be stopped by changing external factors, however as Li plates to the NAM it is mostly irreversible which means that most of the Li will be passivated on the next cycle causing a LLI. Thermodynamic plating will the stop once there is enough LLI. Excessive Li plating can cause Li-dendrites to pierce the separator causing an internal short circuit.

2.5.1.2 Solid Electrolyte Interface Growth

SEI growth occurs when the electrolyte is unstable across the working potential of the battery. When electrolyte decomposes it consumes Li developing the SEI, thus reducing the cells overall capacity. A thicker SEI also contributes to an increase in interfacial resistance which plays a large role in a LIBs power capability. SEI growth can be slowed by reducing polarization by either lowering current, increasing temperature or lowering upper cut off voltage. The growth of the SEI layer on the PAM is minimal and does not impact degradation [54].

2.5.1.3 LLI Effects on the Voltage Curve

Figure 7 shows that as Li is lost the full cell curve shifts to the right and the percentage of LLI is equal to the percentage of capacity loss. For the charge cycles shown in Figure 7 the end of charge remains unchanged for the PE as it is releasing Li^+ so it always becomes fully de-lithiated, while the NE will not become fully lithiated due to the LLI. It should be noted that if SOC_{NE} initial (%) was taken as the horizontal axis and this was a discharge curve then the NE curve would remain constant and the PE curve would shift to the right. The area under a dQdV curve represent capacity, thus a decrease in the peaks is observed during LLI. In the dVdQ this causes peaks to shift towards the left as the curve of 0-100% SOC at 50% LLI will look same as the curve of 0-50% SOC at 0% LLI (excluding the voltage extremities).

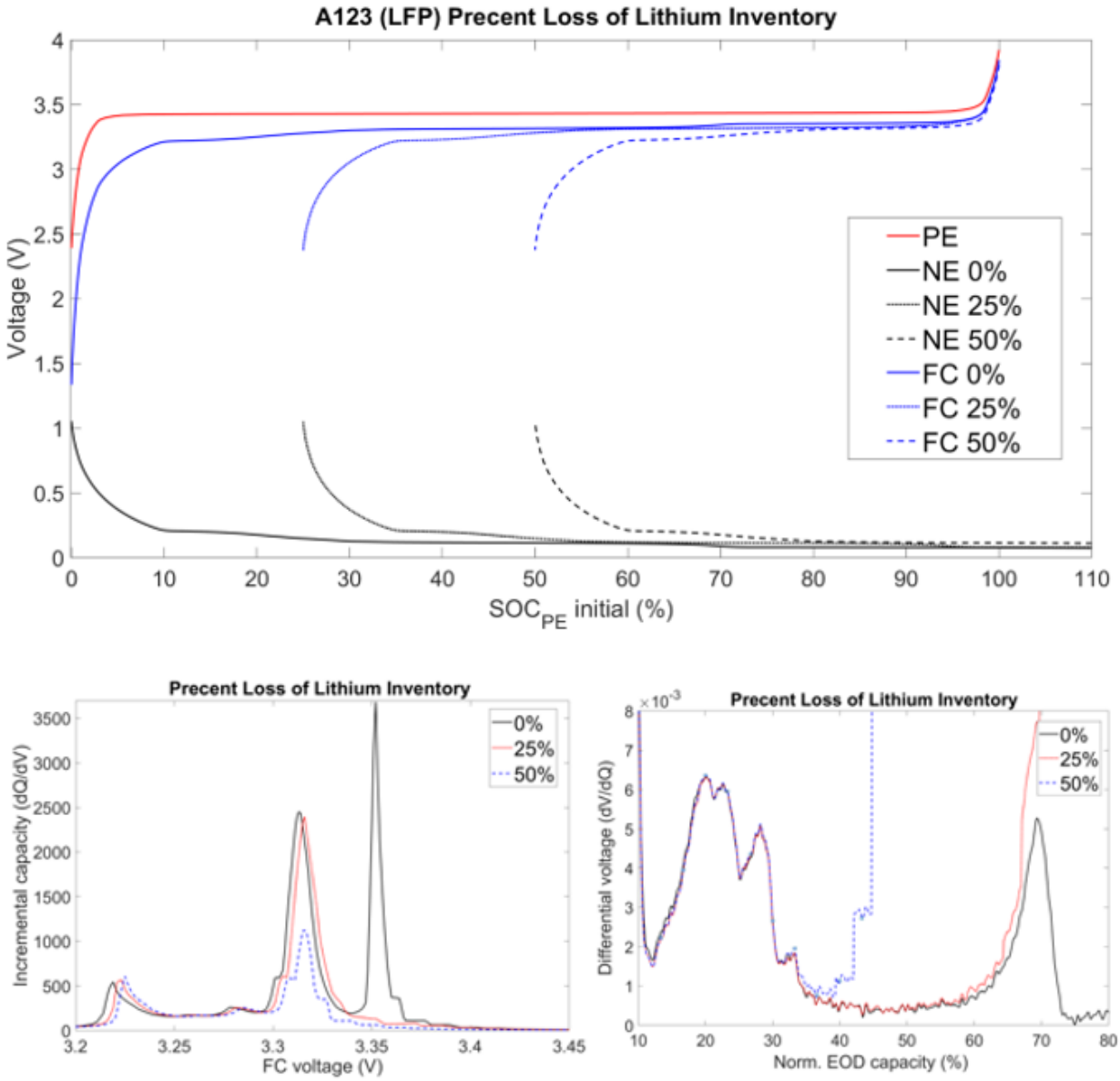

Figure 7 Loss of Lithium Curves

2.5.2 Loss of Active Material

LAM in a LIB can be caused by isolation of the grains of the AM, dissolution of transition metal into the electrolyte solution, and change in the electrode composition and/or crystal structure of the AM.

LAM causes a capacity fade in the battery. If lithiated AM is lost then the Li inside the material is lost causing both LAM and LLI, causing further capacity fade. LAM will also increase the current density (Ah/g) on the affected electrode, as LAM decreases both the material content that can accept charge and the active surface area. This causes both an increase in ohmic resistance and interfacial impedances.

2.5.2.1 Gas Evolution

Electrolyte decomposition leads to gas evolution in a LIB. Gas evolution in LIBs can lead to gas bubbles causing AM to separate. AM separation either reduces the ionic and conductive pathways for lithium/electrons causing a rise in ohmic resistance or if the AM is completely separated LAM will occur. Furthermore, if the AM is lithiated while complete separation occurs this will cause LLI as the Li has loss an ionic pathway. Gas evolution was physically observed in degraded cells in Figure 8 and is more predominate in the EA cells of the NMC+LMO as they were held at higher voltages more often thus increasing electrolyte decomposition.

Oxygen evolution at the electrode/electrolyte surface of transition metals have been reported and particularly for LMO and NMC where the oxide itself can act as a source of oxygen for these oxidation reactions in the formation phases [55]. This oxygen evolution can cause changes in the crystal structure of the PAM causing dense rock salt (cation densification) which can add to the SEI and/or spinel like surface phases, decreasing ionic conduction in the material, which leads to an increase in interfacial impedance. Currently surface dopants/coating are being developed to enhance oxygen retention in these PAMs [56].

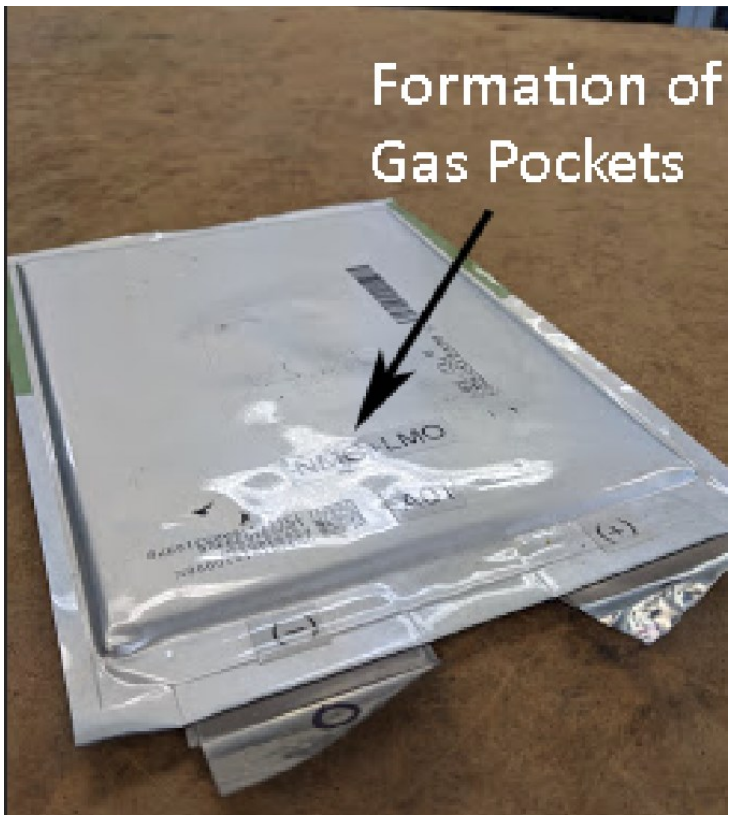

Figure 8 Gas Evolution in degraded LGC EA Cell

2.5.2.2 Active Material Dissolution

PAM dissolution is common in LMO. This phenomenon has also been observed in much smaller amounts of other transition metal ions such as Co^{+3}, Ni^{+2} or Fe^{+3} ions from LCO, NMC, or LFP. PE materials can dissolve and move to the NE which can accelerate SEI growth, and is amplified at higher temperatures and higher voltages [57] [58].

2.5.2.3 Material cracking/Binder degradation

As Li^+ (de)intercalate the molar volume of the AM changes, which causes mechanical stress. When this stress is too high it causes the AM to crack, this phenomenon is amplified when conversion materials are used in the AM such as silicon which experiences several time volume change when intercalating Li^+ [57]. This can cause LAM and LLI from loss of ionic/conductive pathways. This is known as binder degradation as the binder does not reattach to the material. The rate of reattachment of the binder depends on the

material used for the binder, volumetric change of the AM, and the total amount of (dis)charge cycles the cell has experienced [59]. When cracking occurs “fresh” AM is exposed to the electrolyte causing further growth to the SEI layer which further causes AM deformation and loss of adhesion between the binder and the AM thus compounding.

Graphitic NEs, LMO and LFP [36] undergo defined phase transitions which can cause distortion of the crystal lattice which causes further mechanical stress on the material and increases risk for material cracking [60].

2.5.2.3.1 Effects to the Voltage Curve

LAM in the PE shifts the PE curve to right and causes decrease in capacity, similarly LAM in the NE would cause NE curve to shift right.

It should be noted that when 0% SOC on the NE is reached before 100% SOC on the PE, then the PE scale the cell is at risk of thermodynamic Li plating, this is because the NE is fully lithiated before the PE completely releases all its Li^+ [53].

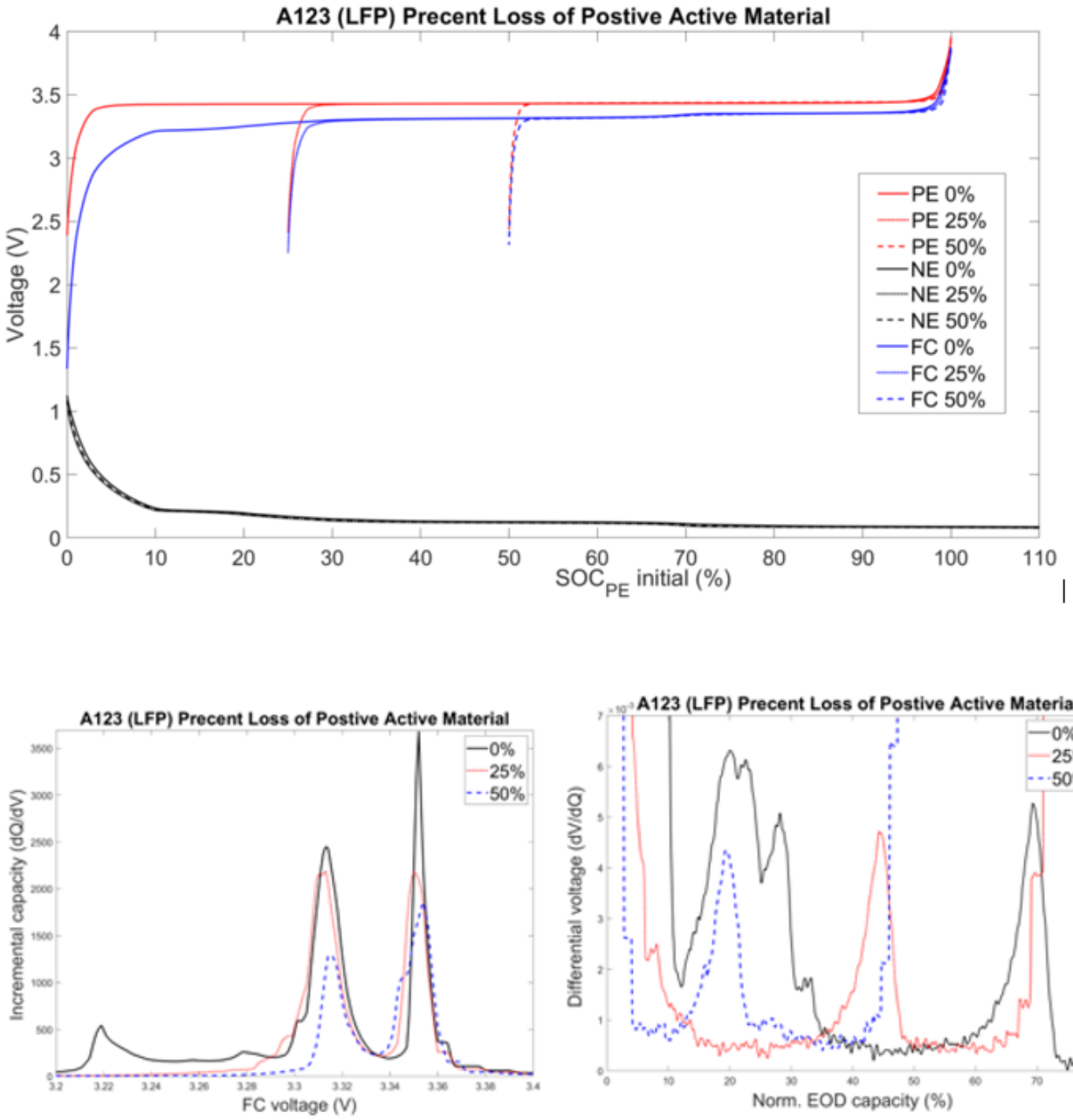

Figure 9 Loss of Active Material Curves

As PAM is lost the NAM will stay partially lithiated when the cell is fully discharged, this is most easily observable in Figure 9 of the dVdQ charge curve. Peaks in dVdQ curves represent phase transitions and the main identified graphite staging completely disappears after 25% LAM PE. The main staging peaks on most GICs occur at approximately $X = 0.25$ and $X = 0.33$ in Li_xC_6 of lithiation [38]. Once enough PAM

is loss, the NAM will always remain above the state of lithiation where these peaks occur and therefore will not be visible on dVdQ curves.

2.5.3 Impedance Changes

2.5.3.1 Current collector corrosion

Corrosion on the current collector has been observed on both the NE and PE but predominately it occurs on the cathodic aluminum foil from electrochemical oxidation of solvent molecules, like ethylene carbonate, at high potentials (<4.0 V). Corrosion increases the contact resistance.

2.5.3.2 Effects on the Voltage Curve

During discharge the increase in ohmic resistance in each electrode will shift the NE potential higher and the PE potential Lower thus decreasing the overall voltage of the cell. This phenomenon happens vise versa during charge as shown in Figure 10.

In a dQdV curve the shifting of all the peaks towards lower potential during discharge and higher potential during charge. Figure 10 shows a clear indication that the resistance of the cell is increasing. This is because as resistance increases the voltage change also increases when an external load is applied. If voltage limits are neglected, ohmic resistance increase does not change the dVdQ curves and will not impact the capacity of the cell [53].

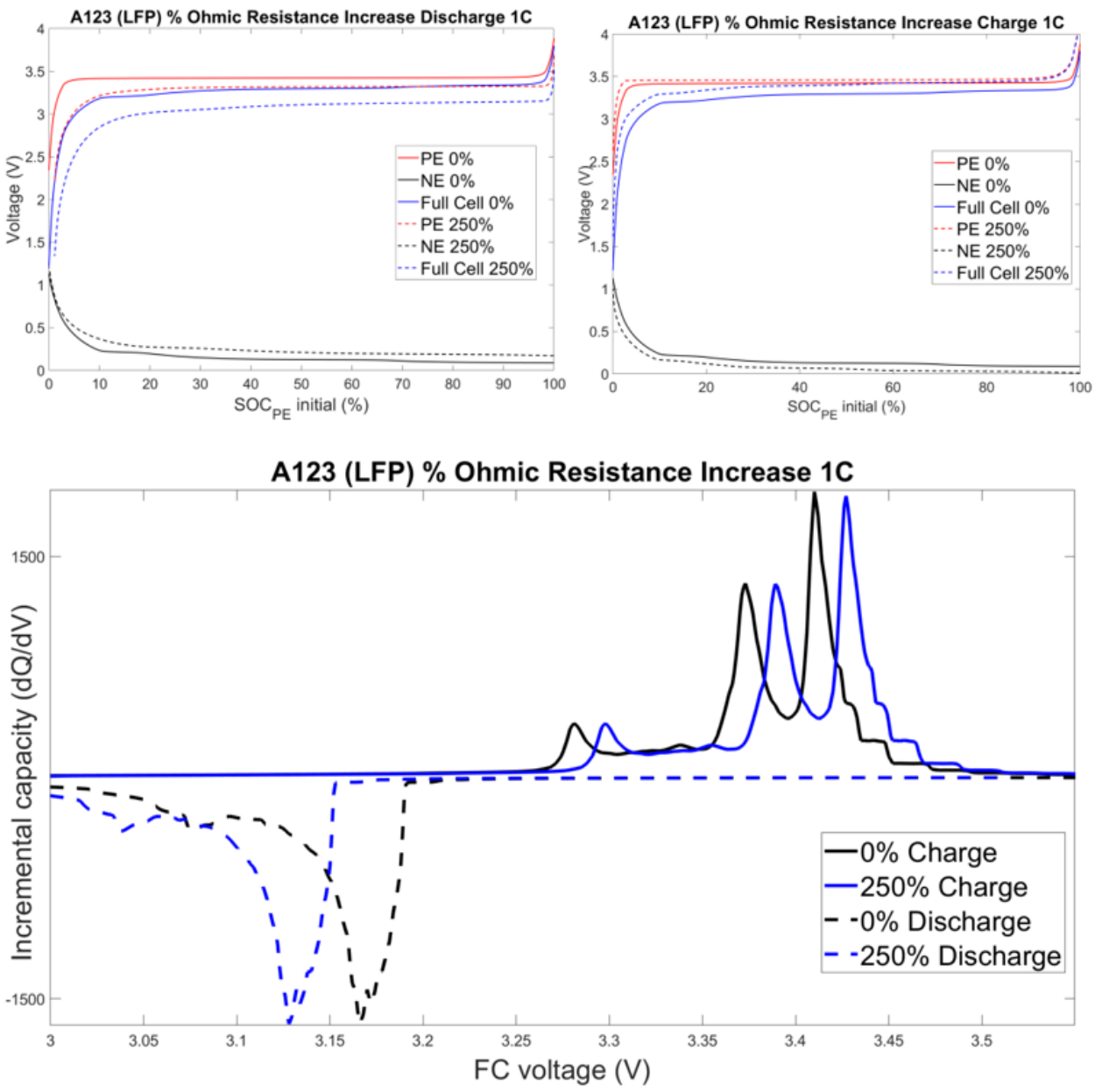

Figure 10 A123 (LFP) % Ohmic Resistance Increase 1 h rate

Interfacial impedance (or faradaic impedance) is the impedance acting on the surface of the electrode and is composed of the charge transfer resistance and the double layer capacitance. A rise in interfacial impedance occurs when an electrode does not react with Li^+ at the same kinetic rate in aging. This

essentially slows down the rate capability as shown in Figure 11. A 5 h rate with high interfacial impedance will look like a 1 h rate with low interfacial impedance. Running a battery with high interfacial impedance at high (dis)charge rates will cause large voltage changes and optimal conditions for uncontrolled SEI growth. This further increases interfacial impedance. For this reason, it is important for battery operators to understand that this can cause rapid degradation of the battery.

2.5.4 Rate Changes

A good measure of battery power performance is rate capability. The rate capability of a cell is the ability to deliver stored capacity when the (dis)charge rate increases. It can be calculated by dividing the capacity obtained at a fast rate (> 2 h rate) by the capacity at a slow rate (< 5 h). At a 1 h fast rate and 24 h slow rate, the rate capability for the LGC and A123 cells were found to be 0.93 and 0.97 respectively.

In open circuit voltage (OCV) curves of intercalation materials, the different types of lattice sites can be identified by voltage plateaus. The peaks in dVdQ curves represent phase transitions in the intercalation of Li (Lithium Ordering) and is further explained in mean field theory [61]. Peaks in dQdV represent phase equilibrium. Having highly ordered Li means when a phase transition happens leads to a large change of voltage over a small change of capacity. This causes large peaks on the dVdQ curve. When (dis)charging fast the Li^+ place themselves wherever they can fit quickly. Fast (dis)charging leading to more randomized intercalation and less prominent shifts in voltage from phase transitions and at very fast rates phase transitions will not happen at all. Thus, when performing a dVdQ/dQdV test it is important to (dis)charge at a minimum of a 15 h rate. A rise in interfacial impedance causes voltage to respond more intensely with capacity change, thus broadening the peaks in the dQdV curve [53]. It should be noted that a rise in interfacial impedance will look similar to an increase in (dis)charge rate.

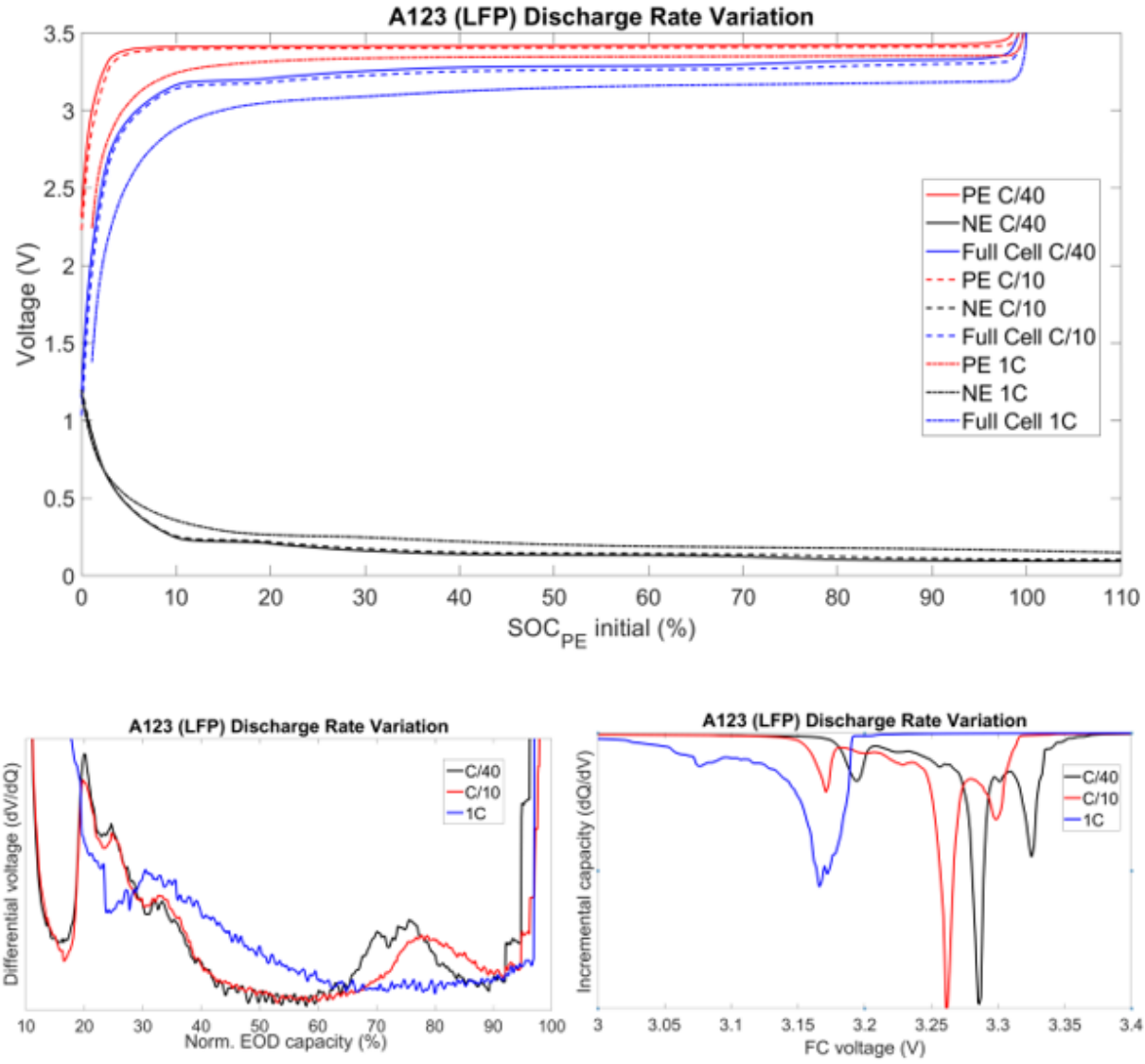

Figure 11 Rate Variation Curves

Chapter 3 Literature Review

Organizations which are involved with research in battery degradation typically come from four different domains: Industrial OEMs, third-party companies, academic researchers, and governmental researchers. Each sector has a unique scope and their own set of advantages and limitation. The latter two domains have the most publicly accessible research and will be the focus of this literature review. Within these domains, this literature review will examine experiments that are very similar to the research in this thesis. Strengths of each experiment will be identified so they can be replicated (when applicable) and weakness will be identified so they can be improved upon.

3.1.1 University of Hawaii

Dubarry et al. [23] work extensively in the battery degradation field at the University of Hawaii. They have analyzed the impact of vehicle to grid (V2G) cycling on commercial EV LIBs. V2G charging could provide a range of electricity grid services and allow more renewable energy onto the grid. A batch of 36 Panasonic NCA cylindrical battery cells rated at 3350 mAh were used in this research, similar to those used in Tesla EVs. The cycling script includes the vehicle being driven from home to work and back again with long periods in between. During these “in between” periods while the vehicle is sitting at work and at home it would either rest or performed a V2G service. The degradation of the batteries at rest and performing V2G were compared and analyzed. Forecasts based on the measurement results found that V2G implementation would decrease the lifetime of the battery packs to under 5 years making the service undesirable to perform for an EV owner.

Strengths in this experiment include a robust statistical analysis of the results using the ANOVA method and a realistic accelerated cycling script imitating different drive conditions and grid services during the “in between” periods. The “accelerated” script, was also identified as a weak point as the extra detail in the script made the experiment more accurate but also longer as only 1 full cycle is completed per day.

This caused the experiment to last over 70 weeks. Only one type of PAM was used (NCA) giving the experiment a narrow range, furthermore the NCA cells were never discharged more than 45% which is unrealistic given how a V2G EV battery would be operated.

3.1.2 University of Aalborg

M Swierczynski et al. [62] at the University of Aalborg in Denmark investigate the prospect of using second life EV batteries for grid storage services. Over 150 NMC pouch cells sized 20 Ah were aged in first life using various EV driving profile. The batteries were then used in an EA grid service and the capacity fade and IR increase of the batteries was monitored throughout the experiment. The IR and battery cell history were found to be the most critical parameters for the suitability of NMC LIBs for second life EA application.

Although this experiment yields reasonable results it had some limitations:

- This experiment accelerated the second life battery ageing by immensely shrinking two years cycling profile into a one-month profile by the elimination of pauses (i.e. calendar ageing).
- Very little information was given about the experimental setup (i.e. temperature control, EA (dis)charging strategy etc.) making this experiment hard to replicate.
- The experiment did not show any energy efficiencies or discharge energies throughout cycle life which are two basic and important parameters when doing battery degradation testing.
- The discussion did not look in depth to why the batteries degraded. Rather it concluded that the cell with lowest internal resistance and high capacity retention is the best.

3.1.3 Wuhan University of Technology

Zhang et al. [63] at the Wuhan University of technology presents an experimental evaluation of two different cycling procedures of EV LIBs as energy-storage systems. LFP cells sized 60 Ah were subjected to a set of comparative experimental tests defined by United States Advanced Battery Consortium that

consider the effects of charge depleting and charge sustaining operations. Incremental capacity analysis and close-to-equilibrium open circle voltage was utilized to evaluate the performance of the LIBs throughout the cycle life. A qualitative relationship between the external factors (the percentage of time in charge depleting/charge sustaining operations) and the degradation mechanism was built with the help of the above methods. It was found that the difference between the two modes in power and capacity degradation were relatively limited.

Strengths in this experiment are the use of multiple experimental methods. However, the scope of this experiment was relatively small (1 chemistry under 2 different use profiles) and improvements could be made by investigating other external factors that lead to LIB degradation.

3.1.4 Pacific Northwest National Laboratory

Crawford et al. at the Pacific Northwest National Laboratory located in Richland, Washington tested commercial NCA and LFP LIBs under a FR and peak shaving cycle [22]. Some cells were testing after being previously subjected to an EV drive cycle. Capacity, energy efficiency, resistance, (dis)charge energy, were the merits used to assess the state of health (SOH) of the battery. The LFP chemistry showed better stability for the energy intensive peak shaving service, while the NCA chemistry was more suitable to the FR service.

This experiment covers a wide scope as 48 total cells are used to assess the degradation characteristics of different chemistries, grid services, and new and repurposed LIBs from EVs.

Weaknesses in this experiment are identified as having no temperature control while cycling and using only direct current resistance pulsing technique to measure impedance which only considers ohmic losses. Furthermore, for the LFP and NCA cells, pulsing was done at a 1/2.7 h and 1/1.45 h rate, respectively; it is noted that pulsing at different rates does not allow the chemistries to be directly compared.

3.1.5 University of Pau

Bodenes et al. at University of Pau in France studied the degradation of an NMC LIB by doing 25 cycles at a 5 hour rate at various temperatures [64]. the loss of capacity of the tested battery was 7.5% when it was cycled at 85 °C, and 22% when cycled at 120 °C. To characterize the change of the binder and SEI during aging, an analysis was performed using SEM at BOL and end of life (EOL), and X-ray diffraction throughout life cycle. They provided two possible reasons for the aging degradation:

1) the polyvinylidene fluoride binder migrated to the surface of anodes and impeded the intercalation of Li^+.
2) the carbonates species disappeared, and inorganic species increased at the SEI layers at high temperature, which led to the increase of impedance inside the LIBs.

Only two cells with two different temperatures were used thus having a narrow scope. Furthermore, LIBs working between temperatures of 85 °C - 120 °C are only required for a very few unique applications so it would be beneficial to test at least three cells per temperature at lower temperatures. The reference performance test was not specified, and the definition of a “cycle” is vague. Strengths include doing SEM at both BOL and EOL thus allowing observation of the changes of morphology in the electrodes.

3.1.6 Nanyang Technological University

Leng et al. at Nanyang Technological University in Singapore investigated the temperature effect on the rate of capacity degradation of prismatic LCO LIBs at 25 °C and 55 °C using an electrochemistry-based model [65]. Cells cycling at higher temperatures increased the capacity but accelerated the degradation rate. The increase of degradation rate was mainly caused by the degradation of electrodes, where the phase change and SEI growth were exacerbated at high temperatures.

The electrochemical model decomposes the causation of degradation in the cell effectively using a Warburg element. However, different LIB chemistries beyond LCO should be cycled to observed if the results are consistent across all LIB chemistries.

3.1.7 Chungnam National University

Kwon et al. at the at Chungnam National University in South Korea studied the performance and degradation characteristics of two different NMC LIBs with varying Ni contents [66]. $LiNi_{0.5}Mn_{0.3}Co_{0.2}O_2$(NCM532) and $LiNi_{0.6}Mn_{0.2}Co_{0.2}O_2$ (NMC622) were analyzed through hour-rates, performance tests, direct current resistance test (DCR), dVdQ, degradation testing, and electrochemical impedance spectroscopy (EIS) with equivalent circuit models. 4 main conclusions were drawn from these tests:

- Lower Ni content cells had a drastically reduced degradation rate as the higher Mn ratio improved battery stability.

- The higher Ni content LIB had better power output characteristics and lower resistance at all test temperatures and in all SOC regions. At low temperatures (>15 ˚C) the resistance of the NMC532 increases significantly. Therefore, NMC532 may not be able to meet power output requirements above a 0.25-hour rate, especially at low temperatures.

- At all experimental temperatures and hour-rates, the NMC622 demonstrated higher efficiency than the NCM523.

- EIS results show no significant impedance increase at different SOCs, however the large rise in impedance throughout cycle life from the NMC622 was dominated by the charge transfer resistance.

This was a very robust paper as 6 different tests were performed on 2 different types of NMC LIBs, unfortunately it was quantity over quality. All tests lacked information on experiment procedure and conclusions were not clear or thoughtful. The dVdQ section should be omitted from the paper completely as they do not explain the experimental method, the results, and give no conclusions from the testing. Conclusions from other tests were not clear and had to be carefully picked out from the body of the paper. Other weaknesses in the paper include:

- degradation testing was done at a 0.25-hour rate, which is too high power for most realistic applications and favors the characteristics of Mn.
- Only Ni and Mn ratios were varied. Co is the material most manufactures are attempting to reduce, therefore the ratio of Co in the LIB should have been varied and tested to coincide with the needs of industry.

Chapter 4 Experimental Setup

4.1 Physical Characteristics of Lithium Ion Cells

Pictures of the test cells are shown in Figure 12. The cell types are of similar rectangular pouch format, and of similar size. The dimensions and ratings of the cells is given in Table 2. The LFP cell is slightly larger, weighs more, and has correspondingly larger capacity.

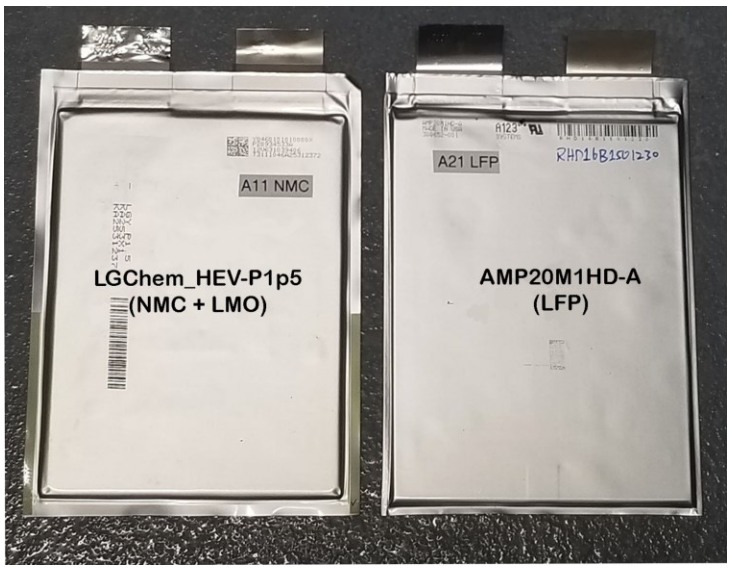

Figure 12 Physical Comparison of Cells

Table 2 Dimensions and Performance Specifications of Cells

Cell Type	LGChem_HEV-P1p5 (NMC+LMO)	AMP20M1HD-A (LFP)
Dimensions (t ,W,H) (mm)	7.1 x 148 x 205	7.25 x 160 x 227
Weight (kg)	0.375	0.496
Nominal Capacity BOL (Ah)	16	19.6
Nominal Energy BOL (Wh)	55	65
Nominal Discharge Power (W)	416	1200
Nominal Voltage (V)	3.75	3.3
Specific Capacity (Ah/kg)	43	40
Specific Energy (Wh/kg)	147	131

A cell from each type was deconstructed to measure the internals components of the cells. The deconstruction also allowed to view manufacturing methods and for the use in SEM/EDS to evaluate cell components.

Due to the stacked nature of the electrodes, there is potential for short circuiting the cell while cutting through it with a knife, which could cause an electrical short that would spark and ignite the electrolyte; therefore cells had to be completely discharged to 0 V before deconstruction could happen.

The cells were discharged by putting a resistor across the cell. A five-ohm resistor was chosen to discharge the cell slowly which give a maximum current of 0.84 A. After 48 h with the resistor the voltages of the cells were measured to be ~0.02 V. Next the cell was shorted by connecting the wire across the positive and negative tabs and any remaining energy was discharged from the cell over the next 24 h. At this point the cell is ready to be deconstructed.

The cells were placed in a fume hood and were cut along the three sides of the outer edge of the heat seal, excluding the side where tabs are located to attempt to avoid cutting through electrodes.

It was found that the LFP cell was a stacked configuration with one continuous zig zagging separator with an extra separator on top and bottom as shown in Figure 13. The NMC+LMO cell was also a stacked configuration with the distinct difference of having individual separators between the positive and negative electrodes. Small samples of both the positive and negative electrodes about 1 cm^2 were cut with standard scissors and was used for the SEM (Section 4.2).

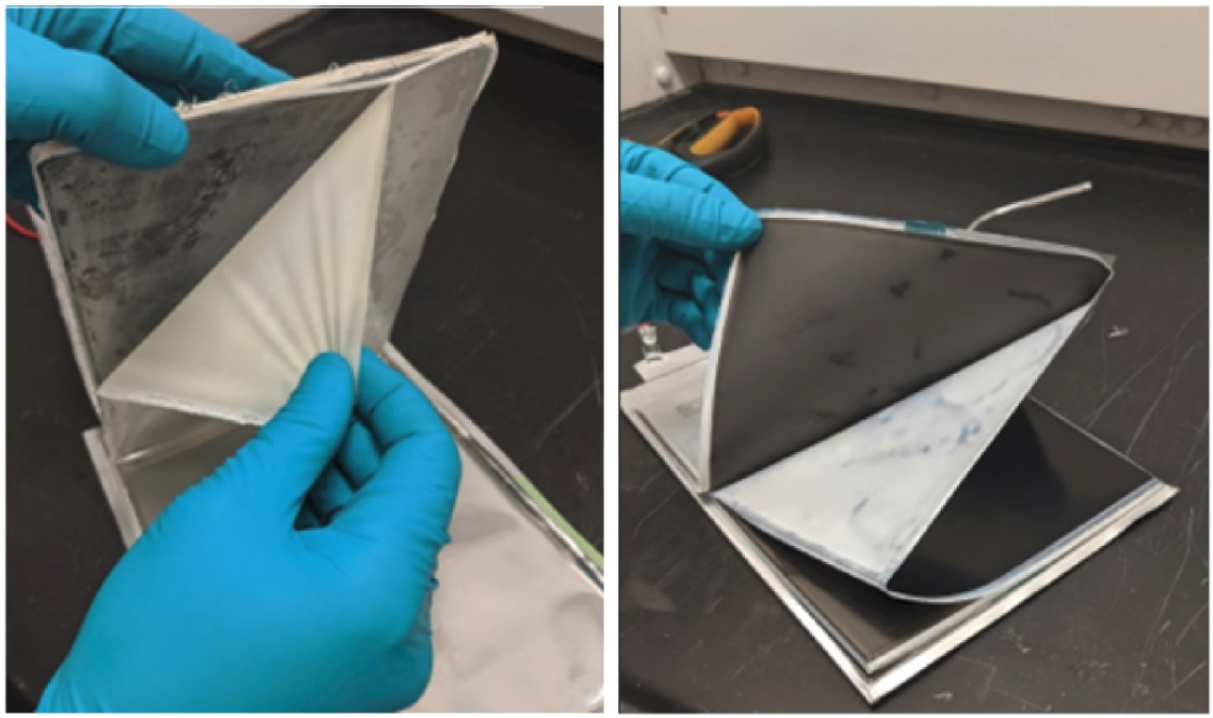

Figure 13 LGC Stacked Separator (left) vs A123 Zig Zag Separator Z-type separator (right)

Each internal component of the cell was measured with the results given in Table 3.

Table 3 Cell Geometry

Dimensions in mm	LGC Positive Electrode (NMC+ LMO)	LGC Negative Electrode (GIC)	LGC Separator	LGC Aluminum Pouch	A123 Positive Electrode (LFP)	A123 Negative Electrode (GIC)	A123 Separator	A123 Aluminum Pouch
Height	196.85	193.6	196.85	196.85	193.675	196.85	196.85	196.85
Width	142.88	142.875	142.88	142.88	149.225	146.05	196.85	149.225
Thickness	0.16	0.17	0.06	0.15	0.17	0.11	0.0023	0.155
Layers	16	17	36	2	21	22	46	2

4.1.1 Cell Geometry

Electrode thickness vs. surface area plays an important roll with the energy to power ratio of a cell. A thick electrode with low surface area allows a high energy cell but has poor power capabilities. This is because many Li^+ can be stored within the electrodes; but the low surface area of the cell cannot transfer ions to the other electrode fast enough when high power is demanded. Conversely, a cell with a high surface area and low thickness, can de-lithiate and intercalate more freely across the entire surface area of the electrode giving high power when needed; but the electrode fills with lithium quickly leading to lower energy capabilities. From Table 3 the A123 NE (GIC) is significantly thinner than the PE (LFP), this is likely because LFP has high power capability so a thin NE is needed, furthermore LFP has a lower energy density making it necessary to have a higher PE/NE material ratio. Since NMC+LMO is a more energy dense and versatile cell (used in energy and power applications) the thickness of the PEs and the amount of material used in the PEs is very close to that of the NEs (within 6%).

4.1.2 Cell Variations

A study by Taylor *et al.* [67] showed that environmental and procedural variations that differences in the experimental setup could induce up to 4% difference in experimental results on similar cells. This different is enough to influence conclusions so much attention should be used to ensure cells are highly similar to each other at the beginning of the test and kept under the same conditions for the duration of the test.

It was necessary to chose cells from a population of 70 cells that were as “close” to each other as possible to enhance confidence. The 3 merits initially assessed were weight, OCV and IR measured from the AC pulse method. After choosing cells based on the qualities mentioned from each chemistry, reference performance tests (RPTs) were then run which assess the state of health (SOH) of the battery.

From the RPTs the cells with the closest discharge capacity were chosen to be used in the experiment. A full list of cells weight, OCV and IR can be found in Appendix B.

4.2 Scanning Electron Microscopy

SEM is used to generate high-resolution images of shapes of objects and to show spatial variations in chemical compositions at very high magnification (20 to 30,000 times spatial resolution of 50 to 100 nm). This is done by using a focused beam of high energy electrons which carry high amounts of kinetic energy. The beam causes different interactions with the atoms of the target sample. Accelerated electrons can either pass through the sample without interaction, undergo elastic scattering or can be inelastically scattered [68]. Elastic and inelastic scattering cause the signals shown in Figure 14

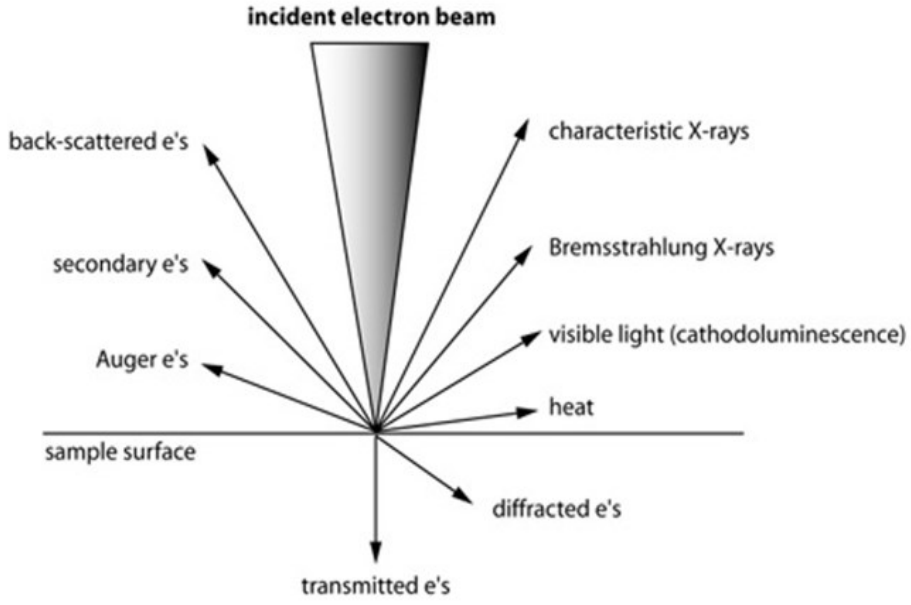

Figure 14 Types of Scattered Electrons [27]

Scattering signals can be used for imaging, quantitative information of the target sample and generation of an X-ray source. In this experiment secondary electrons and backscattered electrons were used for imaging, while characteristic X-ray signals were used for elemental analysis.

The elemental analysis is known as Energy Dispersive X-Ray Spectroscopy (EDS) and is part of the SEM analysis. EDS measures inelastic collisions between incident electrons and the electrons in the discrete orbital of atoms in the sample [69].

The electron beam excites the electrons of the element and as the electron goes back to a lower energy state, the difference of energy levels of the electrons between the adjacent shells of an element emits a unique X-ray of a fixed wavelength. Each wavelength is unique to each element thus EDS can deduct the elements in the sample.

EDS is an elemental analysis tool meaning it can only identify elements present. Therefore, no information is given about the oxidation states of the compound. Furthermore, Li has very low energy radiation characteristics and is not detectable on most modern SEMs (including the one used in this analysis) while Hydrogen (H) and Helium (He) do not produce characteristic radiation at all and cannot be detected. This proves limiting to many battery researchers and therefore a similar technique called X-ray photoelectron spectroscopy (XPS) is used when know the oxidation state of the element is useful. Resources did not permit the use of XPS in this experiment.

SEM and EDS of the LGC and A123 cells were taken at BOL to verify the materials in the cell, compare particle sizes and look for abnormalities in the material. Figure 15 presents NAM values and Figure 16 presents PAM values.

4.2.1 Negative Electrodes

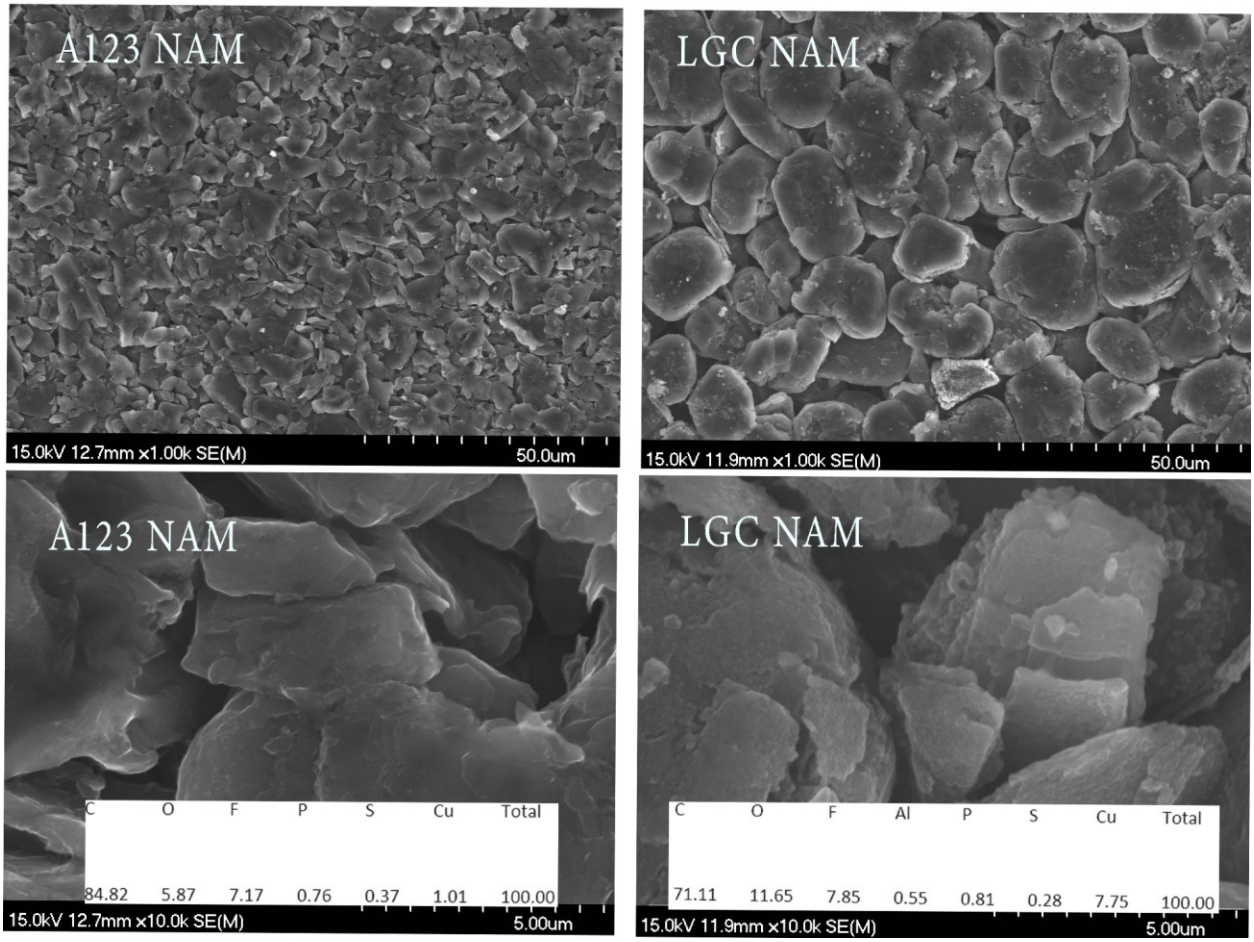

Figure 15 SEM Negative Active Material

LGC and A123 cells both use GIC as the NAM. Graphite pieces in the A123 cell are approximately ¼ the size of the LGC pieces. This plays a significant roll in the high-power capabilities of A123. The total amount of graphite has more exposed surface area on the A123 cell which gives Li^+ more surface area to bond with at the electrode-electrolyte interface. Solid-state diffusion happens much slower through the electrode (i.e. into the basal planes of the graphene sheets) than through the electrolyte. Having more surface Li^+ available at the electrode/electrolyte interphase leads to higher power capabilities as more

Li^+ can move to the PAM at once. The larger holes in the graphite of the LGC means a smaller charge transfer resistance as Li^+ can move through the electrode easier.

Since LCG and A123 both have graphite NAM pasted onto a copper current collector, the Carbon (C), Copper (Cu), and Oxygen (O) were expected. Fluorine (F), Phosphorous (P), Sulphur (S) and Aluminum (Al) were also found in the NAMs. F and P can be accounted for from the Li Salt ($LiFP_6$) that is added to the solvent to make the electrolyte. S is likely used in the solvent portion of the electrolyte however this cannot be confirmed. Since the cell was aggressively discharged to 0 V there is the possibility of Al oxide from the current collector on the PAM moving to the NAM and plating onto the graphite.

4.2.2 Positive Electrodes

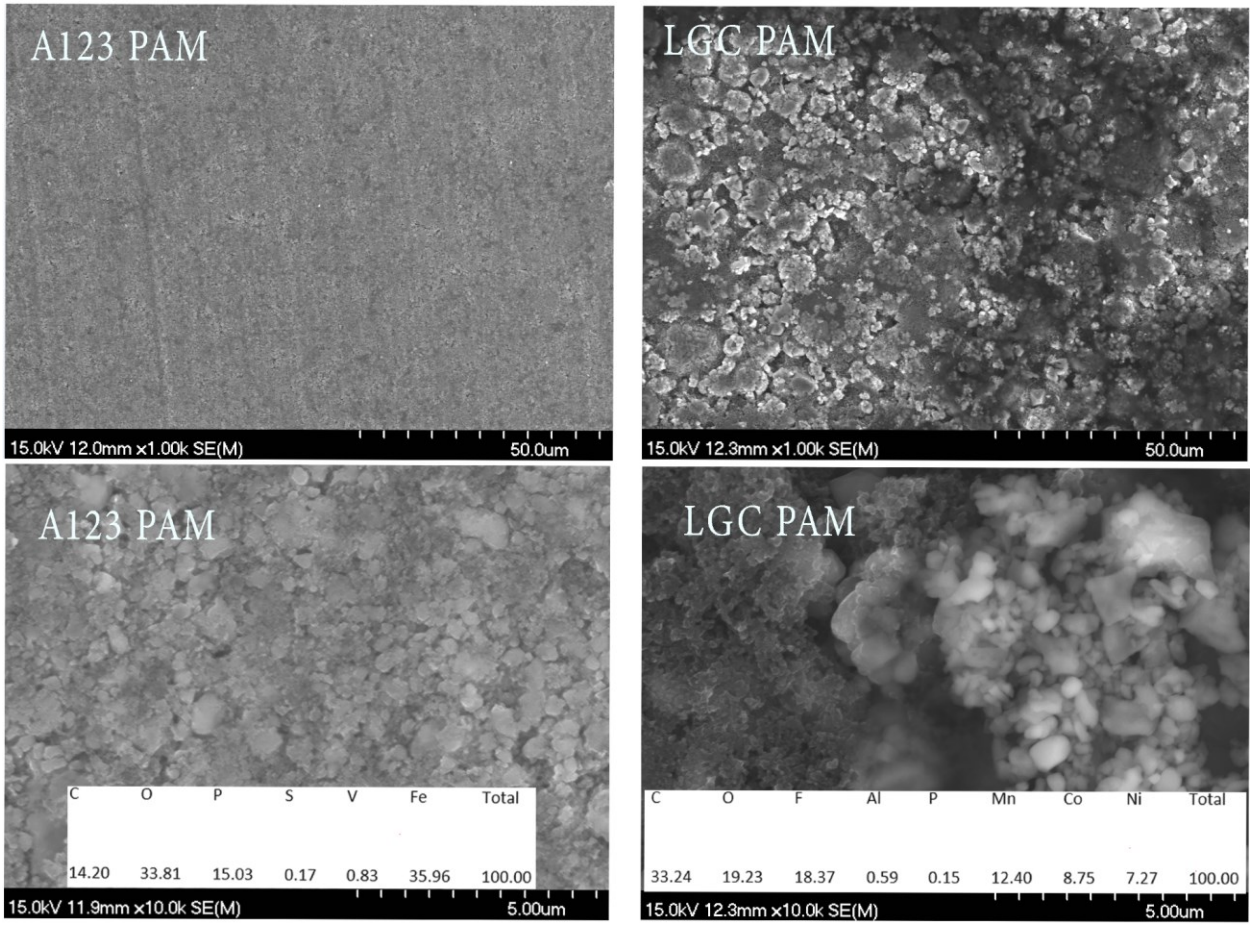

Figure 16 SEM Positive Active Material

Similarly, to the NAM the A123 PAM (LFP) has a much finer grain size due to the nano scale phosphate used in the material than the LGC PAM (NMC+LMO). Since different materials have different theoretical capacity and lattice structures they cannot be compared directly, however the smaller grain size increases surface reactions and enhances power capabilities. Al was used as the current collector in both the A123 PAM and LGC PAM. the only material that was unexpected was the Vanadium (V) In the A123 PAM. V could likely be used as a "dopant" in the PAM to increase capacity and power capabilities but cannot be confirmed.

4.2.3 Chemical Composition and Theoretical Capacities

EDS gives the chemical composition of the subject in mass percentage. The measured chemical composition vs the theoretical composition of each cell can be calculated using this information.

Table 4 shows the percent error of the theoretical chemical composition vs the measured composition through SEM. Limitations of Table 4 are as follows:

- The cells were exposed to open air before EDS and had time to oxidize, thus the total amount of Oxygen contributed to each material was unknown.
- The mass ratio of NMC vs LMO was not specified by the manufacturer
- The ratio for the NMC (i.e. NMC 811 or NMC 111 etc.)
- The structure of the LMO (spinel or layered) was not specified by the manufacturer and spinel was assumed.

Table 4 SEM Mass Fractions

$LiFePO_4$	SEM Weight (%)	Mass Fraction	Molecular Weight (g/(mol*atoms))	Number of atoms	Theoretical Molecular weight (g/mol)	Theoretical Mass Fraction	Error (%)
Lithium (Li)	NA	NA	6.9	1	7	4%	NA
Iron (Fe)	35.96	42%	55.8	1	56	35%	19.90%
Phosphorus (P)	15.03	18%	31	1	31	20%	9.80%
Oxygen (O)	33.8	40%	16	4	64	41%	1.80%
Total (%)	84.79	100%	103		157.7		

$LiMn_2O_4$ (Spinel)	SEM Weight (%)	Mass Fraction	Molecular Weight (g/(mol*atoms))	Number of atoms	Theoretical Molecular weight (g/mol)	Theoretical Mass Fraction	Error (%)
Lithium (Li)	NA	NA	6.9	1	7	4%	NA
Manganese (Mn)	5.15	63%	54.9	2	110	61%	4.00%
Oxygen (O)	3	37%	16	4	64	35%	4.00%
Total (%)	8.15	100%	71		180.7		

$LiNi_{1/3}Mn_{1/3}Co_{1/3}O_2$	SEM Weight (%)	Mass Fraction	Molecular Weight (g/(mol*atoms))	Number of atoms	Theoretical Molecular weight (g/mol)	Theoretical Mass Fraction	Error (%)
Lithium (Li)	NA	NA	6.9	1	7	7%	NA
Nickel (Ni)	7.27	20%	58.7	0.33	19	20%	0.9%
Manganese (Mn)	7.25	20%	54.9	0.33	18	19%	5.7%
Cobalt (Co)	8.75	24%	58.9	0.34	20	21%	15.4%
Oxygen (O)	13.23	36%	16	2	32	33%	9.2%
Total (%)	36.50	100%	189		96.41	100%	0.0%

From Table 4 It was estimated that the molar ratio between the Ni, Mn, Co was 1:1:1 (i.e. NMC 111) ($LiNi_{\frac{1}{3}}Mn_{\frac{1}{3}}Co_{\frac{1}{3}}O_2$) . The mass ratio between the NMC and LMO was estimated to be 4:1.

Using the information from Table 4 the theoretical capacities of each cell can be calculated by Faraday's law.

Taking the LFP for example:

$$Q_{theoretical} = \frac{nF}{3.6W}\frac{\text{mAh}}{\text{g}} \tag{13}$$

where *n* is the number of charge carrier, *F* is the Faraday constant and *W* is the molecular weight of the active material used in the electrode.

$$LiFePO_4 \rightarrow FePO_4 + 1Li^+ + 1e^- \tag{14}$$

$$W_{LiFePO_4} = 157.7\ \frac{\text{g}}{\text{mol}}$$

$$F = 96485.3329\frac{\text{C}}{\text{mol}}$$

$$1\text{mAh} = 3.6\ \text{C}$$

Since only 1 Li^+ is in the reaction, n=1, we obtain

$$Q_{theorectical_{LFP}} = 170\ \frac{\text{mAh}}{\text{g}}$$

Similarly, for NMC and LMO:

$$Q_{theorectical_{NMC}} = 278\ \frac{\text{mAh}}{\text{g}}$$

$$Q_{theorectical_{LMO}} = 148.3\ \frac{\text{mAh}}{\text{g}}$$

For the LGC and A123 Cells:

$$Q_{theorectical_{A123}} = Q_{theorectical_{LFP}} = 170\ \frac{\text{mAh}}{\text{g}}$$

$$Q_{theorectical_{LGC}} = \frac{(4 * Q_{theorectical_{NMC}} + Q_{theorectical_{LMO}})}{5} = 252.1\ \frac{\text{mAh}}{\text{g}}$$

4.3 Experimental Design

Two LIB chemistries will be tested under two different types of grid-services, requiring $2 \times 2 = 4$ cells. As there is variation in the cells and testing conditions (i.e. manufacturing tolerances, separate channels on power cycler, different locations in test chamber) it was necessary to have 3 cells of each type. This produces a range of results with a minimum, median, and maximum value for each cell type and service combination. If the results of the three cells for a given type and service are close together, it gives confidence in the results, especially when comparing across cell types and different services. To achieve this 12 cells were required for the experiment ($4 \times 3 = 12$ cells) as listed in Table 5 and shown graphically in Figure 17 .

Table 5 Test Cell Counts

Grid Service	NMC+LMO	LFP
Frequency Regulation	3	3
Deep Discharge	3	3
Total number of cells	12	

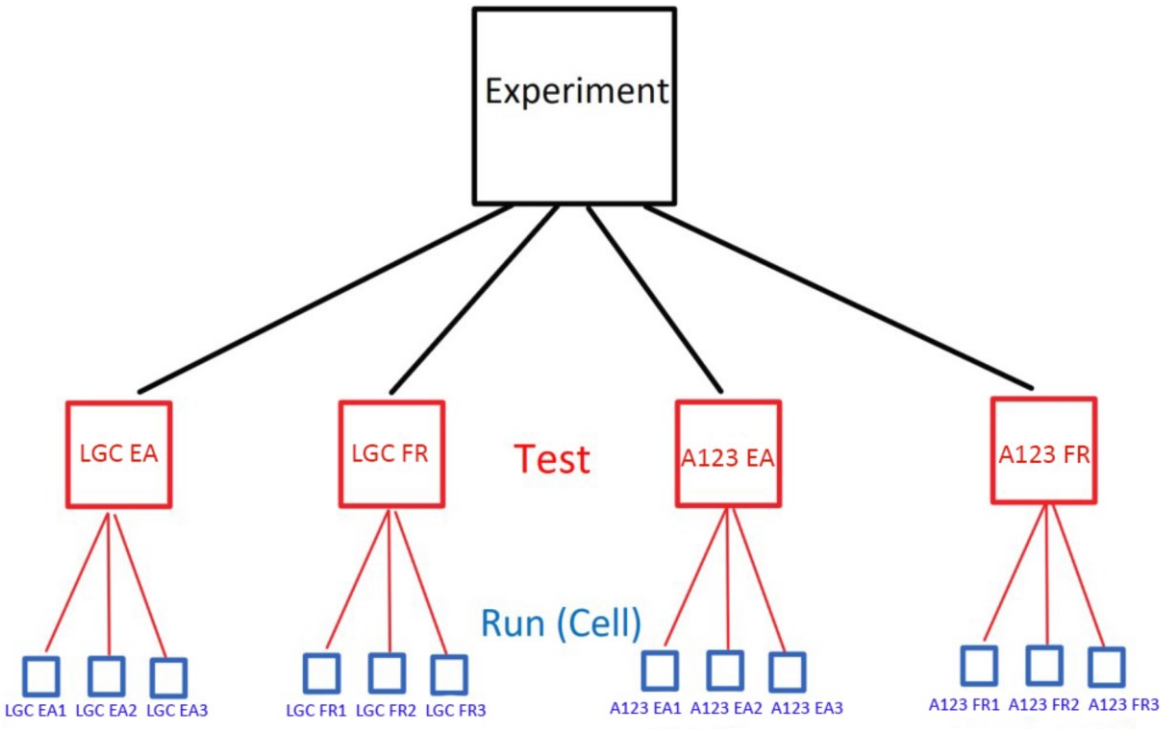

Figure 17 Experimental Setup Overview

LG Chem manufactured the HEV-P1p5 (NMC+LMO) cells and A123 systems the AMP20M1HD-A (LFP) cells. Each chemistry can be considered from the same population. The cells were kept in a temperature and pressure-controlled room at 20 °C, any slight variations in room temperature and pressure are considered negligible.

The LGC (NMC+LMO) and A123 Systems (LFP) LIBs will be cycled using a Neware power cycler to imitate the desired grid service. The cells are cycled using constant power (CP), constant current constant voltage (CCCV), constant power constant voltage (CPCV) and frequency regulation power (FR). The current (A), voltage (V), and cell temperature (°C) is recorded in real time and put into a spreadsheet (.XLS).

4.4 Testing Apparatus

Testing twelve large format Li^+ pouch cells requires a testing area appropriate to meet the unique needs of battery cycling. Before cycling could begin a test area had to be designed that met the following requirements:

1) Neware power cycler and test chamber must fit within a 6 ft x 9 ft space in the Test Area as shown in Figure 18.
2) In the event of a cell going into thermal runaway the condition would not propagate to any other cells in the chamber
3) In the even of cell failure, the test chamber must resist the initial short pressure burst of the cell combustion and possibly a long period of exhaust to remove smoke and heat [70].
4) Test Area must be thermally conditioned.

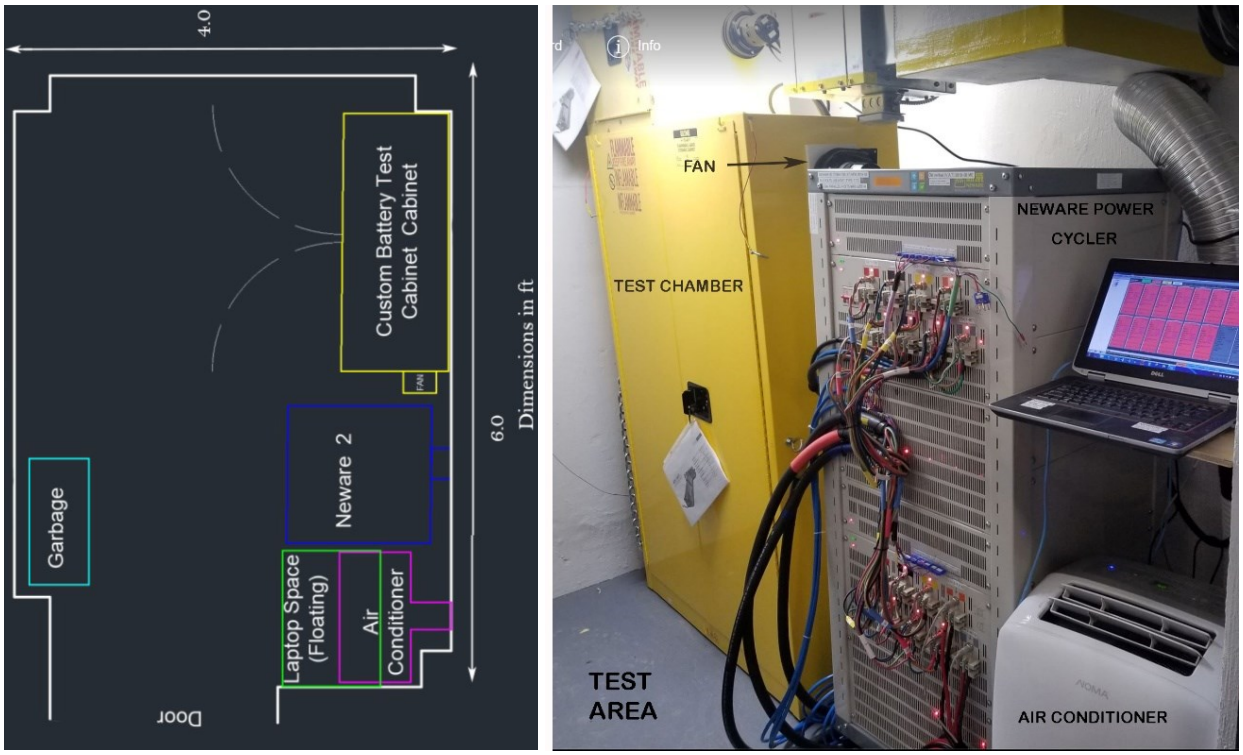

Figure 18 Test Area Floor Plan and final design

4.4.1 Test Chamber

The test chamber was thermally conditioned to promote cell uniformity, provide safe cycling inside a cabinet, and to mitigate propagation in the event of a cell failure.

If a Li^+ cell is short-circuited, exposed to high temperature, or over/under charged exothermic reactions can be triggered, resulting in a self-enhanced increasing temperature loop known as “thermal runaway” this can lead to battery fires and explosions. Doing degradation testing increases this risk. As the battery degrades lithium plating occurs on the negative electrodes this increases the potential for an internal short circuit and a battery explosion. Furthermore, as the battery degrades the IR increases thus making voltages fluctuate more significantly and less predictably than an uncycled cell; at voltage extremities the IR is at its highest putting the cell at its minimum efficiency. This low efficiency means that much of the energy transferred through the cell is dissipated as heat thus increasing the cell temperature and the chances of an occurrence of thermal runaway.

As shown in Figure 19, type-T thermocouples were adhered with tape to the center of each cell which is the warmest part of the outside of the cell. A ½” x ½” piece of insulating tape was adhered on top of each thermocouple to eliminate the effects of surrounding air, but not big enough to insulate the cell and cause an inaccurate reading. While cycling, If the thermocouple reads a value over 40 °C the test will stop and notify the lab staff through error messaging. This should stop any dangerous cell before thermal runaway would begin. This method serves as the first line of defence to mitigate the risk of a fire.

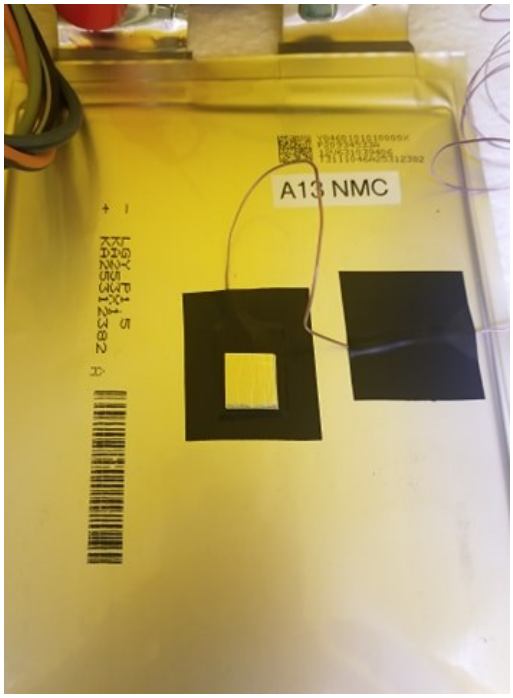

Figure 19 Type T Thermocouple attachment

To reduce high temperatures the fire chamber was air cooled using a blower at the top right side which sucked air through the only large opening in the chamber on the bottom left side. This meant that the air would have to travel through the entire chamber and thus continuous flow and cooling would occur. Holes of 3” diameter were drilled on each level of the inside wall of the chamber. On the blower side this was done to facilitate airflow through the chamber and to make sure the air was not just being sucked through the plenum of the chamber. Furthermore, each set of cells was distributed through each level of the chamber to receive equal cooling as shown in Figure 20. This would reduce risk of any of the cell groups being at a consistent higher ambient temperature. The blower also served the purpose of mitigating damage in the occurrence of a fire as the outlet of the blower points back directly toward a concrete wall and directly under the exhaust outlet of the lab. In the event of a cell fire it would be forced out into the concrete wall and smoke/fumes would be sucked in by the exhaust fan and out of the lab to the outside.

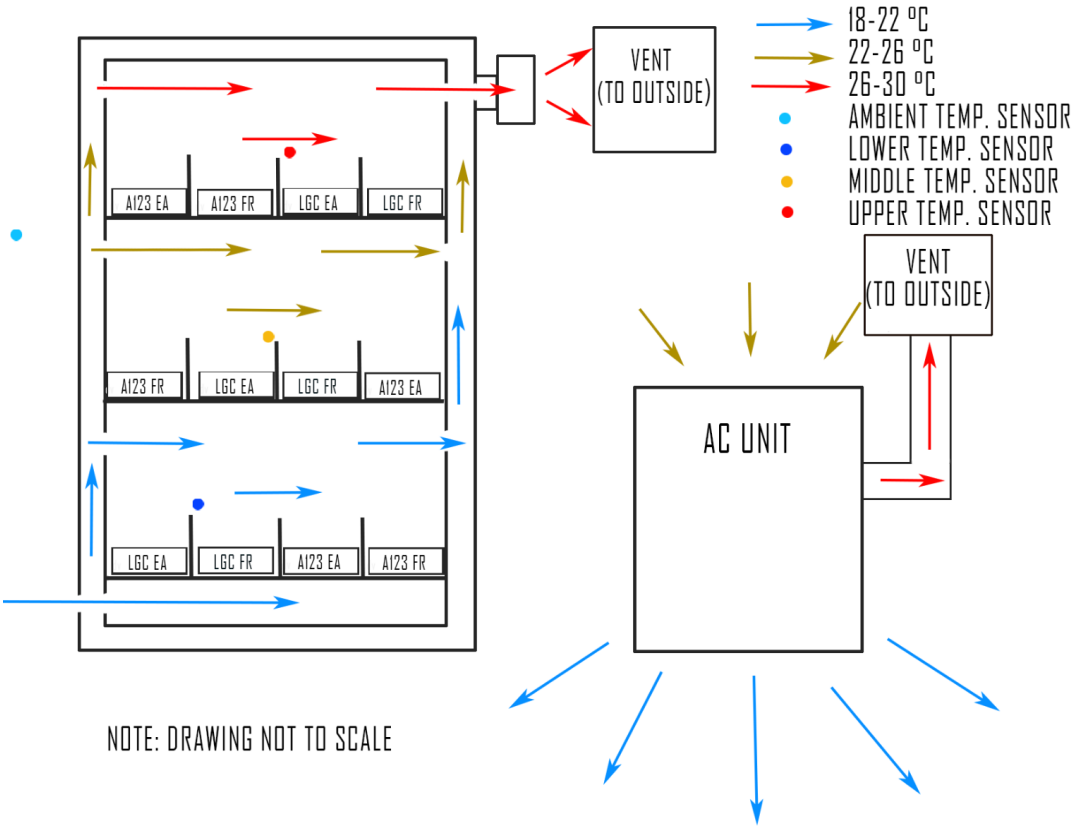

Figure 20 Thermal Conditioning of Test Chamber

To prevent fire propagation to cells on above shelves, fire resistant drywall was placed under each shelf. As shown in Figure 21 to prevent propagation of adjacent cells 1/16” aluminum sheets were used as a fire shield separating each cell. Fire cloth was place on the bottom of the cell to stop heat transfer through the metal shelves into adjacent cells.

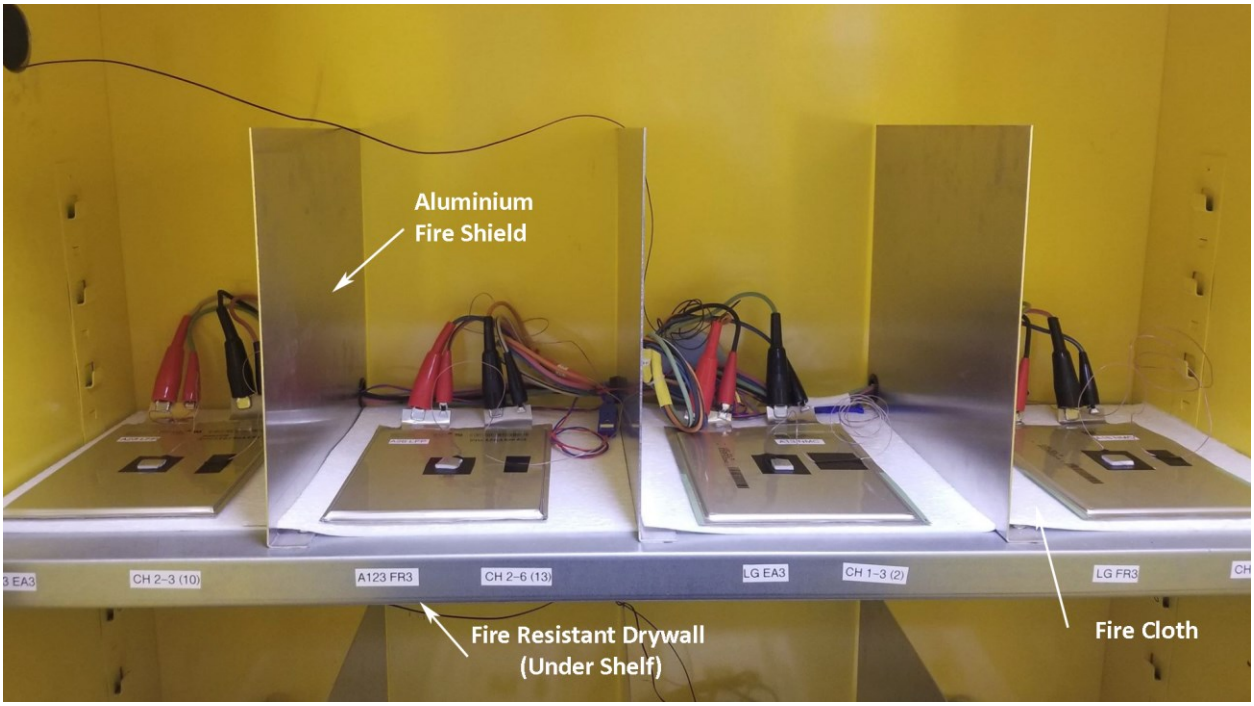

Figure 21 Adjacent and Parallel Fire Protection

Fire suppression was placed inside the test chamber. It was decided the best practice to mitigate human injury would be to let the fire burn until the external fire suppression system (sprinkler) located directly on top of the fire chamber would activate.

As shown in Figure 22, two eyelets were tapped through the chamber and a 3/8” stainless steel chain was loosely attached via clips to facilitate depressurization of the chamber during an explosion of a cell. The latch of the fire cabinet was permanently locked in the open position so that it could not become a pressure chamber. If an explosion happened the door would burst open about 14” to release the gasses created in the explosion, then would be stopped by the chain. This would reduce the risk of the door hitting someone in the unlikely event they were present in the test area during an explosion. The door would then close shut and the unpressurized fire would continue to burn safely inside the fire chamber.

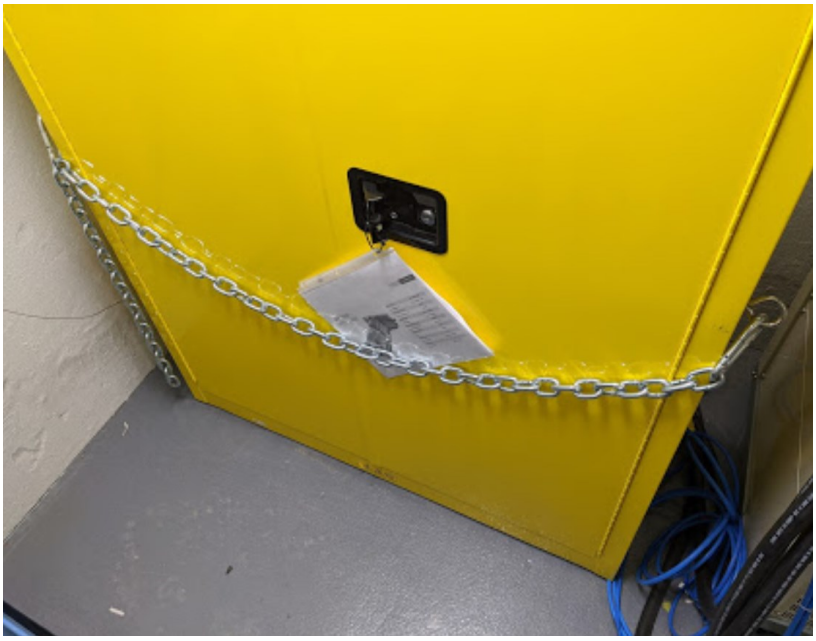

Figure 22 Explosion Release Mechanism

A self closing door was installed at the entry of the test area. This ensured the door remained closed to mitigate external temperature effects from the rest of the laboratory and other experiments.

The Neware Power Cycler was in a closed room with the 12 cells. During 1 h discharge periods the batteries transfer $864\ W$ ($20\ A \times 3.6\ V \times 12\ Cells$) into the test area. As the ambient temperature in the test area would rise, it was necessary to cool the air to reduce the risk of thermal runaway of the cells. An air conditioning unit placed in the test area. An exhaust duct was mounted on the wall and put through an existing hole in the concrete and heat was expelled through a one way valve (to keep cold air out during the winter months) keeping the ambient temperature of the test area at a consistent 20 °C ± 2 °C.

Lastly, a webcam was installed so the tests area can be viewed remotely.

4.4.2 Neware Cycler Accuracy

Before cycling began the 16 channel Neware power cycler was verified for accuracy. Four currents (-10 A, -1 A, 1 A, 10 A) were demanded to be delivered to a test battery from the Neware. The output current from the Neware would then be measured internally by the Neware and manually using a recently calibrated Fluke 289 meter which has a verified DC current accuracy of ±0.05% [71]. Maximum acceptable error for the Neware was as follows:

- ±2.0% difference between the measured Neware currents and the measured Fluke currents
- ±0.5% difference between the measured Neware currents and demanded Neware currents

As shown in Figure 23 the Neware was found acceptable for use.

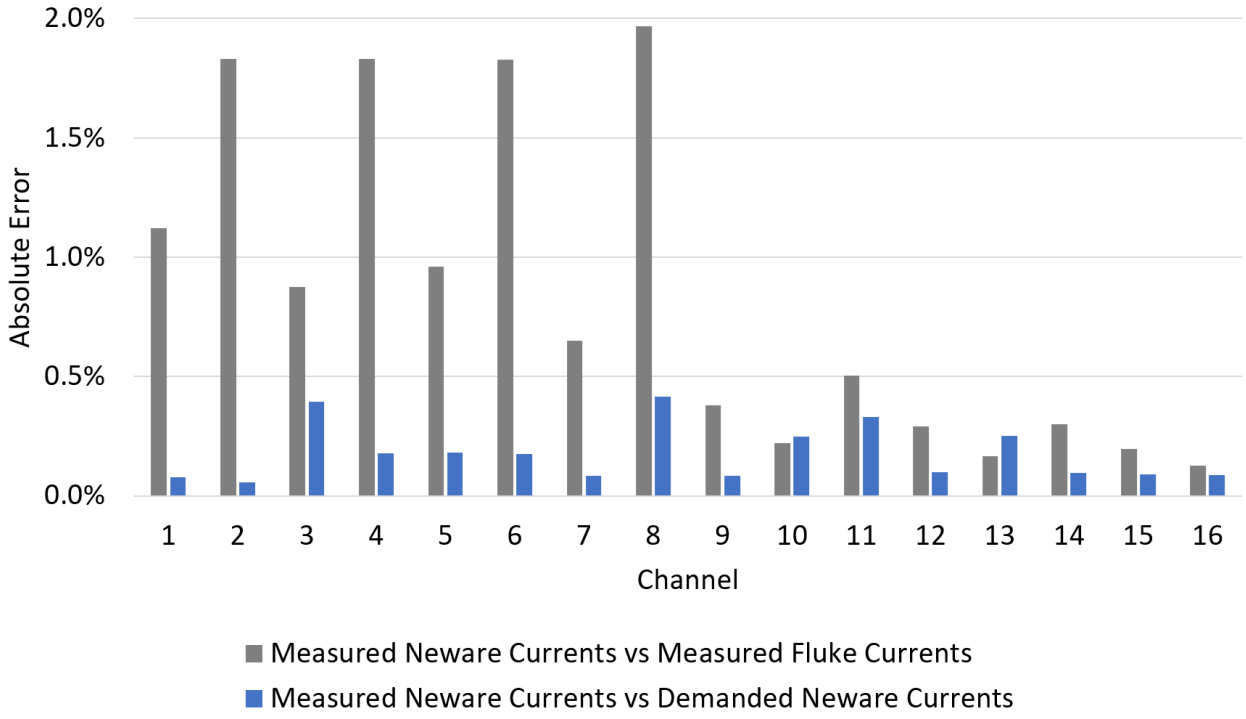

Figure 23 Neware Accuracy Verification

Chapter 5 Experimental Methods

5.1 Cycling

Depending on the grid service being imitated each cell will either cycle under a deep discharge constant power (CP) or a partial discharge frequency regulation (FR) service. Every 21 days (176 Δ100% SOC equivalent rated cycles), reference performance tests (RPTs) were conducted (1 h CCCV, 1 h CPCV, 24 h CCCV, Pulse) on the cells. This allowed the EA and FR tests to be time synced and produced 6 data points every 1000 cycles which was considered acceptable resolution without pausing excessively to perform RPTs.

A comparison of the cycling procedure for both EA and FR is shown in Table 6.

Table 6 EA and FR Cycling Procedure

Energy Arbitrage	**Frequency Regulation**	**# of Cycles**	**Total Test Time (Including Rests)**
1 h CP	24 h FR Signal	EA- 250 cycles (176 Δ100% SOC equivalent rated cycles)	EA - 540 h
		FR- 21 cycles (176 Δ100% SOC equivalent rated cycles)	FR - 540 h
1 h CCCV	1 h CCCV	3 Δ100% SOC equivalent rated cycles	7 h
1 h CPCV	1 h CPCV	3 Δ100% SOC equivalent rated cycles	7 h
24 h CCCV	24 h CCCV	2 Δ100% SOC equivalent rated cycles	72 h
Pulse	Pulse	20 pulses (1 Δ100% SOC equivalent rated cycles)	4 h

The procedure is repeated until the end of the experiment or a cell failure to complete the cycle.

To mitigate effects of thermal variation, cells were timestep synchronized during reference and EA/FR cycling, meaning all cells will start the (dis)charge cycles simultaneously. Cells expel heat as they

discharge, thus the ambient temperature inside the test area varies about 5 °C. If the cells were not timestep locked some cells would be discharging at higher ambient temperatures than others. As cells perform more efficiently at higher temperature this means that the discharge energies of the cells at higher temperature would be skewed high. The temperature profile because of this synchronous cycling during a reference performance tests is shown in Figure 24. Locations of each thermocouple can be found in Figure 20.

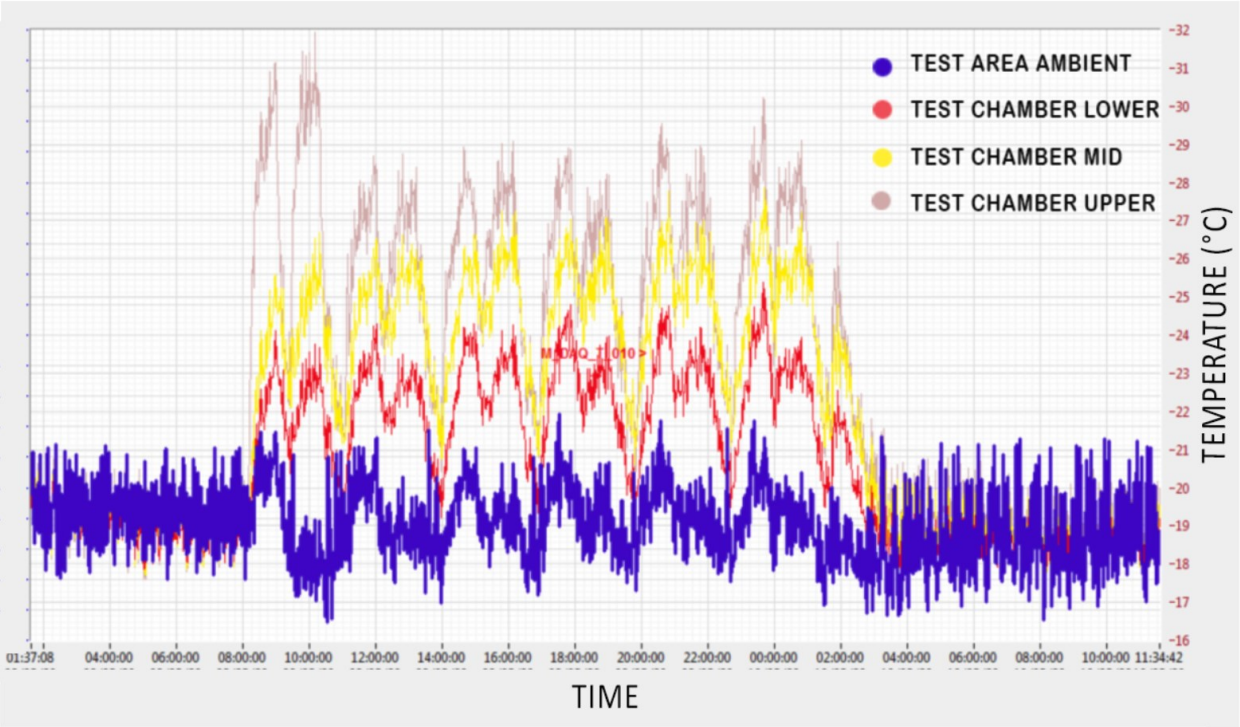

Figure 24 Ambient Temperatures Inside Test Chamber

The bottom shelf experienced the lowest average temperature, the middle shelf the median temperature and the top shelf the highest temperature. There is not enough available data to make conclusions on temperature trends in the transverse (left to right) or latitudinal (front to back) directions. However, these temperature deviations, spanning several degrees Celsius indicate it was proper experimental setup to included 1 or more cells of each type in each service on each shelf.

5.1.1 Energy Arbitrage Cycle

Cycling in EA is imitated on the power cycler by (dis)charging at a constant power to a specified upper and lower cut off voltages as shown graphically in Figure 25.

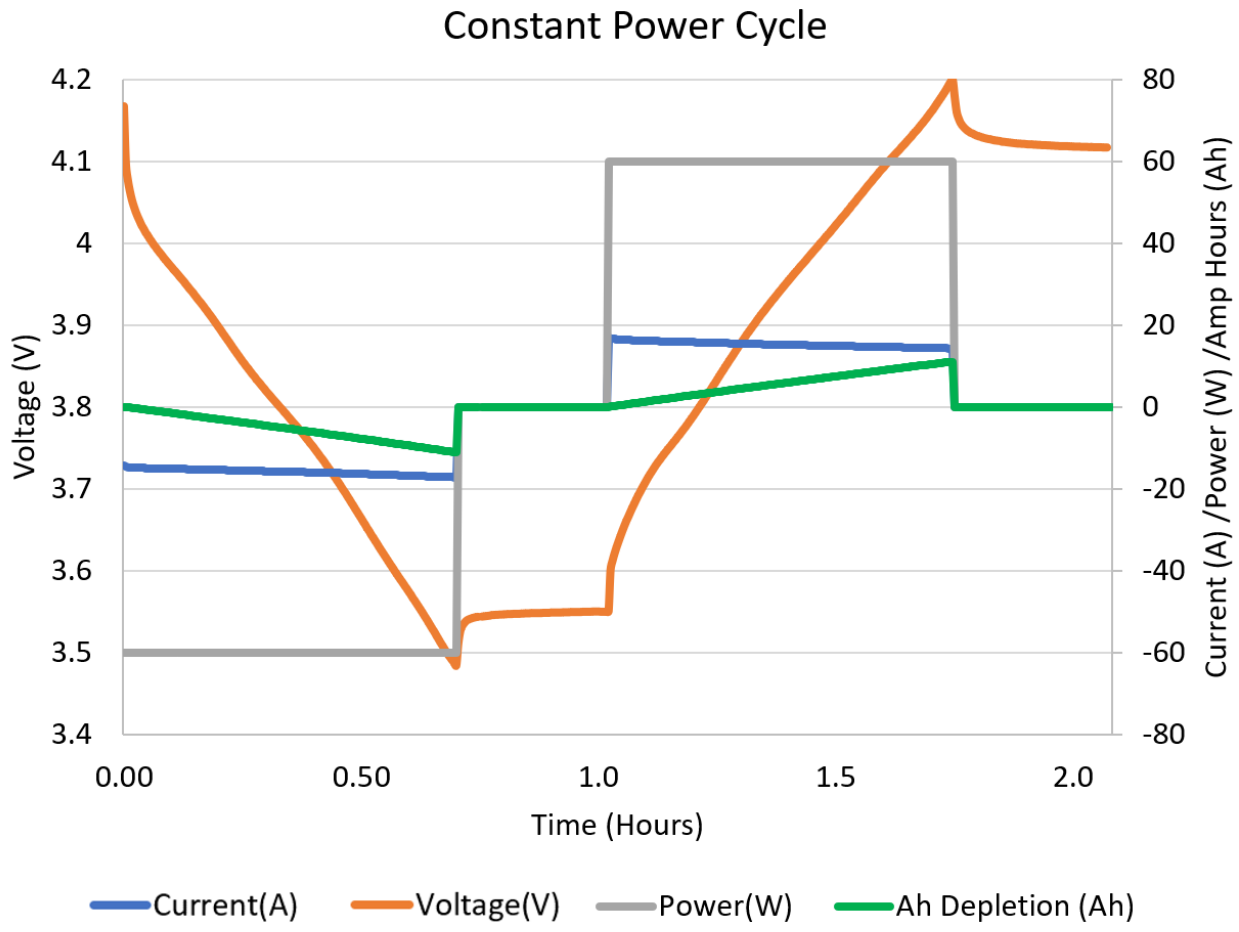

Figure 25 CP Cycle

A simplified EA cycling script is shown in Table 7. The entire EA code implemented on the power cycler can be found in Appendix C.

Table 7 EA Cycling Protocol

Step	Name	LGC		A123	
		Value	Stop Condition	Value	Stop Condition
1	CC Charge	16 A	4.2 V	20 A	3.6 V
2	CP Discharge	60 W	0.7 h	65 W	0.7 h
3	CP Charge	60 W	4.2 V	65 W	3.6 V
4	Loop	Step 2	252 Times	Step 2	252 Times
5	End				

At BOL the EA cells (dis)charge from 90% SOC- 20% SOE (State of Energy) (70% SOE range). The amount of energy discharged from the cells on each EA cycle remained constant throughout the entire experiment. As the cells degrade and lose capacity the SOE range the cells cycle in is expanded, as shown in Figure 26. This method was chosen for the following reasons:

- To avoid high and low voltage extremities. Cycling at these SOEs cause an acceleration in degradation and anyone providing grid services with batteries should avoid these SOEs to prolong battery life and energy throughput.
- To avoid hitting upper and lower cut off voltages prematurely. A Δ70% SOE swing at BOL was used to keep a consistent (dis)charge capacity value while cycling in EA throughout the entirety of the experiment.

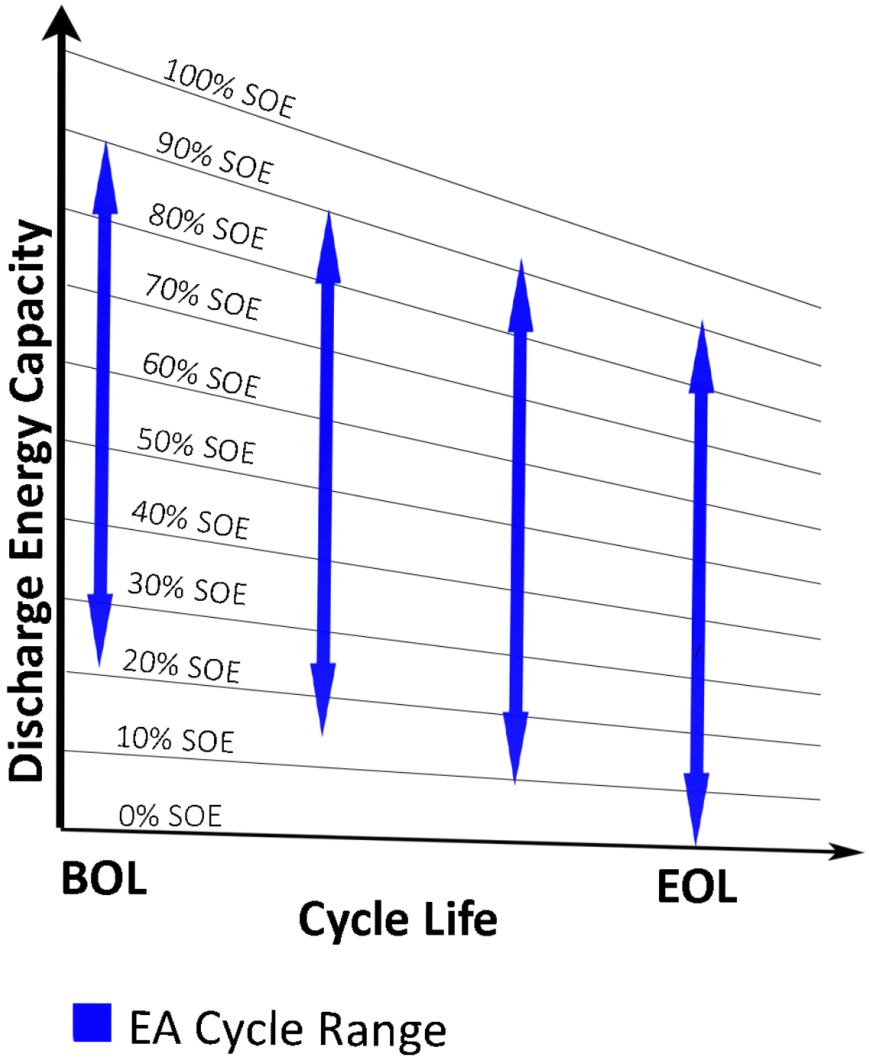

Figure 26 EA SOE Cycling Script

5.1.2 Frequency Regulation Cycle

FR cycling is a partial state of charge service, meaning that the battery should never reach the upper or lower voltage limit. However, the battery is expected to have higher power for short durations (<5 seconds). To show the variable power requirements of FR a 2 h block of a 24 h cycle is shown in Figure 27. In this figure, negative current and negative power correspond to discharge. A simplified FR script is shown in Table 8. The entire FR code implemented on the power cycler can be found in Appendix C.

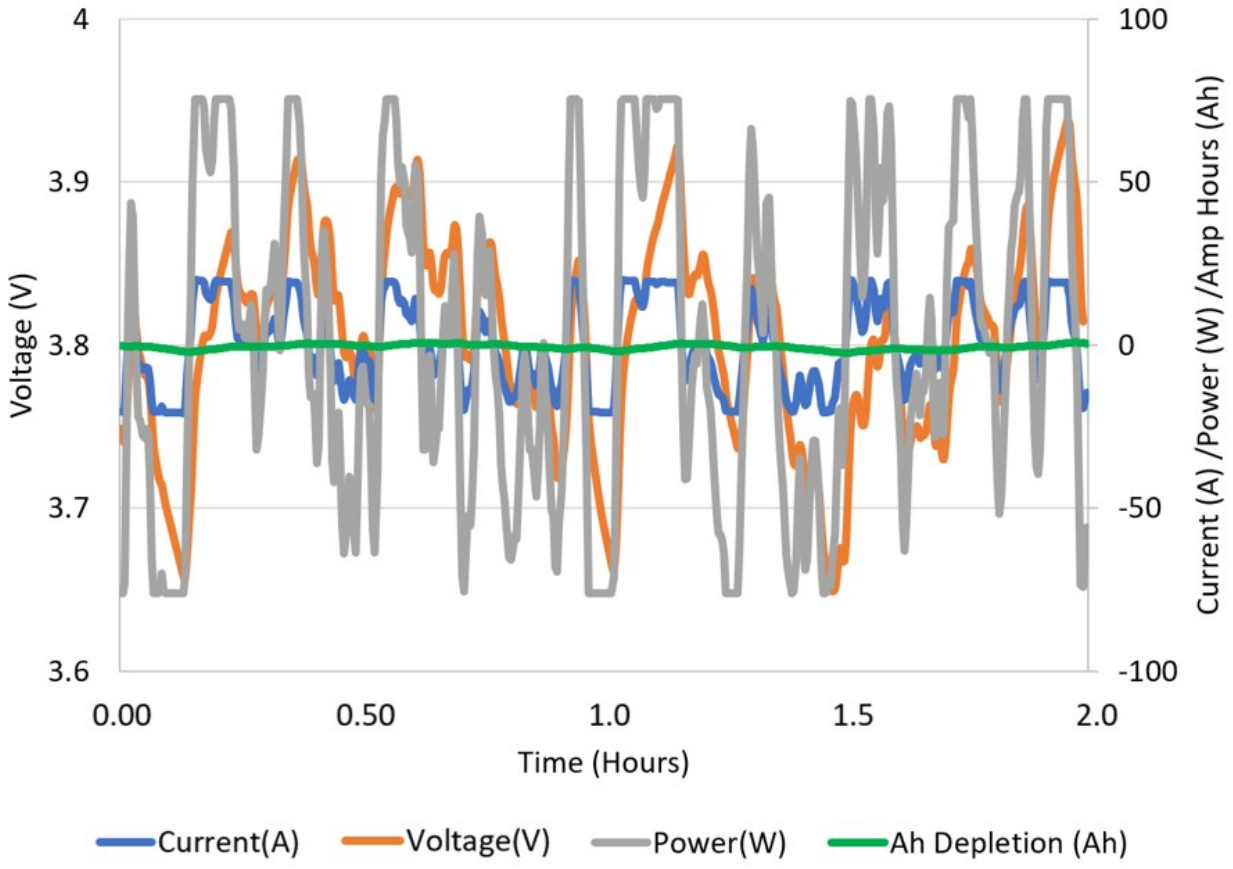

Figure 27 FR Cycle

Table 8 FR Cycling Protocol

Step	Name	LGC		A123	
		Value	Stop Condition	Value	Stop Condition
1	CC Charge	16 A	4.2 V	20 A	3.6 V
2	CV Charge	4.2 V (Taper Current)	1 h or 0.01 A	3.6 V (Taper Current)	1 h or 0.01 A
3	CC Discharge	16A	0.45 h	20A	0.45 h
4	FR Cycle	PJM December 18th,2017 (76.2 W Power Multiplier)	24 h	PJM December 18th,2017 (83.0 W Power Multiplier)	24 h
5	CC Charge	16 A	(Ahd Step 4 + Ahd Step 5) > 0	20 A	(Ahd Step 4 + Ahd Step 5) > 0
6	Loop	Step 4	3 Times	Step 4	3 Times
7	Loop	Step 1	7 Times	Step 1	7 Times
8	CC Charge	16 A	4.2 V	20 A	3.6 V
9	End				

Ahd = (charge coulombic capacity - discharge coulombic capacity)

There is little FR signal data available to the public. In 2012, Sandia National Laboratories developed a 24-hour FR duty-cycle for energy storage systems research [72]**,** composed of select segments of 4-second FR signal data published by PJM, a Pennsylvania-based electricity grid operator. PJM now publishes 2-second FR signal data covering every day of the year [73], and a representative 24-hour period of this raw data better reflects practical FR service than the composite duty-cycle from Sandia. The 24-hour period of December 18th, 2017 from PJM was chosen for this study for the following reasons:

- One repeating day gives consistency to testing. While a multitude of days could have been used, each was unique and most had energy bias that would cause over discharge or over charge.
- 2017 was the latest available data when this test started in mid 2018.
- December 18th was chosen as it is an aggressive power signal day, is energy neutral over the 24-hour period and has relatively small energy deviations. Being power aggressive will wear batteries faster and is beneficial for this study. Being energy neutral means that the cell should

start and end the 24-hour period at approximately the same SOE. Having small energy deviations means that the cell will not be come over discharged or over charged at any point throughout the signal period.

In Figure 28, the energy graph of December 18th (blue lines) is compared against 2 other representative days.

- Jan 30th (red lines) has a high energy throughput but is far from energy neutral.
- November 24th (green lines) has close to a energy neutral signal but does not have a high total energy throughput.

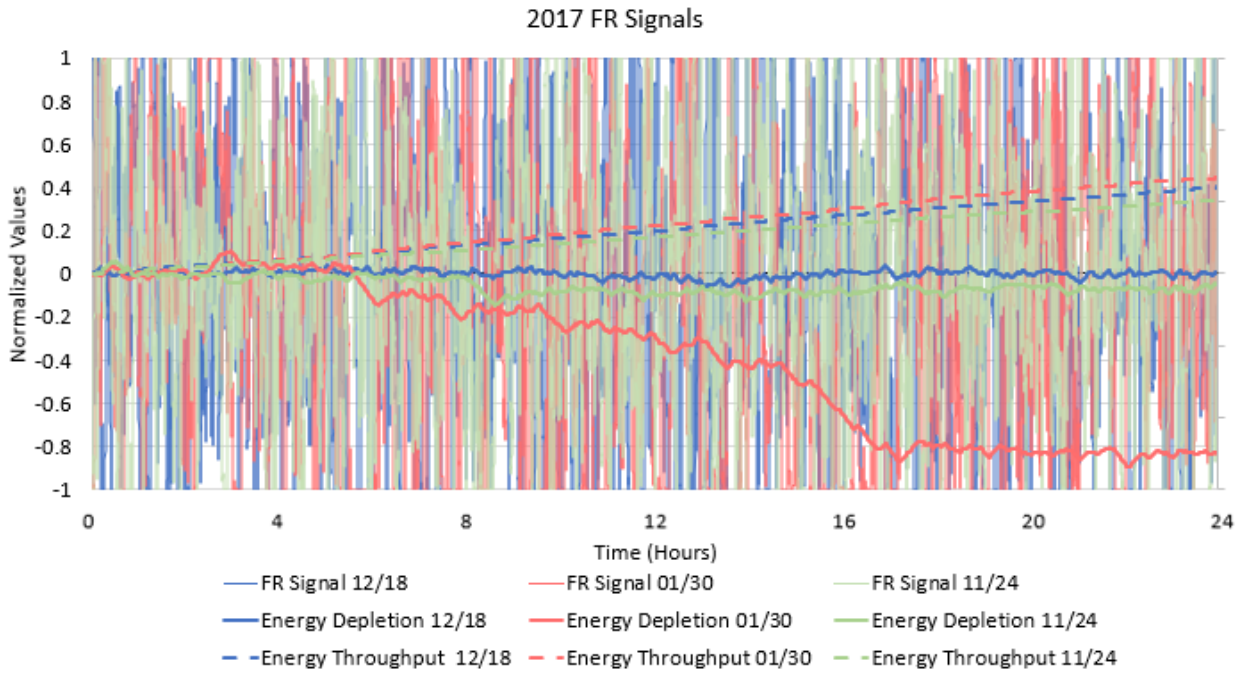

Figure 28 FR Day Variations (2017)

During FR the cell is initially discharge to 55% SOC. It is intended for this to represent 50% SOE, with a +5% buffer to account for battery inefficiency which will cause a walkdown in SOE and SOC during the

24-hour period. The FR signal is then implemented. The FR cycle is repeated 21 times, charging (topping up) to the upper voltage limit (90% SOC) every three cycles as explained below.

During experimental trials, it was found that the battery would decrease slightly in voltage from the previous cycle, even with the top-up that occurred at the end of each day. A small positive bias power was added to the signal to overcome the inefficiency of the cell in an attempt to mitigate this. However, it did not solve the problem. It was deduced that the voltage slip was not from degradation or inefficiency of the cell, rather from inaccuracies in coulomb counting of the power cycler over long periods. During a FR cycle with end of day top up the power cycler would charge and discharge the exact same amount of coulombs. It was found that the inaccuracies in the machine caused a slight biased favouring discharge. Over many cycles this bias inaccuracy accumulated and ultimately reduced the cell SOC and caused the tests to stop. To overcome this problem, it was decided to charge the battery to the upper voltage limit every three FR cycles. Charging to a set voltage will "reset" the cell as inaccuracies in coulomb counting are not present when charging to a cut-off voltage.

Table 9 shows the power multipliers associated with the FR signal of each cell and the corresponding total energy throughput, and maximum/minimum power demanded during a FR cycle.

Table 9 FR Signal Multipliers

	Day	FR Signal Multiplier	Charge Bias Multiplier	Total Energy Throughput (Wh)	Max Power (W)	Min Power (W)
LGC	December 18th 2017	76.2	1.02	1013.4	75.38	-76.22
A123	December 18th 2017	83.0	1.02	1109.3	83.00	-82.95

5.1.3 Reference Performance Test

The RPT should give as much information as possible on SOH of the battery without damaging the cell or degrading it excessively. The RPT should be short so it does not significantly interrupt the EA and FR cycling, and not stress the cells, but still characterize the thermodynamic and kinetic changes [74]. In this experiment the main goal of the RPT is to gain an accurate measurement of discharge capacity, energy efficiency, OCV and IR throughout cycle life. This information will serve as the basis of the degradation analysis.

CCCV (Table 10) and **CPCV** (Table 11) cycles are typical RPTs used by both industry and academia to characterize the SOH of batteries. CCCV is relevant to the battery manufacturing industry as it focuses on coulombic performance and gives information about the active material, while CPCV focuses on deliverable energy and is relevant in the electricity industry as it is a better indicator of the total energy a battery can provide.

Table 10 CCCV Cycling Protocol

Step	**Name**	**LGC**		**A123**	
		Value	**Stop Condition**	**Value**	**Stop Condition**
1	CC Discharge	16 A	2.5 V	20 A	2.5 V
2	CC Charge	16 A	4.2 V	20 A	3.6 V
3	CV Charge	4.2 V (Taper Current)	1 h or 0.01 A	3.6 V (Taper Current)	1 h or 0.01 A
4	Loop	Step 1	3 Times	Step 1	3 Times
5	End				

Table 11 CPCV Cycling Protocol

Step	Name	LGC		A123	
		Value	Stop Condition	Value	Stop Condition
1	CP Discharge	60 W	2.5 V	65 W	2.5 V
2	CP Charge	60 W	4.2 V	65 W	3.6 V
3	CV Charge	4.2 V (Taper Current)	1 h or 0.01 A	3.6 V (Taper Current)	1 h or 0.01 A
4	Loop	Step 1	3 Times	Step 1	3 Times
5	End				

The information from the 3rd cycle of the CCCV and CPCV tests will be extracted for the degradation analysis. The 3rd cycle was chosen because the 1st cycle is subject to rest time from the previous test and the 2nd cycle allow the cell to thermally acclimate. CCCV, CPCV are cycled at a 1 h rate because this is a typical rate for a grid service application and is a good rate for characterizing kinetics of the cells.

24 h CCCV is an RPT used to assess thermodynamic aspects of the cell by giving a pseudo OCV curve. Kinetic losses are minimized at such slow cycling rates thus effects of thermodynamic losses on the battery can be easily observed using differential voltage and differential capacity analysis.

5.1.4 Data Extraction

During each test data was collected at time intervals of 5 seconds. It was necessary to be able to extract the useful information reliably and efficiently. Computer code was written in MatLab and Visual Basic to extract the necessary information.

- The Neware power cycler stores test data in a MySQL database. Data was exported to CSV and files were named to give all necessary information about the file in the remarks section as shown in Figure 29.
- Files were then put into the appropriate folder by a macro code written by Chris White at the RESL using AutoHotkey [75].

- MatLab was used to take the raw data in each file and convert variables of interest into a Microsoft Excel Spreadsheet.
- Visual Basic code was written so that specific cells could be called upon and compared via a drop down of many different graphs.

The entire code can be found in Appendix D.

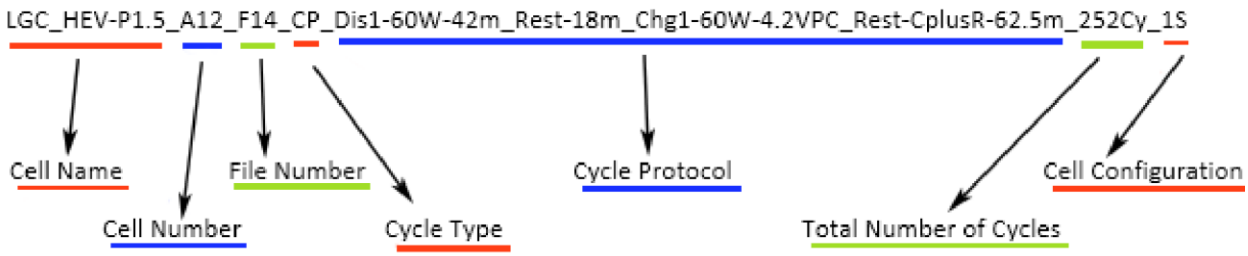

Figure 29 File Naming Protocol

5.2 Impedance

Many methods exist to quantify the amount of impedance in a circuit, such as calorimetry, electrical impedance spectroscopy, direct current resistance (DCR) and the AC method. The DCR method was used in this experiment.

Impedance increases as the LIB is near voltage extremities. At the start of discharge Li^+ is released from the NE and has space to intercalate into the PE wherever it pleases with little near neighbor interactions. As the cell discharges the PE starts to fill with Li^+ and the Li^+ is now restricted on where in the PE it can intercalate. Furthermore, the Li^+ are released from further back in the NE the more discharged the cell becomes, this increases resistance further [76]. This resistance is amplified with thicker electrodes and at

colder temperatures as Li^+ move and intercalate slower, electrolyte becomes more viscous and chemical reactions are slowed.

Larger capacity cells generally have a smaller resistance per Ah as they have less inert components per Ah. These inert components (i.e. current collectors, tabs, separators) add to the resistance. Therefore, all resistance results in section 6.4 are presented in ohms/Ah so the LGC and A123 can be fairly compared.

5.2.1 Direct Current Pulse Method

The DCR technique measures ohmic resistance in the cell by applying a current and measuring the voltage change. Following Ohm's law ($\Delta V/\Delta I = R$) the ratio between the change in voltage and the change in current gives the cell ohmic resistance.

Batteries are nonlinear and time dependent systems and the resistance measurement will vary greatly with pulse frequency and amplitude, this leads to highly varying methods throughout literature onto how to conduct pulsing for ohmic resistance determination.

Ohmic resistances were measured periodically throughout the life of each cell using DCR in two different ways, the pulse method and the voltage gap method.

The pulse method applies a nominal 2 h rated current for 300 seconds followed by a 30 second 1 hr rated pulse (double nominal). The rest/pulse was repeated until the cell reached the upper voltage limit. After a total of 9000 seconds (including rest) the sequence was repeated using negative currents until the cell reached the lower voltage limit. Voltages and currents were noted two seconds before the pulse began and two second before the pulse ended. This allowed enough time for the voltage to settle at the nominal and pulsing levels, thus decreasing chances of taking a data point while the current was still varying significantly. The value of 300 seconds was chosen as the rest period as this was experimentally

shown to be enough time for the voltage to settle and become constant. The cell temperature varied within 1°C of the same data point taken in the last test.

Useful results can be easily obtained using DCR methods but it does not allow for the decomposition of the different contributions which make up the total cell impedance and neglects reactance components within the cell. Therefore, DCR methods are not useful in measuring the total impedance of the cell in operation but can measure how the ohmic resistance of the cell is increasing throughout cycle life.

5.2.2 Voltage Gap Method

The voltage gap method uses a constant current charge and discharge cycle from 0-100% SOC. The voltage vs capacity is plotted for both the charge and discharge and the difference between the 2 curves at any given SOC is used as a proxy for changes in the cell resistance. Growth in the gap between charge and discharge voltage over the cycle life indicates higher resistance. And that growth can be identified as be an effect on charge or on discharge.

5.3 Half Cells

+Half cell testing was performed at the University of Hawaii under the supervision of Dr. Matthieu Dubarry and Dr. George Bauer.

This section will explain the procedure of making half cells, the method of forming and cycling the cells.

The purpose of half cell testing is to isolate each individual electrode and measure the voltage across the full SOC range when compared to Li metal which has a quasi-stable voltage across its SOC range. This differs from the full cell where the voltage is measured against the opposing electrode which also experiences a voltage change across its range of SOC. This makes it difficult to identify which electrode is changing voltage. Half cell testing allows the observation of how each specific electrode of the battery is

performing thus gaining an understanding of the workings of the entire system (full cell). The same results can be achieved by inserting a reference electrode into the full cell, but this has proven to be very difficult to do with pouch cells without damaging the cell considerably.

5.3.1 Dissection of Full Cells

Using a shunt or power cycler, each cell must be completely discharged (< 2 V) so it can be safely opened.

Once discharged the cells can be placed in an antechamber for 24 hours (Figure 30). Argon gas is pumped into the antechamber until no other gases remain. Argon is a noble gas and will not react with other elements so is used to avoid oxidation reactions. This is important as many electrolytes are unstable in air and Li metal will react with any moisture present in the air.

The pressure between the antechamber and glovebox is then equalized and the antechamber can be opened from inside glovebox and the cells can now be brought into the glove box.

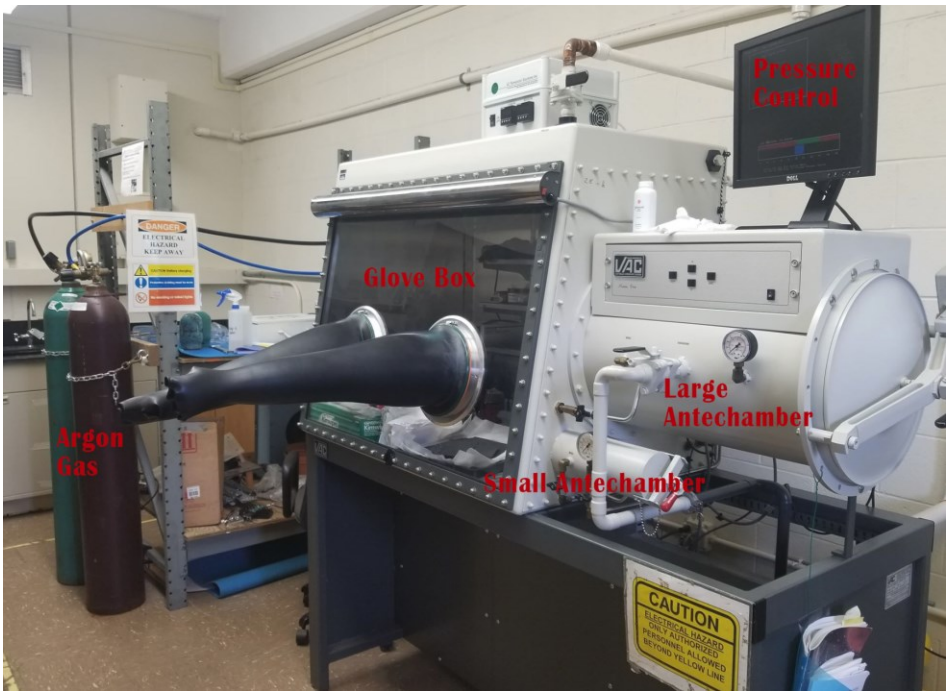

Figure 30 Glove Box

To reduce risk of short circuit, the cell can be opened using ceramic tools. A pipe cutter and electric Dremel tool can be used on cylindrical cells, while a ceramic knife is used for the pouch cells in this experiment.

Samples of each electrode are cut and placed in a beaker filled with dimethyl carbonate ($C_3H_6O_3$) (DMC). If ageing is visibly present (i.e. discolouration of the electrode) multiple samples of the electrodes should be taken to achieve statistical significance. The electrode sits in the DMC for at least 10 minutes. This will clean the electrode and remove any electrolyte of Lithium hexafluorophosphate ($LiPF_6$) (Li salt) which can react with air and can make Hydrogen fluoride (HF) which is dangerous to inhale.

The DMC can be re-used on other electrodes to conserve the solvent.

Once all electrode samples are collected they are removed from the glovebox and antechamber.

Place samples into vacuum oven to let any remaining DMC/electrolyte dry off but avoid leaving the sample in for prolonged times (> 24 h) to mitigate the risk of cracking the electrode.

5.3.2 Cleaning Previously Used PAT Cell and Electrodes

The PAT cell (Figure 31) is a re-usable LIB that allows the user to insert their own electrodes. This was chosen over making a classic coin cell as Dr. Dubarry and Dr. Bauer have experienced more reliable results using a PAT cell.

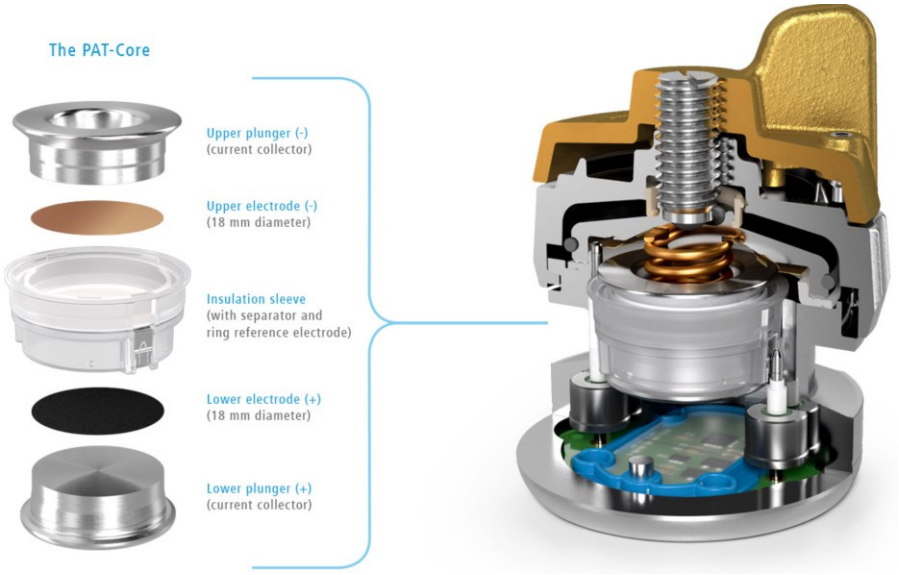

Figure 31 PAT Cell Exploded View [77]

Before making the PAT (half) cells, the previously used PAT cells should be cleaned by screwing apart the used PAT cells and placing used materials In EDC solvent, except for Li metal or any materials in direct contact with Li. These materials can be placed in a two-liter water jug. Typically, the Li is place in mineral oil to avoid reaction but since this was a minuscule amount (<1 g) it can be dissolved in water and put down the drain. Adding Li makes water more basic and if it does not exceed a pH of 12 it is safe to put down the drain. Li reacts when placed in water (Figure 32) so caution should be used.

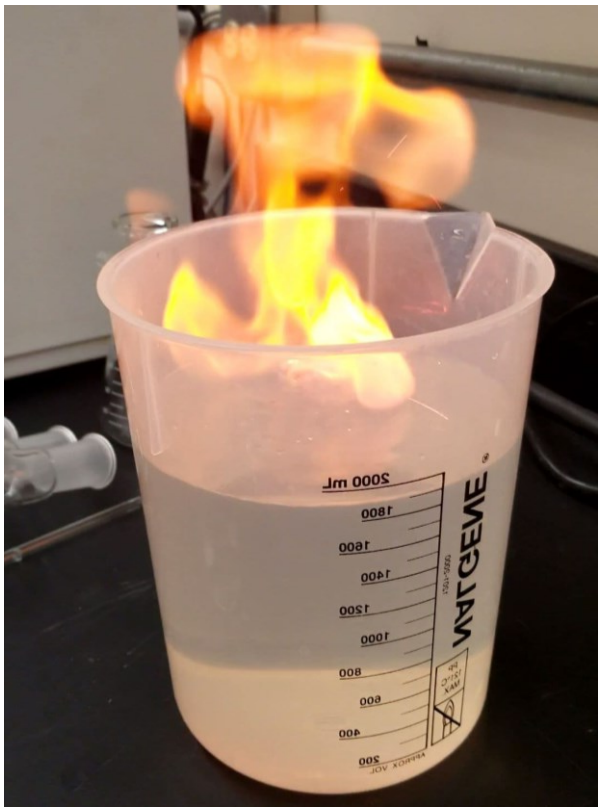

Figure 32 Lithium Reacting with Water

The PAT cells should be placed in the sonicator bath (Figure 33) with deionized water to removed inorganic salts, then ethanol to remove the de ionized water then acetone which cleans off any organic materials. PAT cells can then be placed in the vacuum chamber to dry.

Figure 33 DMC, Sonicator Bath, Assembled PAT Cell

Generally, when using commercial cells both sides of the electrode are coated with AM. To allow for a conductive pathway for the electrons to flow in the PAT cell one side of the AM needs to be removed to expose the current collector.

Dipping a cotton swab in N-Methyl-2-Pyrrolidone (NMP) solvent, and rubbing the AM in a circular motion, the swab will slowly take off the AM, repeating this process will reveal the current collector.

Once one side of the coating is cleaned, the specialized punch (EL-Cut) made for the PAT cells to punch out a circular piece of AM can be used.

The circular AM piece can now be placed in EDC solvent to remove any impurities. The electrode can now be placed in the vacuum chamber to dry.

The half cell is now ready for assembly.

5.3.3 Assembly of Half Cells

One glass fiber and two supereon separators can be cut using separators sheets and a specialized punch. This reduces the risk of shorting the cell. This is common when assembling cells in a lab as the assembly standards do not match that of industry. Having three separators increases the IR of the cell but also adds stability, if impendence becomes an issue the cell can be ran at a higher temperature.

The PE of the cell is constructed outside the glovebox, a disposable O-ring is used on the top and bottom of the PAT cell to keep it airtight. The half-assembled cells can be placed in the glovebox so Li metal can be added as the NE.

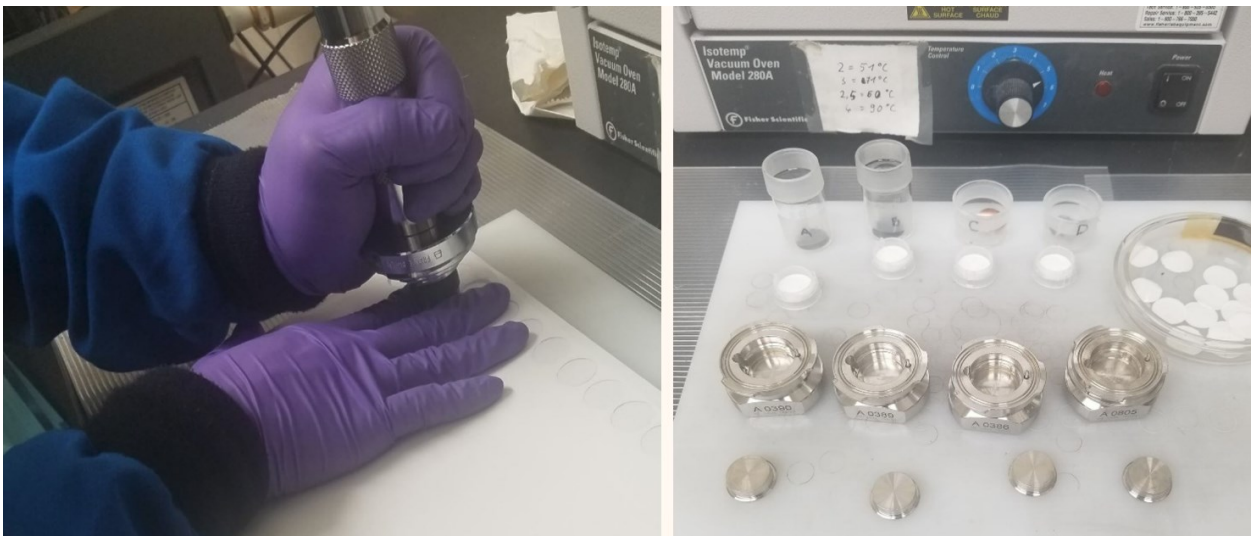

Figure 34 Separator Punch and Half Cells Ready for Glovebox

Inside the glovebox using a pipette, about 400 µL of electrolyte should be added on top of the separators until it becomes saturated and a small amount of electrolyte remains on top.

The exact electrolyte used in a commercial LIB is generally unknown so a common blend of 1:1 mixture by volume of DMC /EC were used as solvent and $LiFP_6$ as the salt. Not using the exact original electrolyte should not have a large impact on the results. Differences in electrolytes affects mostly the kinetics of

the cell and the cells are to be (dis)charged at very slow rates (24 h (dis)charge) where kinetics on the cells are virtually eliminated.

Li can be cut out of a punch and crimped to the top side of the PAT cell to insure good conductivity. The top of the PAT cell is then added to the bottom and screwed together.

The half cell is now ready for formation cycling.

5.3.4 Formation Testing and OCV Curves

The PAT cell is considered a new cell so formation testing must be done. This allows for the formation of the SEI layer and to ensure the cell was built correctly. Formation testing was cycled at a 2 h rate and is considered finish when consecutive cycles are within 1% capacity from each other.

It is undesirable to see the effects of current on the voltage curve so once formation testing is finished it is important to obtain an OCV vs. SOC relationship at the current SOH. However, it is recommended to wait four hours before taking a voltage reading after a current is applied so getting a proper OCV vs. SOC curve can take weeks of testing and it is not convenient to repeat the process at various SOHs. To expediate this lengthy process a very slow discharge is applied to the battery (24 h duration or longer) so effects of current are negligible over the time step being recorded. The result is a pseudo OCV curve measured from 0-100% SOC.

A 40 h, 20 h, 10 h, 5 h, 2 h, and 1 h (dis)charge were cycled consecutively to assess performance of the cell. Different rates give pseudo OCV curves and information about resistances and kinetics of the cell. Furthermore, running at various rates yields best results in the Alawa battery diagnostic tool [53] as less interpolating of the software is required.

Chapter 6 Experimental Results

The test cells LGC-EA, LGC-FR, A123-EA, and A123-FR were cycled over 1200 cycle equivalents of Δ100% SOC, constituting 8 months of testing. Throughout cycle life the discharge capacity, energy efficiency, thermal variation, internal resistance and dVdQ/dQdV were assessed periodically to provide information as to their evolution throughout cycling wear.

6.1 Coulombic and Energy Capacities

Table 12 Rated Capacity and Energy vs BOL measured values

Cell Group	Rated Coulombic Capacity (Ah)	Mean Coulombic Capacity at BOL (Ah)	BOL Percent of Rated Coulombic Capacity	Average Deviation of BOL Coulombic Capacity from Mean	Rated Energy Capacity (Wh)	Mean Energy Capacity at BOL (Wh)	BOL Percent of Rated Energy Capacity	Average Deviation of BOL Energy Capacity from Mean
LGC EA	16	16.1	100.7%	0.8%	60	60.1	100.1%	0.3%
LGC FR	16	16.2	101.6%	0.1%	60	60.2	100.3%	0.6%
A123 EA	20	20.7	103.7%	0.2%	65	65.5	100.8%	0.2%
A123 FR	20	20.8	103.8%	0.1%	65	65.7	101.0%	0.3%

At BOL, the average coulombic capacity and energy capacity within each cell group is higher than the rated value given by the manufacturer. The BOL percent of rated coulombic capacity is higher than that of the BOL percent of rated energy capacity within each cell group. At BOL all cell groups are within 1% of the mean for averaged coulombic capacity and energy capacity. This indicates a high degree of cell consistency at the start of the testing.

The coulombic and energy capacity of cells, as measured by the RPT, are plotted throughout their cycling lifetime in Figure 35 and Figure 36 respectively. It is important to note that the capacity of each cell was measured using the uniform RPT schedule, but that between RPT point, the cycling is in

accordance with the unique services of EA and FR, which are very different. However, they have equal discharge energy throughput during those periods.

Figure 37 is based on the same data but is normalized by initial values for ease of comparison and identification of differences in trends. The cells are normalized to the initial measured energy and capacity of each cells and plotted against Δ100% SOC equivalent cycles of the initial measured value. All charts are color coded by cell type (LGC=blue, A123=yellow), and the line type indicates the service type (EA=solid, FR=dashed). Range bars are added on each data point taken by RPT, and gives the minimum cell and maximum cell, with the colored series marker being the mean cell.

It is apparent in all cases that coulombic capacity and energy are reducing due to degradation throughout cycling. Both the coulombic capacity and the energy capacity degrade with similar trends. This indicates that degradation is associated with substantial coulombic capacity changes rather than insubstantial operating voltage changes. Examination of the results reveals the following, and each will be discussed in detail in the following paragraphs:

- Between BOL and the first subsequent reference test, there is a substantial reduction in coulombic capacity and energy capacity. This is followed by a reduce rate of degradation that appears either linear or with a slight asymptotic decay.
- Cells cycling in EA service degrade approximately twice as fast as those operating in FR, for the given same discharge throughput.
- LGC (NMC+LMO) cells and A123 (LFP) cells have similar degradation patterns for partial state of charge FR service. In contrast, the LGC cells degrade substantially faster than A123 cells in deep discharge EA service.
- Minimum and maximum cells deviations from median cell grow with quantity of degradation.

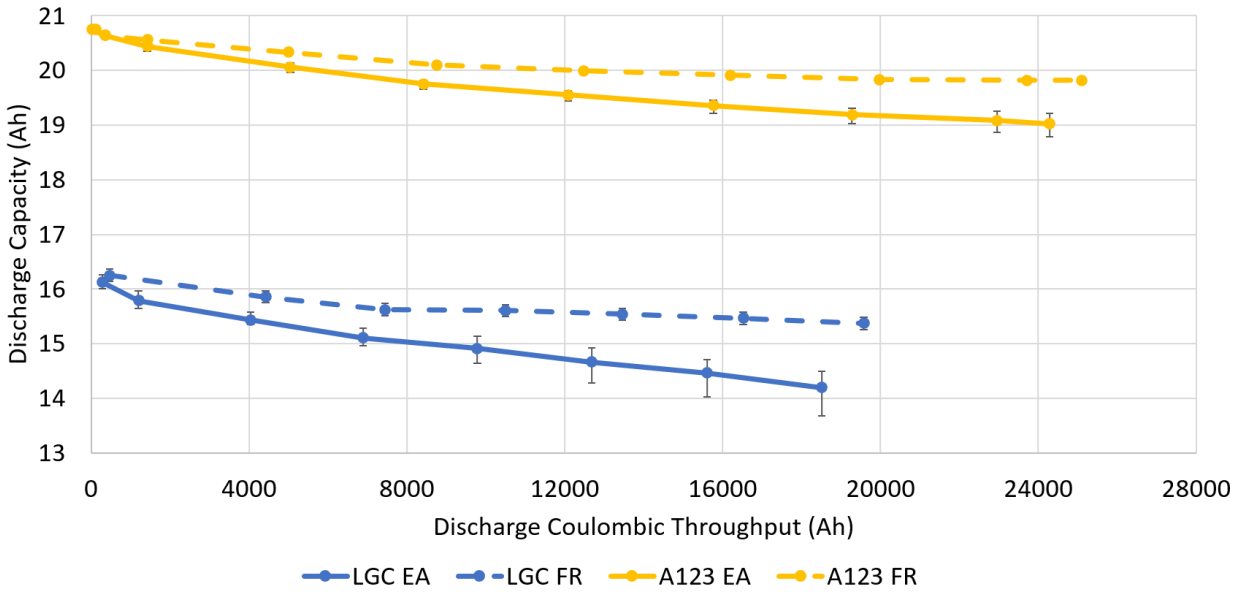

Figure 35 Discharge Capacity vs Capacity Throughput

Figure 35 show coulombic capacity curves begin with a steep decline of capacity and energy followed by relatively linear decline with a slight asymptotic decay for the remainder of the experiment. The LGC cells have degraded in coulombic capacity 37.5% and 20% faster than the A123 cells under EA and FR, respectively. Cells cycling in EA degraded 120% and 100% faster than cells cycling in FR for LGC and A123, respectively.

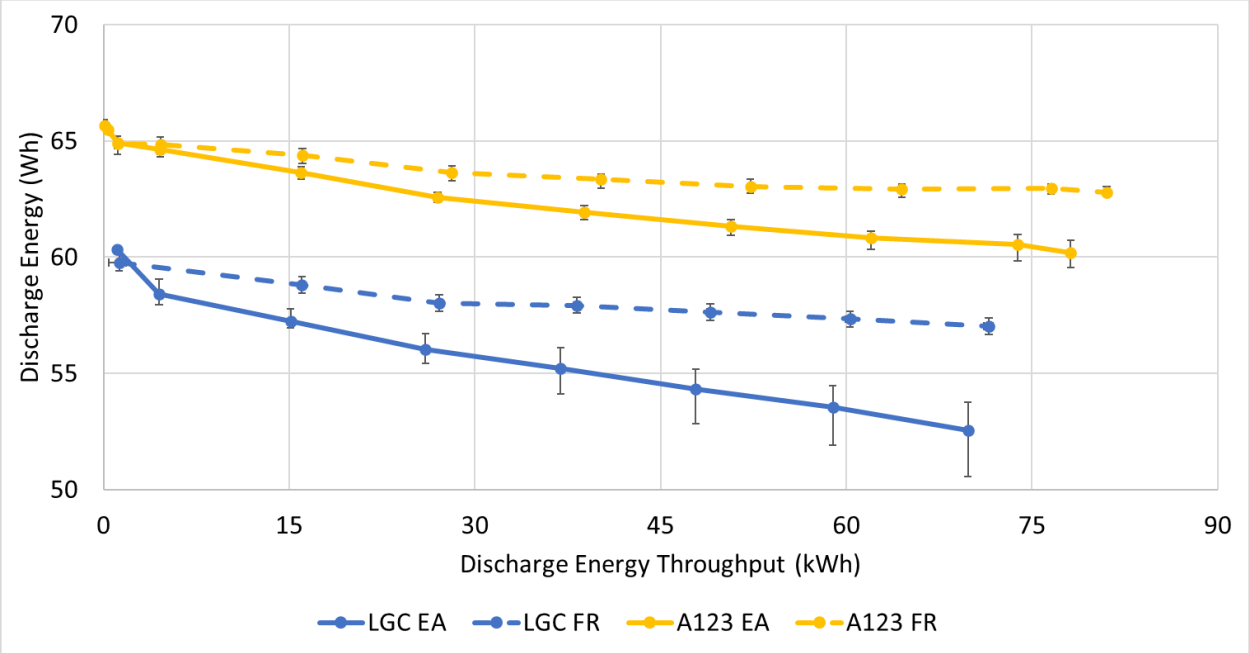

Figure 36 Discharge Energy vs Energy Throughput

Figure 36 show the energy capacity trends are similar to the coulombic capacity trends of Figure 35. There are a few distinct differences. When measuring on the merit of discharge energy (Figure 36) the cells become closer on both the vertical and horizontal axis (i.e. there performance becomes increasingly similar) compared to Figure 35. LCG (NMC +LMO) has a higher working voltage than A123 (LFP), giving it more energy per capacity and thus the LGC cell can deliver closer to the same amount of energy as the A123 cell compared to capacity.

The LGC cells have degraded in energy 59% and 12% faster than the A123 cells under EA and FR, respectively. Cells cycling in EA degraded 180% and 84% faster than cells cycling in FR for LGC and A123, respectively.

Figure 37 shows normalized values where the variations in degradation rates become immediately apparent. A cycle life of 1000 cycles equivalent is a nominal metric used by industry. The degradation rate in each service for each cell type over the first 1000 cycles is extracted from Figure 37 and given in Table 13.

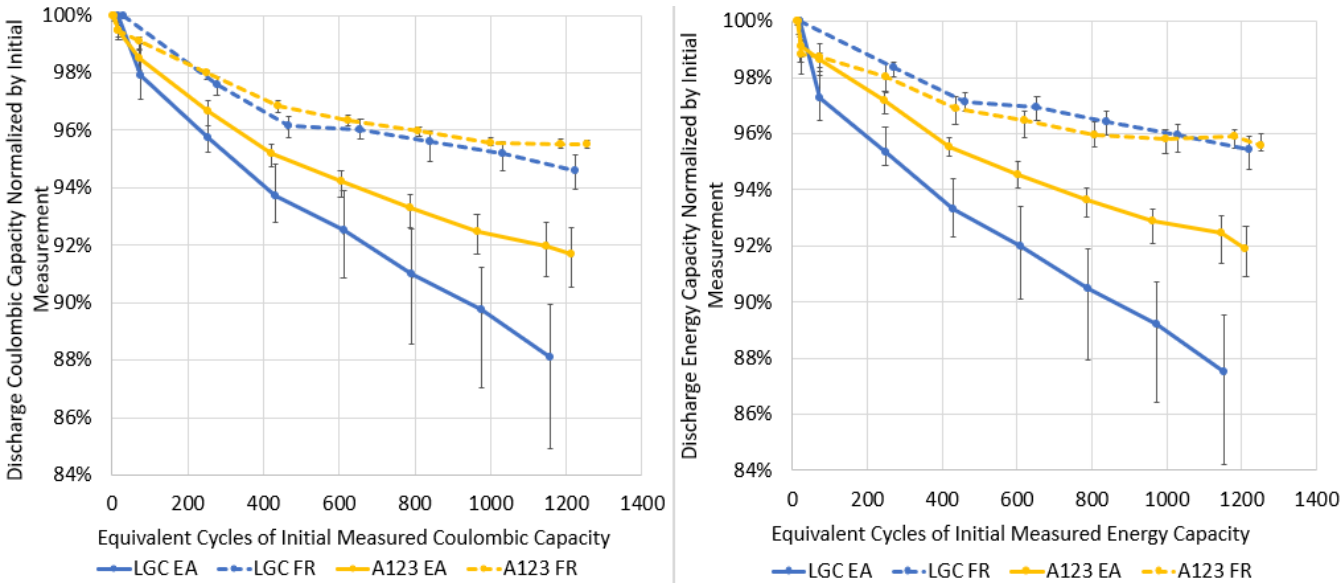

Figure 37 Normalized Discharge Coulombic Capacity and Discharge Energy Capacity vs. Cycles

Table 13 Degradation Results

Cell Group	Mean Coulombic Capacity Decrease per 1000 Rated Cycles	Mean Energy Capacity Decrease per 1000 Rated Cycles
LGC EA	11%	13%
LGC FR	5%	5%
A123 EA	8%	8%
A123 FR	4%	4%

Coulombic capacity and energy capacity loss begin with a steep decline followed by a relatively linear decline for the remainder of the experiment. When a brand-new cell is cycled, capacity is lost from LLI to form the SEI over the exposed active material at the electrolyte-electrode interface. This SEI layer formation is necessary to block electrons in order to prevent further electrolyte decomposition and degradation within the cell. This drastic decrease in capacity at BOL suggests that the manufacturers did not fully form the SEI.

All cells begin with a steep decline of capacity/energy followed by relatively linear decline. From a similar preliminary experiment shown in Appendix E, the LGC cells were cycled under EA and FR for 2200 cycles and degradation remained linear, thus linearity is not expected to change until at least 2200 cycles of beyond for the LGC cells. Near linear degradation is useful for an energy storage system operator because battery augmentation can be easily planned and installed at intervals. A battery augmentation strategy refers to a plan to maintain the performance of a battery storage system over its life, typically by adding more batteries to the base system. For example, an LFP energy storage system may need to retain 80% of its original energy to function properly and is designed to do two EA Δ100% SOC equivalent rated cycles daily. From Table 13 a conservative 9% linear degradation per 1000 cycles is estimated. This means every 3 years, 20% of the original capacity of this system will need to be added to keep it maintained ($\frac{365\ days}{year} \times \frac{2\ cycles}{day} \times 3\ years \times \frac{9\ \%\ Capacity\ Loss}{1000\ cycles} = 20\ \%\ Capacity\ Loss$) . Alternatively, an annual replacement of 6.6% capacity will keep the system operating properly.

For both LGC and A123, the cells cycling in FR have degraded in capacity at about half the rate as the cells cycling in EA. This indicates deep discharge energy services, such as EA, peak shaving, time shifting, or self consumption of PV, will degrade batteries faster than partial SOC services like power services such as FR or frequency response. This also suggests that the addition of FR service operating on top of EA via stacked services should not dramatically increase the degradation rate compare to a battery operating in EA alone.

A123 cells have retained more energy compared to LGC when cycling under the same service. This suggests LFP will be better for long life services where total lifecycle energy throughput is important such as time shifting and FR. In other use cases such as infrequent demand charge mitigation or backup power supply (UPS) this advantage may be less valuable.

A battery management systems (BMS) is a hardware/software unit that measures voltage, current, and temperature to ascertain the state of charge, operating envelope, and degradation of a battery. The BMS manages the (dis)charging output current and provide critical safeguards by protecting cells from over (dis)charging. Range bars (thin black lines attached to each data point in Figure 35-Figure 37), show deviations within cell groups. At BOL, the range bars are on average at 0.3 % deviation from the median discharge coulombic capacity and energy capacity within cell groups. As the cells degrade the deviation within cell groups become larger. At cycle 1200 the average deviation from median within cell groups is 1.1 %. The cell groups that have degraded more show a larger deviation. The most degraded cell group (LGC EA) shows the largest (2.5 %) deviation from median by cycle 1200. Therefore, the general trend can be discerned that deviations within cell groups grow proportionally with degradation. Discharge capacity deviations from median are 480% greater for EA (higher degradation service) than FR (lower degradation service). This could become an issue as the BMS must be designed to handle the significant cell deviations at EOL, not the small deviations at BOL. The capacity of a conventional series configuration battery pack is limited to that of the lowest capacity cell. The BMS balances all cells to the lowest performing cell and shunts any extra energy from the less degraded cells. If balancing is excessive, it can impact the overall energy efficiency of the system.

6.2 Energy Efficiencies

Energy Efficiency is defined as the ratio of discharge energy (Wh) to charge energy on a cycle. The round-trip energy efficiency of each cell while conducting reference cycles at the prescribed intervals is shown in Figure 38. Note that these energy efficiencies were obtained during the RPT and are not the energy efficiency of a cell doing EA or FR service.

It is apparent that energy efficiency capability of a cell conducting a RPT is not impacted by the normal service duty (i.e. FR is same as EA when reference tested). This is shown by the energy efficiency of EA

and FR cells being very similar at each RPT. Efficiency curves also remain essentially flat over cycle life. LGC cells (NMC+LMO) have a higher energy efficiency than A123 cells (LFP). This is in part because of cell design, but is also impacted by the lower operating voltage of the LFP cell.

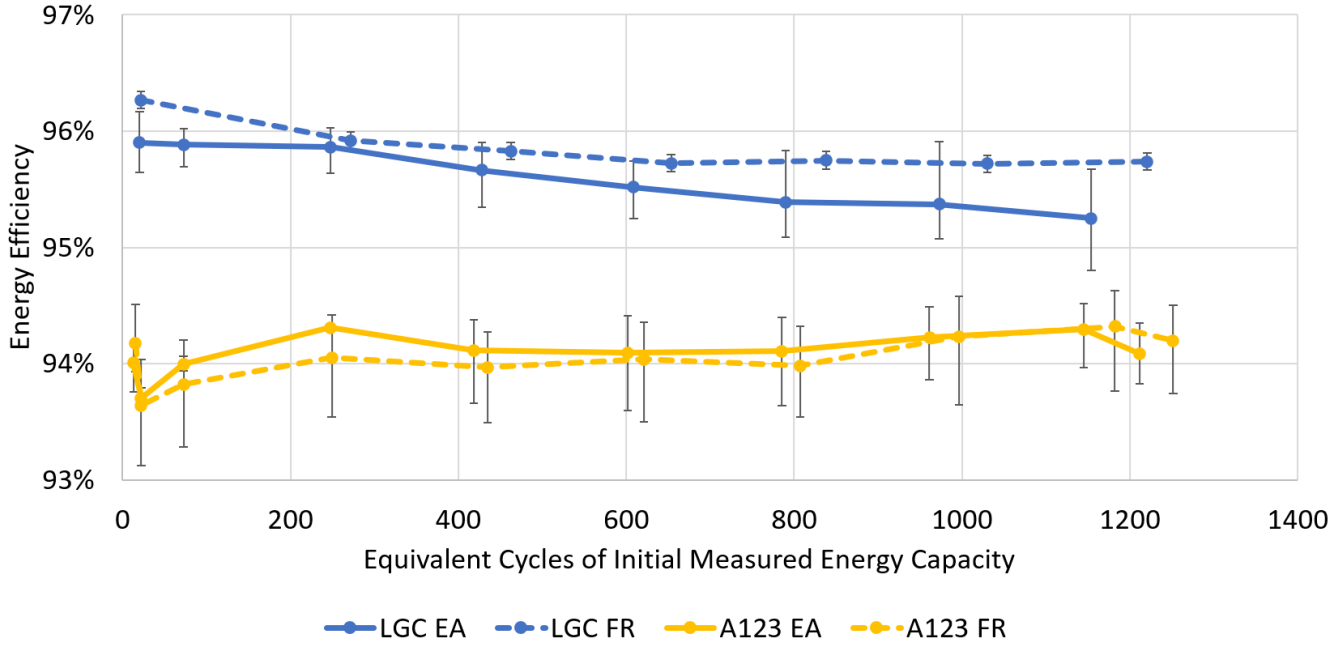

Figure 38 Energy Efficiency at 1 h rate vs Cycles

After 1250 cycles, energy efficiency remains ± 1% from BOL and appears not to be impacted by the degradation of the cells. The LGC (NMC+LMO) has a 1.5% higher energy efficiency than the A123 (LFP) cells. From a similar experiment (see Appendix E) the LGC cells were cycled under EA and FR for 2200 cycles and energy efficiency remained constant, thus energy efficiency is not expected to change until at least 2200 cycles for the LGC cells in this experiment.

Energy efficiency is dependent on the resistance in a cell as there are losses incurred due to this resistance. In a completely ohmic system the resistance remains constant, however LIBs have non-linear ionic and reactance components and can cause the total resistance to grow with increasing currents

[78]. Therefore, the same cell (dis)charged at a 5 h rate compared to a 1 h rate will have a lower resistance and a higher energy efficiency. NMC+LMO has a higher working voltage than LFP and needs less current to deliver the same amount of energy over a given time step. As the energy efficiency is compared during a 1 h rate CP test this increases the energy efficiency of NMC+LMO compared to LFP. Many other factors impact energy efficiency such as cell size, cell design, lattice structure, and cycling temperature. Thus, energy efficiency can not be based off resistance measurements alone.

The results from Figure 38 are useful for cell pack designers. Degradation in energy efficiency means an increase in losses and consequently an increase in cell temperature when cycling. Therefore, the NMC+LMO cells will need less cooling than the LFP when a pack is being designed. Furthermore, for both the NMC+LMO and LFP, the temperature profile of the cells when cycling should not change significantly over cycle life. This means the thermal system designed at BOL will work for EOL.

As the NMC+LMO has a better energy efficiency there will be less energy costs when cycling NMC+ LMO vs LFP. This suggests NMC+LMO will be better in services where retaining and using as much of the energy stored as possible is important such as off-grid storage and solar storage or in infrequent cycling services such as black start.

6.3 Thermal Impacts of Test Infrastructure

The thermal chamber was laid out as 3 shelves (one above the other), each with 4 cells per shelf. It had previously been noted that temperature affects capacity and degradation. Temperature sensors were placed between each shelf and the locations shown in Figure 20.

The temperatures on each shelf were recorded during the experiment. Figure 24 showed temperature values throughout a 34-hour period during a RPT.

The temperature varied inside the three-tiered test chamber by a maximum of 5 °C. The bottom shelf experienced the lowest average temperature, and the top shelf the highest average temperature throughout the entire experiment. Because the thermal conditioning system (fans and plenum) was laid out with cross flow, it is expected that cells located toward the right-hand side of the cabinet would be warmer and cells towards the left will be the coolest. There was not enough available data to make conclusions on temperature trends in the front to back directions.

The experiment was set up in such a way that each set of 3 cells (LGC-EA, LGC-FR, A123-EA, and A123-FR) would have a cell on the bottom shelf (low temperature), middle shelf (medium temperature) and top shelf (high temperature). Figure 39 shows the normalized deviation for each cell group (LGC-EA, LGC-FR, A123-EA, A123-FR) from their mean value for both discharge energy capacity and energy efficiency at cycle 1000. The figure attempts to investigate if the thermal variation inside the test chamber was substantial enough to cause a bias within the experiment.

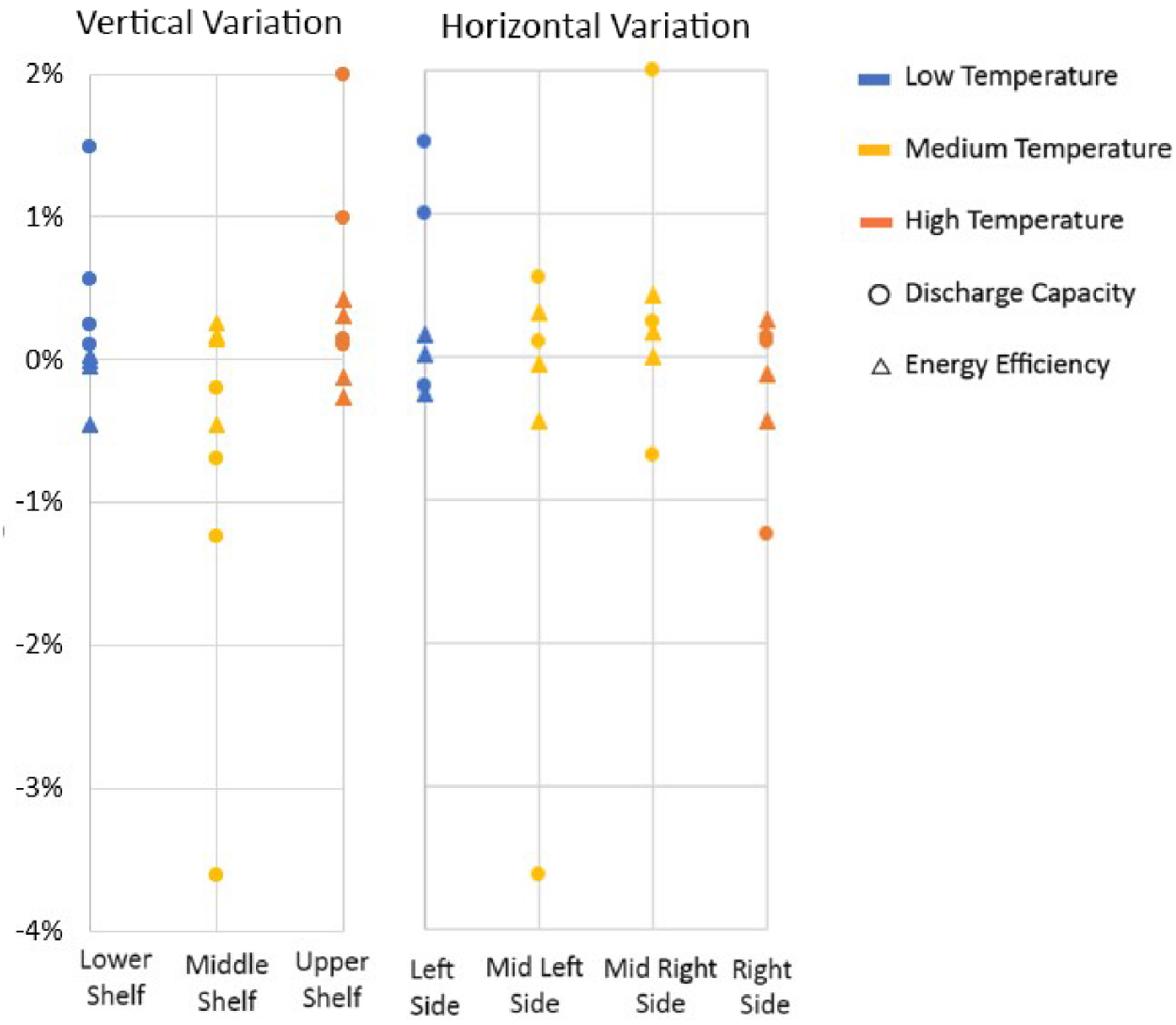

Figure 39 Normalized Discharge Capacity and Energy Efficiency Deviation from Mean Cycle 1000

From Figure 39 the middle shelf cells tend to have the lowest discharge capacity while the upper shelf cells have the highest. No other meaningful trends can be discerned. Figure 39 verifies that the temperature variation inside the test chamber plays little to no role in the degradation of the cells. Differences in cell performance within groups likely comes from variation in cells during the manufacturing process and it can be concluded that the measures taken to mitigate thermal variation throughout testing have worked.

6.4 Resistances

6.4.1 DC Current Pulse Results

The resistances of the cells were quantified using the DC current pulse method and are presented in Figure 40.

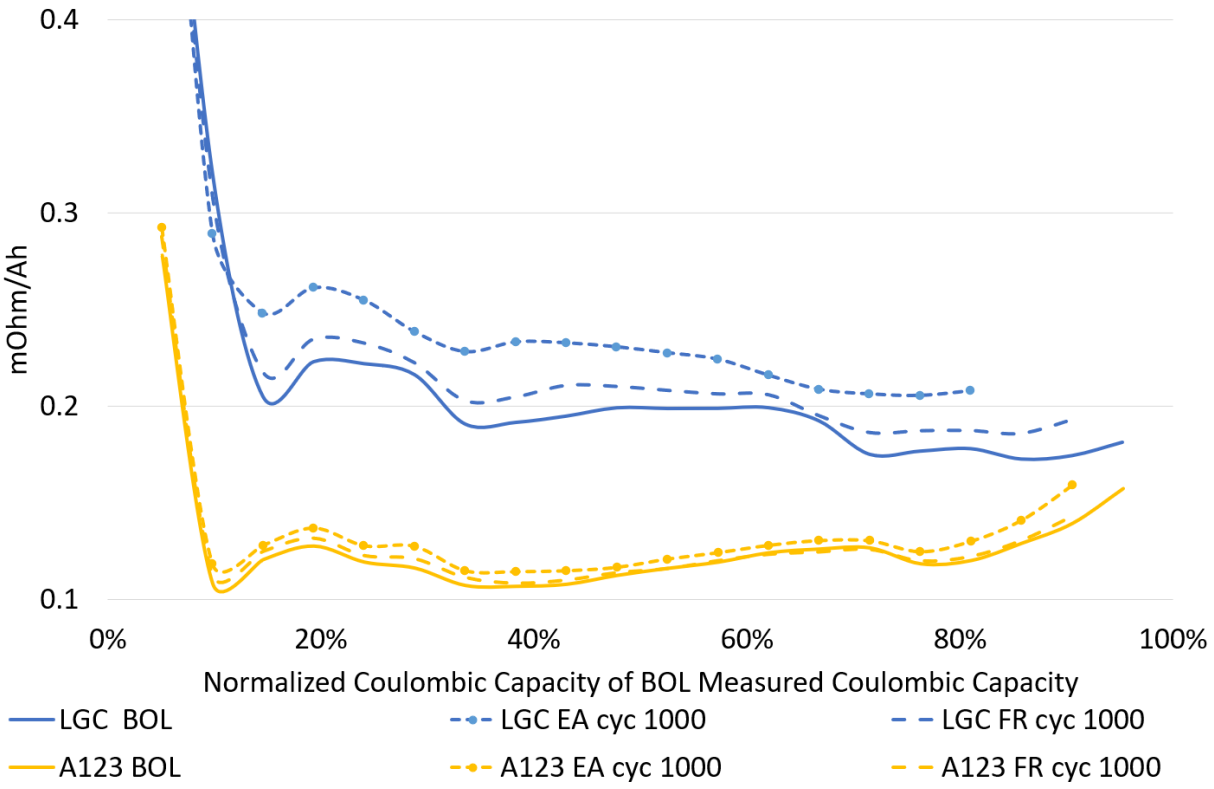

Figure 40 Resistance DC Pulse Method Charge Cycle

Figure 40 shows that IR increases substantially as the cell approaches the fully discharged state. As the cells degraded the IR increases, as shown for cells at 1000 cycle equivalents. The number of data points in Figure 40 reduces as the cell ages because there is less capacity. Throughout the charge and discharge of the DC pulse test, the recorded resistance value during each of the pulses was averaged. This averaged value is used to quantify the operating resistance of the cell and is shown in Table 14.

Table 14 DC Pulse Test Average Resistance (mOhms/Ah)

	BOL	Cycle 1000	Growth
LGC EA Cycle 1000	0.222	0.287	29%
LGC FR Cycle 1000	0.222	0.263	18%
A123 EA Cycle 1000	0.139	0.143	3%
A123 FR Cycle 1000	0.139	0.144	4%

Resistance values for a given cell type are uniform at BOL. The resistance of the A123 cell (LFP) is substantially lower than the LGC cell (NMC+LMO), even though differences in capacity have been taken into account (mOhms/Ah). As per the SEM results given in Section 4.2, the lower measured resistance in the A123 cells is largely due to the finer grain size on the anodic and cathodic material of the cells. This allows for more surface reactions and higher power capabilities. After 1000 cycles differences in resistance emerge, with the LGC increasing substantially for EA service, more so than FR service, while the A123 experience only a minor increase and is uniform for both services.

The LGC cells resistance has grown substantially more over the 1000 cycles than the A123. This is likely contributed to the LGC cell having an upper cut-off voltage of 4.2 V. Above 4.0 V electrolyte decomposition is favorable. This decomposition adds to the SEI layer and causes an increase in resistance. Furthermore, the LGC EA cell is held above 4.0 V more frequently than the FR cell and thus exacerbates SEI growth and therefore shows the largest growth in resistance.

6.4.2 Voltage Gap Analysis

As a proxy for energy efficiency and internal resistance, the voltage gap between discharge and charge is compared for each cell in Figure 41 (LGC) and Figure 42 (A123) at different points in cycle life.

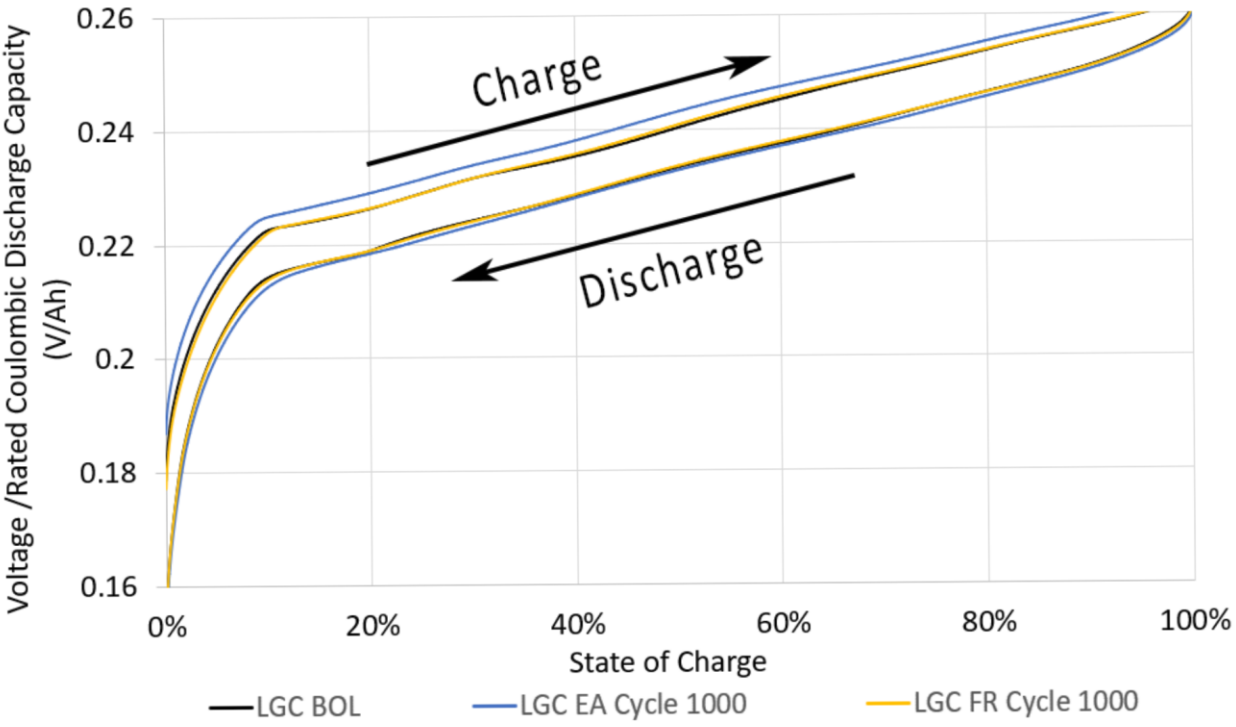

Figure 41 LGC Resistance Voltage Gap Method

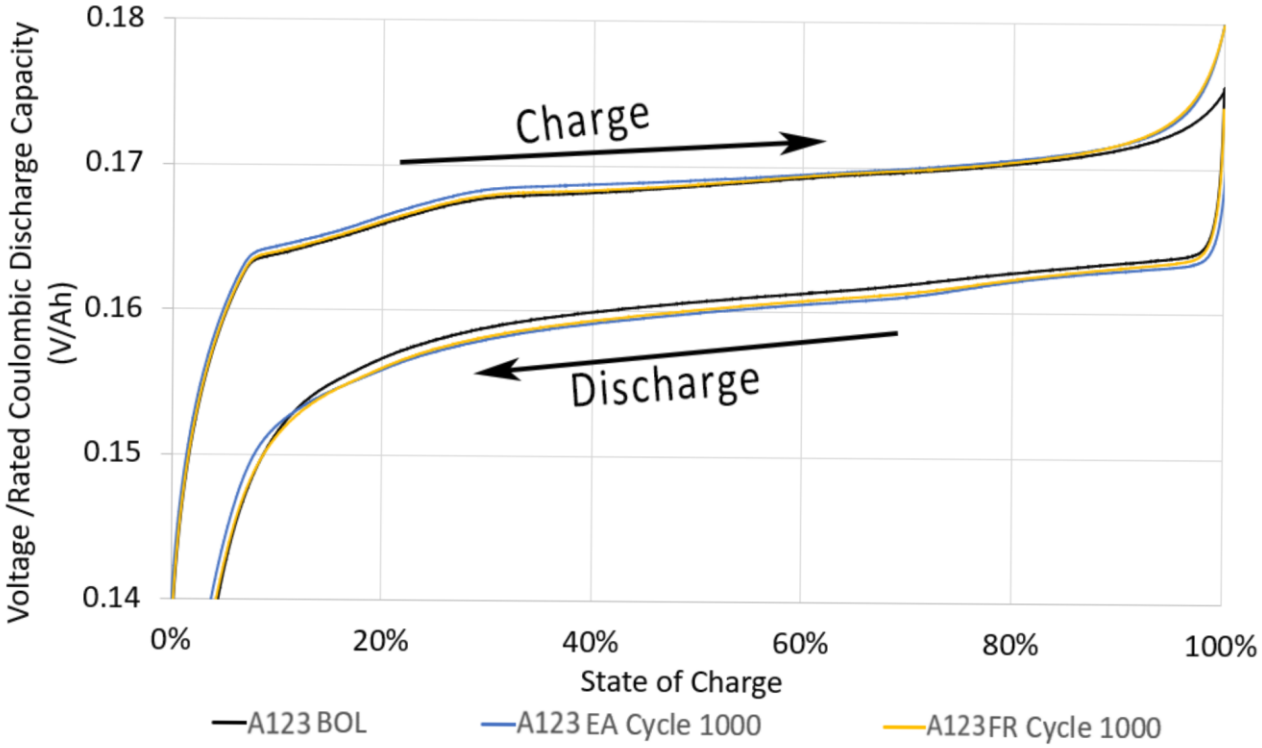

Figure 42 A123 Resistance Voltage Gap Method

Figure 41 shows the magnitude of the gap between the LGC charge and discharge remains close to constant from 10% SOC to 90% SOC and the gap narrows at voltage extremities (0%-10% and 90%-100% SOC). The voltage drops linearly with SOC. The FR curves remain largely unchanged from BOL to 1000 cycles-equivalent with only a 1.8 % increase. However, a 34.1 % increase in the voltage gap is observed in the EA cell, notably on the charge rather than the discharge. This asymmetry from the electrodes when intercalating and releasing Li^+ (i.e. charging and discharging) which causes a larger voltage response from the PE or NE depending on the direction of the flow of Li^+ and electrons. However, no method was set in place to determine where this increase in voltage response was coming from within the cell.

Figure 42 shows the LFP cells, the magnitude of the gap between charge and discharge remains close to constant from 10% SOC to 90% SOC and the gap narrows at voltage extremities for the A123 cells. the

A123 trends are very different than the LGC trends. First, the voltage slope is much flatter, and exhibits two stages, the second occurring below 30% SOC. Second, the discharge voltage is shown to be less at 1000 cycle-equivalents compared to BOL, whereas the charge voltage at 1000 cycle equivalents is similar to BOL. As expected, the EA service causes slightly more voltage gap than the FR.

6.5 Half Cell Results

Figure 43 and Figure 44 show half-cell voltage curves and dVdQ curves obtained from the PAT cell cycling that was completed while at the University of Hawaii. The charge cycle of the LGC and A123 cells are shown respectively at 40 h rate. The voltage is taken relative to Li metal. The full cell voltage is the difference between the PE and NE. The full cell capacity of the battery is the overlapping SOC range between the PE and NE. The PE voltage cut off is generally specified for each individual chemistry while the NE lower voltage cut off generally happens before the NE reaches 0 V. When the working potential of NE is very close to that of metallic Li, Li plating is kinetically favorable.

The ratio of change in voltage to change in capacity (dV/dQ) was plotted against normalized capacity. The loading ratio ($Capacity_{NE}$ /$Capacity_{PE}$) was matched from the full cell 24 h CCCV test data and was found to be approximately 1.3 for both the LGC and A123.

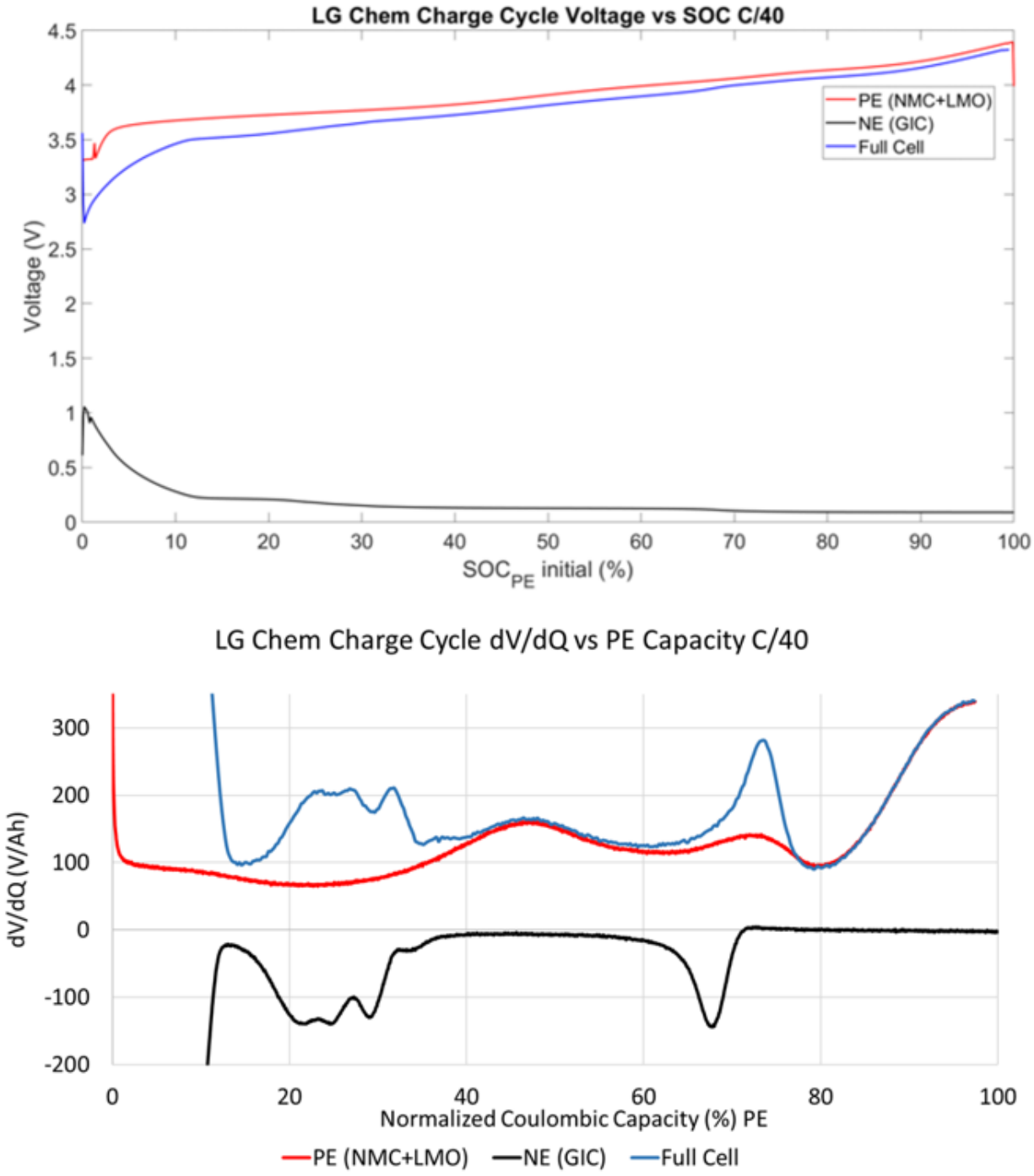

Figure 43 LGC Half Cell and dVdQ Curve

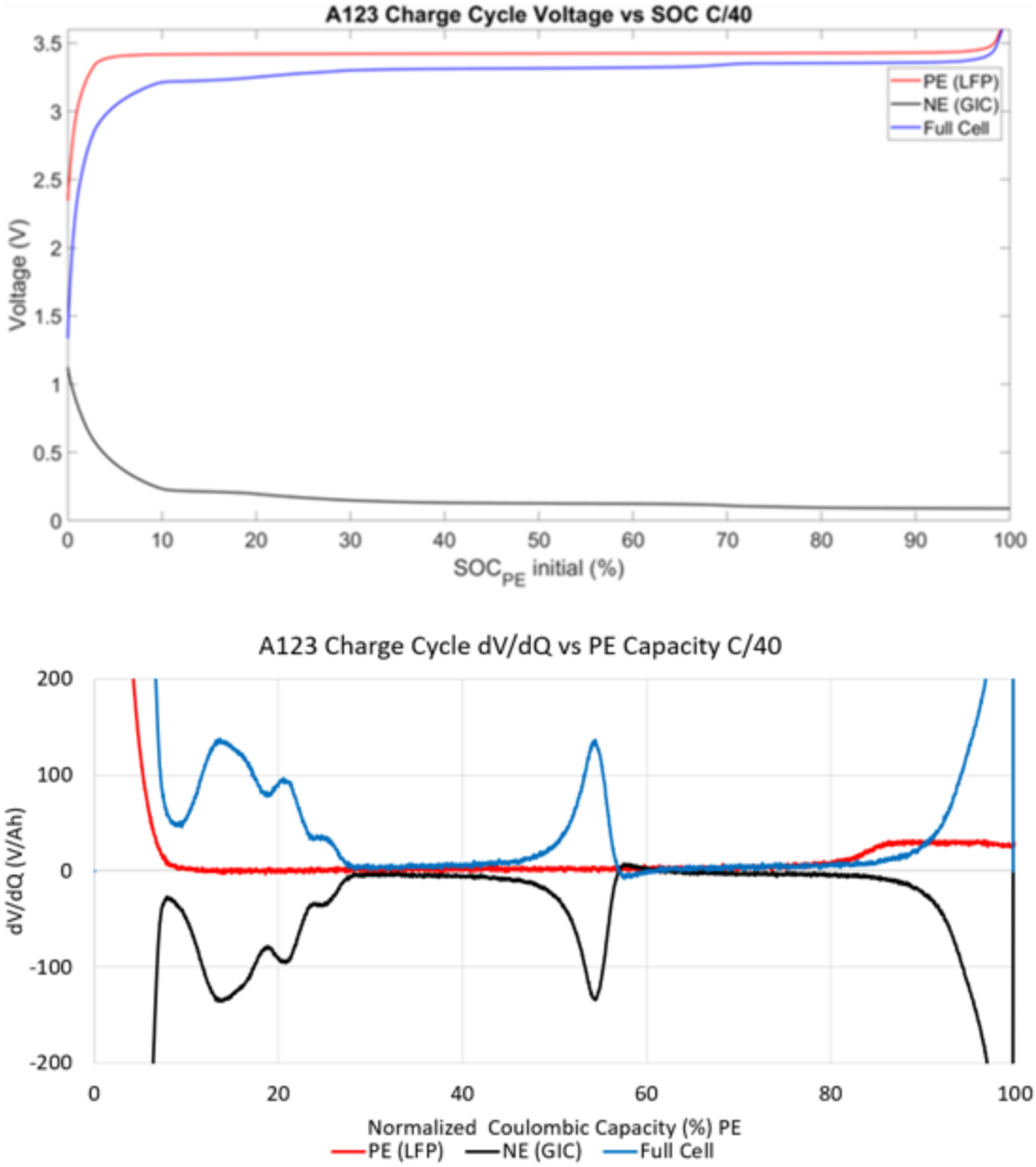

Figure 44 A123 Half Cell and dVdQ Curve

6.6 Differential Voltage / Incremental Capacity Analysis

The dVdQ and dQdV curves change as the cell ages and each change corresponds to a certain phenomenon. Each peak corresponds to either a PAM feature or NAM feature. Analysis of the peak identifies which AM is affected and allows for a more accurate analysis. Throughout this section each change in the curve as the LGC and A123 cells degrade will be analyzed. For each chemistry, the values

of the six cell BOL capacity were averaged and plotted and the values for each set of three EA and FR cells were averaged and plotted making comparison after 1000 cycles-equivalent.

6.6.1 NMC+LMO Differential Voltage / Incremental Capacity Analysis

The LGC cell with a NMC+LMO blended PE and a GIC NE is analyzed using dVdQ/dQdV. From the half cell results PE and NE features can be separated but PE features of NMC and LMO cannot be differentiated with the methods used in this experiment.

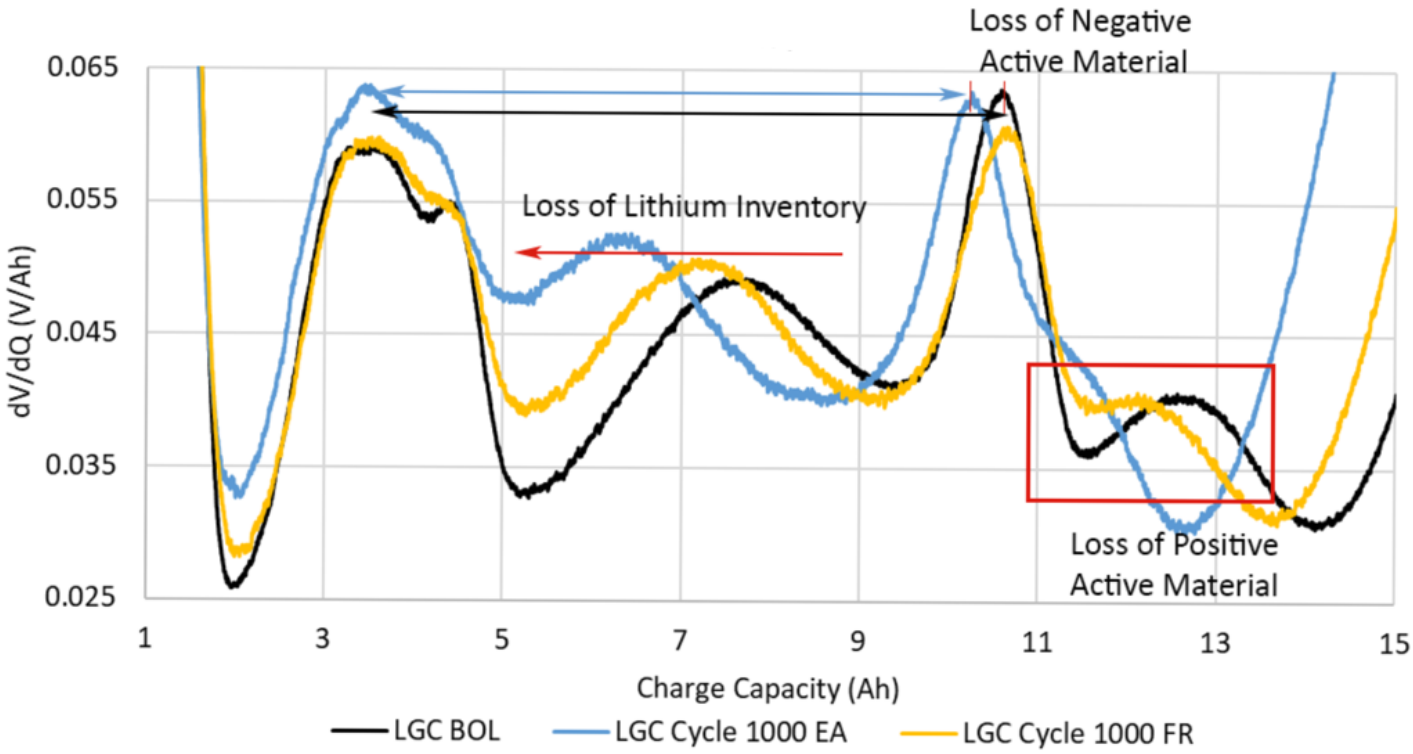

Figure 45 NMC + LMO dVdQ Charge

As the cell charges (left to right on graph) Li^+ leaves the PAM and intercalates into the NAM. PAM features (located at approximately 8 Ah & 12.5 Ah at BOL) shift to the left approximately by 1.3 Ah and 0.6 Ah for EA and FR respectively. This indicates that LLI has occurred as the PAM becomes de-lithiated quicker (i.e. the Li^+/PAM ratio has decreased).

At approximately 12.5 Ah, the peak of the PAM feature almost completely disappear as the cell degrades in EA, this could indicate structural changes to the material (i.e. loss of PAM). This hypothesis is strengthened as the capacity loss is not proportional to the amount of shifting from the PAM features. From Figure 37 the LGC EA cell has degraded to 0.87 from BOL capacity, however from LLI in the dVdQ curve we have $\frac{(16-1.3)}{16} = 0.91$ so there is approximately 4% capacity loss coming from somewhere else. It is likely that LAMPE is happening as this would decrease the overall cell capacity. Although it can only be speculated if it is the NMC or LMO (or both) being loss, Mn dissolution is increased when charging cells above 4.0 V [28]. Having an upper cut off voltage of 4.2 V during EA testing, Mn dissolution is likely the reason from the LAMPE.

LAMNE is proportional to the ratio of the distance between the NE peaks at BOL and cycle 1000 (denoted by black and blue arrows in Figure 45). LAMNE appears to only occur slightly in the EA cell (1.5%) as spacing between negative features on the FR cell have remain unchanged from BOL. Since the loading ratio of this cell (Q_{NE}/Q_{PE}) was estimated to be 1.3 this would have minimum effect on degradation of the cell as it is the “extra” NAM capacity being loss.

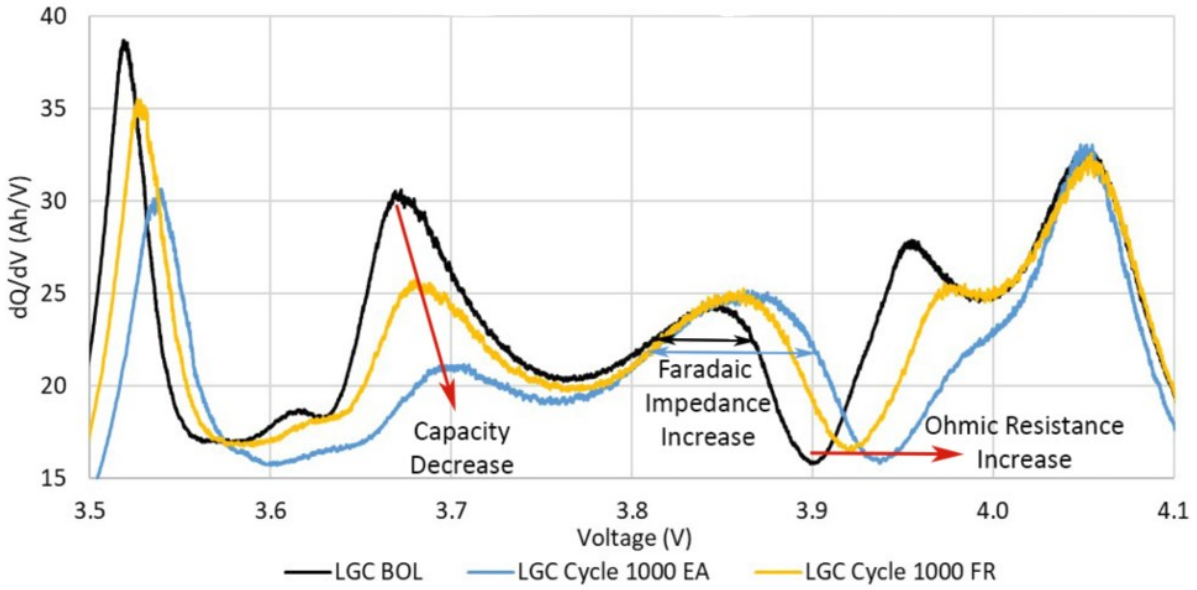

Figure 46 NMC + LMO dQdV Charge

In dQdV curves, the area under the curve represents capacity. Peaks diminishing indicate a loss of capacity and is most significant for the PAM feature of the EA cell at 3.65 V. This reaffirms the hypothesis of a LAMPE. Most features move towards a higher potential during charge indicating an increase in ohmic resistance, while broadening of all peaks indicate a rise an interfacial impedance.

Remarks

The degradation of the cell appears to come primarily from LLI and secondarily from LAMPE. LLI can happen in two ways, SEI growth and Li plating and It is likely that both are happening to some extent. SEI growth and Li plating both increase faradaic impedance, but since the LGC cells are charge to 4.2 V where electrolyte decomposition is favourable, it is likely that most of the LLI is coming from growth of the SEI.

The LAMPE likely comes form Mn dissolution which causes growth in the SEI, thus exacerbating this phenomenon in the EA cell.

This all agrees with theory as the EA cell is more frequently at higher voltages compared to FR where electrolyte decomposition, Li plating and Mn dissolution are more favorable.

The easiest operational solution to mitigate the degradation of the LGC cell would be by reducing the upper cut off voltage from 4.2 V to 4.0 V. This would slow SEI growth, Li plating and Mn dissolution, however this would not be practical for many energy services as It would reduce the amount of energy the cell can deliver by about 30%. A manufacturing solution would be to use electrolyte additives that make the electrolyte stable above 4.0 V, this would decrease electrolyte decomposition thus reducing LLI and SEI growth.

6.6.2 A123 Differential Voltage / Incremental Capacity Analysis

dVdQ/dQdV results are limited for the A123 cell as the LFP half cell dVdQ curve is essentially flat (see section 6.5), thus making it difficult to analyze the features from this material. In Figure 47 and Figure 48 virtually all features are representative of the NE.

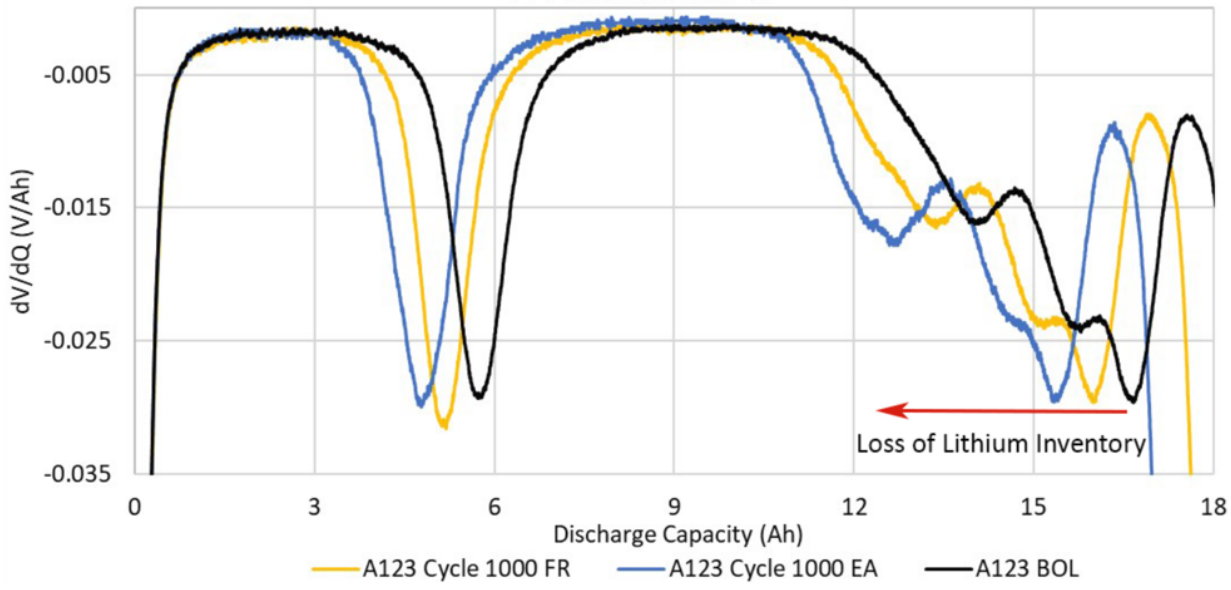

Figure 47 LFP dVdQ Discharge

The peaks in the dVdQ represent phase transitions in the intercalation of Li^+ (Lithium Ordering). In Figure 47 all NE peaks have shifted to a lower discharged capacity which indicates that this phase transition is happening sooner in the discharge. When discharging Li^+ move from the NAM to the PAM (left to right

on graph). The first peak at about 5 Ah represents the shift from LiC_6 to LiC_{12}, since this happening sooner it can be said that there has been an LLI. The amount of shifting of the dVdQ curve is proportional to the amount of capacity loss. There was likely minimal to no LAMNE as spacing between the NAM features of each curve remain virtually unchanged from BOL to cycle 1000.

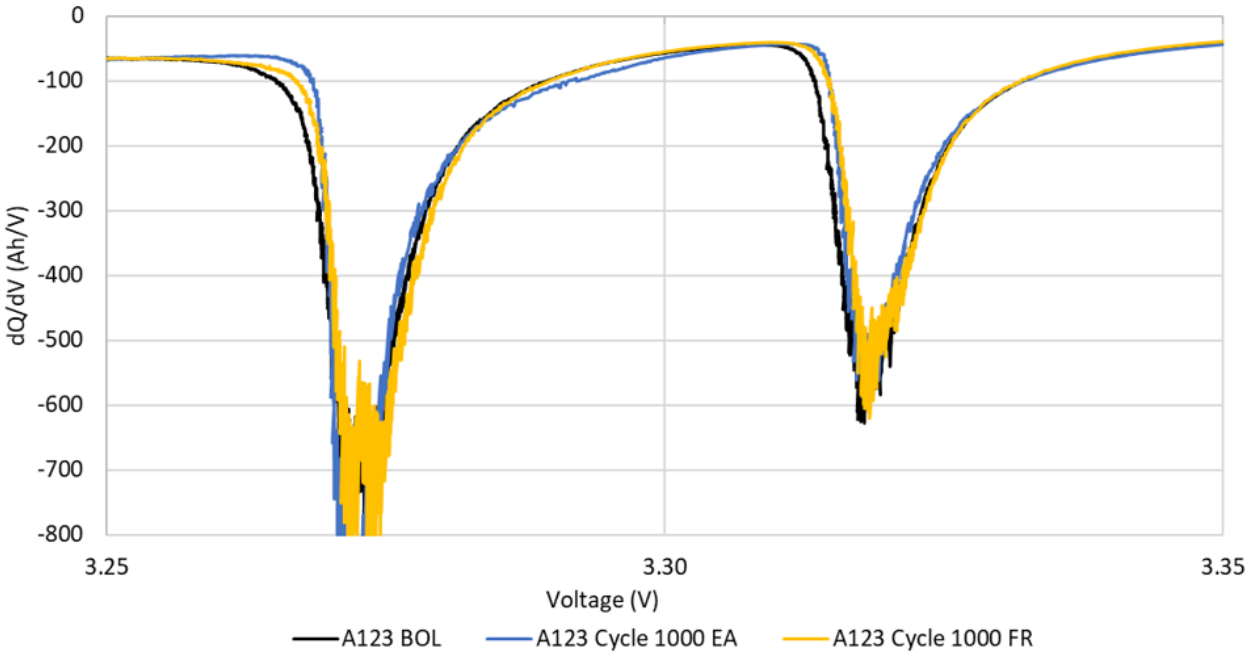

Figure 48 LFP dQdV Discharge

In the dQdV, the curves remain relatively unchanged. Peaks have diminished and shifted slightly, indicating a small capacity fade (from LLI) and only a small increase in overall impedance within the cell.

Remarks

LLI was the main source of degradation within the A123 cells and was more pronounced in the EA cell. Without performing a post-mortem SEM, it is difficult to conclude if the LLI has come from electrolyte decomposition (SEI growth) or Li plating.

Electrolyte decomposition is a function of overall cell potential (i.e. PE vs NE) while Li plating is a function of NE potential vs the potential of Li metal (Li plating occurs when Voltage NE ≈ Voltage Li Metal). Since the working voltage of LFP is kept below 3.7 V it is likely that the electrolyte was stable across the entire potential. A growth in SEI causes a much larger rise an interfacial impedance compared to Li plating and minimum impedance growth is observed on both the dVdQ and dQdV graph. From these analysis, the capacity loss from LLI is likely largely due to Li plating on the NE. Lowering the applied current near upper voltage limits will reduce kinetic Li plating on the NE.

Chapter 7 Conclusions and Recommendations

7.1 Summary

Production of EVs has increased dramatically over the past decade. The use of end-of-life EV batteries presents an opportunity to repurpose them for grid services. Similar sized NMC+LMO and LFP EV LIB pouch cells were cycled in two grid services, energy arbitrage and frequency regulation for 1200 complete-cycle-equivalents. EA is a deep discharge service used to smooth the electricity grids energy consumption while FR is a partial state of charge service used to maintain the electricity grid at a desired frequency. The coulombic capacity, energy capacity, and energy efficiency degradation characteristics from the results of the experiment were analyzed using various scientific methods. The conclusions from this experiment inform the selection of LIB for grid services based on power, capacity, energy efficiency and expected life. This will allow a battery choice that will optimize capacity retention, energy efficiency, and thermal implications.

7.2 Conclusions

EA causes LIBs to degrade in coulombic and energy capacity at twice the rate of FR. This suggests that energy services, such as EA, peak shaving, time shifting, or self consumption of PV, will degrade batteries faster than partial SOC services like power services such as FR. This also suggests that the addition of FR service on-top of EA (stacked services) should not dramatically increase degradation rate of battery operating in EA alone.

Both chemistries degraded linearly and LFP (A123) degraded less than NMC+LMO (LGC). This suggests LFP will be better for long life services where total lifecycle energy throughput is important such as peak shaving, time shifting and FR. Inter-cell degradation variance appears to be a function of total

degradation level, and this requires that a battery management system be designed to handle end-of-life deviations between cells, rather than that at beginning-of-life.

Throughout cycling, energy efficiency stayed essentially constant for both chemistries and grid services. This indicates that the thermals system designed for BOL should work at EOL, for this same reason the cost of operation will remain constant throughout cycle life. NMC+LMO had a higher energy efficiency. NMC+LMO will be better when energy efficiency is important such as off-grid storage and solar storage or infrequent cycling services such as black start.

Accelerated degradation in the LGC cells (especially LGC EA) can be contributed to a LLI to a growing SEI layer. Reducing the cut off voltage of the LGC cells from 4.2 V to 4.0 V will improve the degradation rate but reduce the specific energy of these batteries. A123 cells have degraded mainly from LLI due to Li Plating. Lowering the applied current near upper voltage limits will reduce this phenomenon.

7.3 Recommendations

Based on preliminary tests given in Appendix E using very similar methods, non-linearities in degradation or changes in energy efficiencies, are not expected until at least 2200 cycles or more. No work has been done past 2200 cycles, so it is recommended to keep all cells in long-term cycling until past this point to see if the degradation trend becomes non-linear, or if the energy efficiency becomes non-constant.

A more precise method called electrochemical impedance spectroscopy (EIS) can be performed to get the impedance at BOL and throughout cycling. Doing EIS every 1500 cycles until EOL will allow for decomposition of the different impedances in the cell. This will gain information about how the various electrode-electrolyte interfaces are changing throughout cycle life, thus allowing for a more accurate and better quantification of impedance.

X-ray photoelectron spectroscopy should be performed at BOL and EOL. XPS is a non-destructive tool for elemental analysis and can determine binding energies. XPS identifies compounds analytically and directly giving near surface region chemical composition of a sample (elements in the top few nm of the sample) including the oxidation state. It is therefore useful when concerned about the processes that occur in the top few atom layers of materials such as the growth of SEI layer, which was identified as a source of the degradation of both the LGC and A123 cells.

References

[1] K. Z. M.R. Allen, "Framing and Context. In: Global Warming of 1.5°C. An IPCC Special Report on the impacts of global warming of 1.5°C above pre-industrial levels," IPCC, 2018.

[2] Canadian Wind Energy Association , "Installed Capacity," 2019. [Online]. Available: https://canwea.ca/wind-energy/installed-capacity/. [Accessed 5 03 2020].

[3] M. Gorman, "No more room for wind power, energy minister says in wake of export proposal," *CBC News,* 1 Aug 2017.

[4] A. Rathi, "China added as much battery-storage capacity in 2018 as all previous years combined," *Quartz,* 27 09 2018.

[5] O. S. Abhijith Yenduri, "Lithium Ion Battery Market Overview," Allied Market Research, 2018.

[6] I. E.-Z. J. D.-I. M. A. E.Martinez-Laserna, "Battery second life: Hype, hope or reality? A critical review of the state of the art," *Renewable and Sustainable Energy Reviews,* vol. 93, pp. Pages 701-718, 2018.

[7] P. H. B. W. R. P. B. Ramadass, "Capacity fade of Sony 18650 cells cycled at elevated temperatures: Part I. Cycling performance," *Journal of Power sources,* vol. 112, no. 2, pp. 606-613, 2002.

[8] J. Warner, "The Handbook of Lithium-Ion Battery pack design," Midland,MI,USA, Elsevier, 2015, pp. 169-173, 177-200.

[9] A. D. R. Wachal, "Stationery Energy Storage System Using Repurposed Electric Vehicle Batteries," Manitoba HVDC Research Centre, Winnipeg, 2017.

[10] R. T. M. Swierczynski, "The Second Life Ageing of the NMC/C Electric Vehicle retired Li-ion Batteries in Stationary Applications," Electrochemical Society , Brussels, 2016.

[11] R. C. Kyle Bassett, "Energy arbitrage and market opportunities for energy storage facilities in Ontario," *Journal of Energy Storage ,* vol. 20, pp. 478-484, 2018.

[12] J. H. Eto, "Frequency Control Requirements for Reliable Interconnection Frequency Response," 02 2018. [Online]. Available: https://www.ferc.gov/industries/electric/indus-act/reliability/frequency-control-requirements/report.pdf. [Accessed 12 07 2018].

[13] H. Z. O. M. Vivek Pandurangan, "Frequency regulation services: A comparative study of select North American and European reserve markets," in *North American Power Symposium* , 2012.

[14] Y. L. C. L. C. L. Qian Zhang, "Grid frequency regulation strategy considering individual driving demand of electric vehicle," *Electric Power System Research,* vol. 163, pp. 38-48, 2018.

[15] L. G. S. Jason Leadbetter, "Selection of battery technology to support grid-integrated renewable electricity," *Journal of Power Sources,* 2012.

[16] J. A. R. M. Rahul Walawalkar, "Economics of electric energy storage for energy arbitrage and regulation in New York," Carnegie Mellon Electricity , New York City, 2004.

[17] V. Arangarajan, "Self-discharge level of ESS.," [Online]. Available: https://www.researchgate.net/figure/Self-discharge-level-of-ESS_fig2_292682073.

[18] UNITED STATES OF AMERICA FEDERAL ENERGY REGULATORY COMMISSION, "Essential Reliability Services and the Evolving Bulk-Power System—Primary Frequency Response," 2018.

[19] A. S.-M. a. H. Mohsenian-Rad, "Strategic Selection of Capacity and Mileage Bids in California ISO Performance-based Regulation Market," Department of Electrical and Computer Engineering, University of California, Riverside, CA, USA, 2016.

[20] S. Blumsack, "Introduction to Electricity Markets," [Online]. Available: https://www.e-education.psu.edu/ebf483/node/705. [Accessed 18 04 2020].

[21] S. Santhanagopalan, "Types of Batteries," in *Design and Analysis of Large Lithium-Ion Battery Systems*, Artech House , 2015.

[22] D. C. Alasdair J Crawford, "Lifecycle comparison of selected Li-ion battery chemistries under grid and electric vehicle duty cycle combinations," *Journal of Power Sources ,* 2018.

[23] A. D. Matthieu Dubarry, "Battery durability and reliability under electric utility grid operations: Representative usage aging and calendar aging," *Journal of Energy Storage ,* vol. 18, pp. 185-195, 2018.

[24] B. Univeristy, "BU-205: Types of Lithium-ion," [Online]. Available: https://batteryuniversity.com/learn/article/types_of_lithium_ion. [Accessed 07 11 2018].

[25] H. G. Christian M. Julien, "Comparative Issues of Cathode Materials for Li-Ion Batteries," *inorganics,* pp. 132-154, 2014.

[26] InvestmentMine, "Cobalt Prices and Cobalt Price Charts," [Online]. Available: http://www.infomine.com/investment/metal-prices/cobalt/. [Accessed 28 03 2020].

[27] M. C. Z. I. J. L. J. Hongyang Li, "Is Cobalt Needed in Ni-Rich Positive Electrode Materials," *Journal of The Electrochemical Society,* vol. 166 , no. 4, pp. A429-A439 , 2019.

[28] Y. J. S. a. S. M. O. Dong H. Jang, "Dissolution of Spinel Oxides and Capacity Losses in 4 V Li / Li x Mn2 O 4 Cells," *Journal of The Electrochemical Society,* 1995.

[29] P. N. M. W. C. V. K.-C. M. ,. J. B. J. Vetter, "Surface–electrolyte interactions and formation of surface," *Journal of Power Sources,* 2005.

[30] W. L. Y. W. X. Z. Y. M. H. L. Jing Yan, "Enhanced High-Temperature Cycling Stability of LiMn2O4 by Coating LiNi0.5Mn1.5O4," *JMMCE,* vol. 2, 2014.

[31] A. A. G. L. ,. S. S. M. Saulnier, "Manganese dissolution in lithium-ion positive electrode materials," Université du Québec à Montréal, Montreal, CA.

[32] N/A, "Global and China Lithium Iron Phosphate (LiFePO4) and Battery Industry Report, 2016-2020," Reportlinker, New York, NY, December 2016.

[33] F. W. J. T. L. a. G. Y. Naoki Nitta, "Li-ion battery materials: present and future," vol. 18, no. 5, 2015.

[34] W. X. a. Y. G. J.R. Dahn, "The Falling Cards Model for the Structure of Microporous Carbons," *Carbon ,* vol. 35, pp. 825-831, 1997.

[35] J. F. Victor Agubra, "Lithium Ion Battery Anode Aging Mechanisms," *Journal of Materials,* vol. 6, no. 4, pp. 1310-1325, 2013.

[36] M. T. Liang Hong, "Two-dimensional lithium diffusion behavior and probable hybrid phase transformation kinetics in olivine lithium iron phosphate," *Nature Communications,* vol. 114, no. 8.

[37] X. L. Qiang Li, "Kinetically Determined Phase Transition from Stage II (LiC12) to Stage I (LiC6) in a Graphite Anode for Li-Ion Batteries," *ACS Publications ,* vol. 9, pp. 5567-5573, 2018.

[38] J. Dahn, "Staging in intercalation systems," Halifax, 2015.

[39] T. A. Taketoshi Minato, "Surface and interface sciences of Li-ion batteries-Research progress in electrode–electrolyte interface," *Progress in Surface Science,* vol. 92, pp. 240-280, 2017.

[40] K. Xu, "Nonaqueous Liquid Electrolytes for Lithium-Based Rechargeable Batteries," *Chemical Reviews,* vol. 104, p. 4303–4418 , 2004.

[41] New York Post, "Samsung finally figures out why its phones kept exploding," New York Post, 20 01 2017. [Online]. Available: https://nypost.com/2017/01/20/samsung-finally-figures-out-why-its-phones-kept-exploding/. [Accessed 03 01 2018].

[42] AZO Materials, "Analysis of Separator and Binder Materials in Lithium Ion Batteries," 17 October 2017. [Online]. Available: https://www.azom.com/article.aspx?ArticleID=14583. [Accessed 02 12 2019].

[43] V. F. lvovich, impedance Spectroscopy: Applications to Electrochemical and Dielectric Phenomena, Hoboken: Wiley, 2012.

[44] Gamry, "Electrolyte Resistance," [Online]. Available: https://www.gamry.com/Framework%20Help/HTML5%20-%20Tripane%20-

%20Audience%20A/Content/EIS/Theory/Physical%20Electrochemistry%20and%20Circuit%20Elements/Electrolyte%20Resistance.htm. [Accessed 19 12 2019].

[45] Cadex Electronics, "BU-902: How to Measure Internal Resistance," [Online]. Available: https://batteryuniversity.com/learn/article/how_to_measure_internal_resistance. [Accessed 19 12 2019].

[46] J. H. Z. P. M. O. Xing Zhoua, "Impedance characterization of lithium-ion batteries aging under hightemperature," *Contents lists available at ScienceDirect,* vol. 426, pp. 216-222, 2019.

[47] J. Clark, "Rate Constants and the Arrhenius Equation," 2002. [Online]. Available: https://www.chemguide.co.uk/physical/basicrates/arrhenius.html. [Accessed 07 01 2020].

[48] S. H. M. B. Peyman Taheri, "Investigating electrical contact resistance losses in lithium-ion battery assemblies for hybrid and electric vehicles," *Journal of Power Sources ,* vol. 15, no. 196, pp. 6525-6533, 2011.

[49] P. B. Hans-Georg Schweiger, "Comparison of Several Methods for Determining the Internal Resistance of Lithium Ion Cells," *Sensors,* vol. 10, pp. 5604-5625, 2010.

[50] R. R. a. J. W. D. Halliday, Fundamentals of Physics, 9th ed, Hoboken, N.J: Wiley, (2010).

[51] Diverse Power, "Fundamentals of Electricity," [Online]. Available: http://c03.apogee.net/mvc/home/hes/land/el?utilityname=diversepower&spc=foe&id=4571. [Accessed 02 01 2020].

[52] I. H. M. W. Harald Brandstätter, "Myth and Reality about the Origin of Inductive Loops in Impedance Spectra of Lithium-Ion Electrodes — A Critical Experimental Approach," *Electrochimica Acta,* vol. 207, pp. 218-223, 206.

[53] M. Dubarry, "Synthesize battery degradation modes via a diagnostic and prognostic model," *Journal of Power Sources,* vol. 219, pp. 204-216, 2012.

[54] J. L. C. D. D. M. S. N. D. L. Seong Jin An, "The state of understanding of the lithium-ion-battery graphite solid electrolyte interphase (SEI) and its relationship to formation cycling," *Carbon,* vol. 105, pp. 52-76, 2016.

[55] Y. &. P. K. A. Shin, "Surface morphology and surface stability against oxygen loss of the lithium-excess Li2MnO3 cathode material as a function of lithium concentration," *ACS,* pp. 25595-25602, 2016.

[56] K. A. P. Yongwoo Shin, "Alleviating oxygen evolution from Li-excess oxide materials through theory-guided surface protection," *Nature,* vol. 9, 2018.

[57] G. E. Blomgren, "The Development and Future of Lithium Ion Batteries," *J. Electrochem. Soc. ,* vol. 164, no. 1, pp. A5019-A5025, 2017 .

[58] J. T. L. K. G.G. Amatucci, " Cobalt dissolution in LiCoO2-based non-aqueous rechargeable batteries," *Solid State Ionics,* vol. 83, 1996.

[59] P. P. B.-E. B. P. B. V. D. A. F. D. C. &. V. W. Simon Müller, "Quantification and modeling of mechanical degradation in lithium-ion batteries based on nanoscale imaging," *Nature communications,* no. 9, 2018.

[60] C. Y. Q. L. Wang J., "The Development of Silicon Nanocomposite Materials for Li-Ion Secondary Batteries," *The Open Materials Science Journal,* p. 228 , 2011.

[61] W. M. J. D. S.T. Coleman, "Lithium Intercalation in Lixmo6se8 - a Model Mean-Field Lattice Gas," *Physical Review B ,* vol. 29, no. 7, 1984.

[62] R. T. M. Swierczynskia, "The Second Life Ageing of the NMC/C Electric Vehicle retired Li-ion Batteries in the Stationary Applications," *ECS Transactions,* vol. 74, pp. 55-62, 2016.

[63] R. T. Chi Zhang, "Evaluating the Degradation Mechanism and SOH of LiFePO4 LIBs in," *energies,* 2017.

[64] F. F. Lucille Bodenes, "Lithium secondary batteries working at very high temperature: Capacity fade and understanding of agoing mechanisms," *Journal of Power Sources ,* vol. 236, pp. 265-275, 2013.

[65] C. M. T. M. P. Feng Leng, "Effect of Temperature on the Aging rate of Li Ion Battery Operating above Room Temperature," *Nature,* 2015.

[66] J. K. Soon-Jong Kwon, "Performance and Life Degradation Characteristics," *NDPI Electronics,* 2018.

[67] A. B. T. A. Y. G. M. A.-S. J. M. James Taylor, "An insight into the errors and uncertainty of the lithium-ion batterycharacterisation experiments," *Journal of Energy Storage,* vol. 24, 2019.

[68] nanoScienceInstruments, "Scanning Electron Microscopy," [Online]. Available: https://www.nanoscience.com/techniques/scanning-electron-microscopy/. [Accessed 06 02 2020].

[69] S. Swapp, "Geochemical Instrumentation and Analysis," [Online]. Available: https://serc.carleton.edu/research_education/geochemsheets/techniques/SEM.html. [Accessed 06 01 2020].

[70] S. T. S. D. D. J. C. J. J. D. J. C. B. J. R. Dahn, "Accurate and Precise Temperature-Controlled Boxes for the Safe Testing of Advanced Automotive Li-Ion Cells with High Precision Coulometry," *Journal of the Electrochemical Society,* vol. 160, pp. a251-a258, 2013.

[71] Fluke, "Specifications: Fluke 289 True-RMS Data Logging Multimeter," [Online]. Available: https://www.fluke.com/en-ca/product/electrical-testing/digital-multimeters/fluke-289. [Accessed 07 05 2020].

[72] Sandia National Laboratory, "Dynamic PJM Regulation Signal," Sandia , Albuquerque, NM, 2015.

[73] PJM, "Ancillary Services," [Online]. Available: https://www.pjm.com/markets-and-operations/ancillary-services.aspx. [Accessed 10 03 2020].

[74] G. B. M. Dubarry, "Commercial Li-ion battery testing: Initial Conditioning & Characterization and Reference Performance Tests," Hawai'i Natural Energy Institute, Honolulu, HI, 2019.

[75] "AutoHotkey," 2019. [Online]. Available: https://www.autohotkey.com/. [Accessed 09 03 2019].

[76] J. L. J. G. Rui Zhao, "The effects of electrode thickness on the electrochemical and thermalcharacteristics of lithium ion battery," *Applied Energy ,* vol. 139, pp. 220-229, 2015.

[77] EL-CELL, "PAT Series Overview," [Online]. Available: https://el-cell.com/pat-series/pat-series-overview.

[78] C. Snyder, "The Effects of Cycle Rate on Capacity Fade of Lithiun Ion Batteries," Sandia National Laboratories , Albuquerque.

[79] T. J. Hammond Jules, "Electrochemical biosensors and nanobiosensors," *Essays in Biochemistry,* vol. 60, 2016.

[80] BP, "BP Stats Review," London, 2017.

[81] JoséGoldemberga and S. Coelhob, "Renewable energy—traditional biomass vs. modern biomass," *Energy Policy,* vol. 32, no. 6, pp. 711-714, 2004.

[82] T. K. Kim, "T test as a parametric statistic," *Korean Journal of Anesthesiology ,* pp. 540-546, 2015.

[83] C. R. Birkl, "Degradation diagnostics for lithium ion cells," *Journal of Power Sources,* vol. 341, pp. 373-386, 2017.

[84] H. Sandeson, "Congo, child labour and your electric car," *Financial Times,* 6 July 2019.

[85] S. W. W. K. P. V. P. Po-Han Lee, "The storage degradation of an 18650 commercial cell studied using neutron powder diffraction," *Journal of Power Sources,* vol. 374, pp. 31-39, 2018.

[86] AutoLion-3D, "Battery Safety Simulation," [Online]. Available: https://www.gtisoft.com/autolion-3d/. [Accessed 14 02 2020].

[87] S. W. Leila Ahmadi, "Energy efficiency of Li-ion battery packs re-used in stationary power applications," *Sustainable Energy Technologies and Assessments,* vol. 8, pp. 9-17, 2014.

[8 Nova Scotia Power, "TIME OF DAY RATES," [Online]. Available: https://www.nspower.ca/about-
8] us/electricity/rates-tariffs/domestic-tod/time-of-day-rates. [Accessed 18 04 2020].

Appendix A. Electrochemical Impedance Spectroscopy /Calorimetry

Electrical Impedance Spectroscopy

There are many limitations with the DCR, calorimetry, and AC pulse techniques explained in section 2.4. A more advance and concise technique called Electrochemical Impedance Spectroscopy (EIS) can be used to measure localized impendences within the cell. This is done by using the AC pulse method at many different frequencies. The amplitude of voltage and current is a function of frequency and the ratio of the voltage to the current is the impedance and due to the phase difference (θ) the impendence includes real and imaginary parts.

$$v(\omega, t) = Vcos(\omega t)$$

$$i(\omega, t) = Icos(\omega t + \theta)$$

Using Ohms law

$$Z(\omega) = \frac{Vcos(\omega t)}{Icos(\omega t + \theta)}$$

Using Euler's equation, the impendence can be written as a complex number

$$Z(\omega) = \frac{Ve^{j(\omega t)}}{Ie^{j(\omega t+\theta)}} = |Z|e^{-j\theta} = |Z|cos(\theta) - |Z|jsin(\theta)$$

EIS is a noninvasive technique which allows one to gain information about what is happening to the various electrode/electrolyte interfaces. Equivalent circuit models (ECM) are often used to analyze the EIS data and understand what is happening at these interfaces. ECMs attempt to mimic the behavior of

what is happening within the cell by modelling each type of impedance as a resistor and adding them in series with other elements such as Waburg (diffusion resistance) and capacitance elements. The sum of the impedances Is considered the total cells impedance. As capacitance decreases with frequency and inductance increases one can plot the imaginary vs. real impedance at many difference frequencies. This is called a Nyquist plot and will give you a curve that can be analyzed which can isolate the contact resistance, charge transfer resistance and double layer capacitance. Below shows the simplest and most common ECM (Randles Model) superimposed on a Nyquist curve taken from Hammond et al [79] .

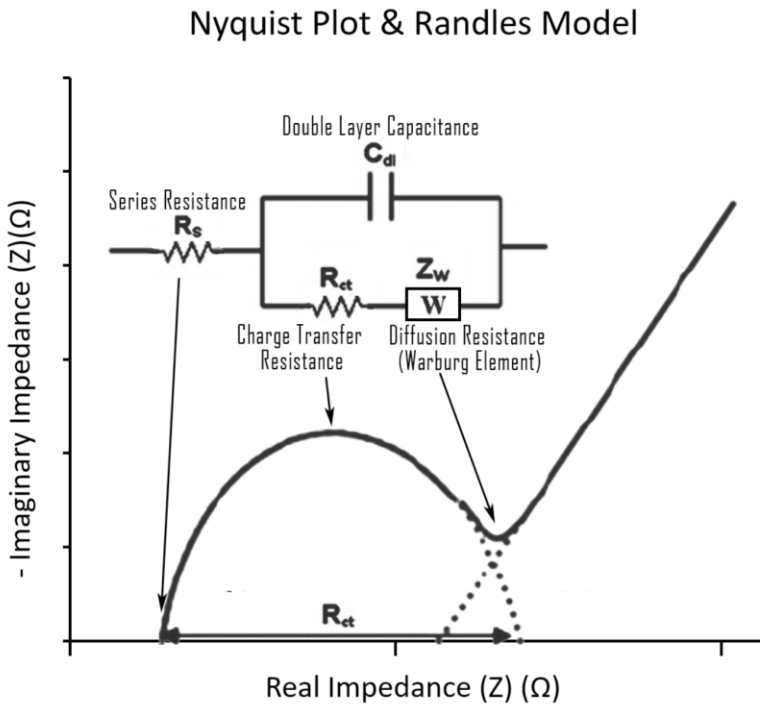

Figure 49 Nyquist Plot and Randles Model

At the RESL however the power cyclers are not sensitive enough to perform such high frequency pulsing, so this was considered out of scope for the purposes of this research.

Calorimetry

Another method of estimating a cells impedance is by using a calorimeter. A calorimeter is a device used to measure the heat flow of a chemical reaction or physical change. Current flowing through a battery generates heat. For all batteries the value of heat is defined by losses resulting from current flowing through the IR of the battery during charging and discharging and is known as Joule heating. Using a calorimeter, it is possible to measure the heat loss in the battery and calculate the resistance [49].

$$Q_{loss} = I^2Rt$$

Where Q_{loss} is the heat generated I is the current(constant), R is the total resistance of the battery and t is time in seconds.

Appendix B. Cell Measurements of Weight, IR and OCV

Column Count	Type	Cell	Weight (g)	IR (Ohms)	OCV (V)
1	LGY P1.5	A01	375	1.32	4.179
2	LGY P1.5	A02	375	1.18	4.182
3	LGY P1.5	A03	375	1.12	4.146
4	LGY P1.5	A04	375	1.14	4.147
5	LGY P1.5	A08	375	1.17	3.586
6	LGY P1.5	A09	375	1.2	3.581
7	LGY P1.5	A11	375	1.18	3.566
8	LGY P1.5	A12	374	1.13	3.573
9	LGY P1.5	A13	376	1.16	3.552
10	LGY P1.5	A14	375	1.15	3.567
11	LGY P1.5	A15	375	1.15	3.566
12	LGY P1.5	A16	375	1.16	3.567
13	LGY P1.5	A28	376	1.25	3.567
14	LGY P1.5	A36	375	1.17	3.574
15	LGY P1.5	A37	375	1.16	3.571
16	LGX P1.5 (P1.7)	A06	375	1.06	3.564
17	LGX P1.5 (P1.7)	A07	376	1.06	3.564
18	LGX P1.5 (P1.7)	A10	376	1.05	3.595
19	LGX P1.5 (P1.7)	A17	376	1.14	3.592
20	LGX P1.5 (P1.7)	A18	375	1.07	3.561
21	LGX P1.5 (P1.7)	A19	376	1.08	3.56
22	LGX P1.5 (P1.7)	A20	377	1.09	3.572
23	LGX P1.5 (P1.7)	A21	377	1.1	3.572
24	LGX P1.5 (P1.7)	A22	376	1.04	3.595
25	LGX P1.5 (P1.7)	A23	377	1.08	3.594
26	LGX P1.5 (P1.7)	A24	377	1.14	3.597
27	LGX P1.5 (P1.7)	A25	376	1.12	3.597
28	LGX P1.5 (P1.7)	A26	375	1.1	3.592
29	LGX P1.5 (P1.7)	A27	376	1.06	3.593
30	LGX P1.5 (P1.7)	A30	376	1.08	3.564
31	LGX P1.5 (P1.7)	A31	377	1.04	3.565
32	LGX P1.5 (P1.7)	A32	375	1.08	3.595
33	LGX P1.5 (P1.7)	A33	377	1.04	3.589
34	LGX P1.5 (P1.7)	A34	376	1.05	3.591
35	LGX P1.5 (P1.7)	A35	377	1.16	3.591

Column Count	Type	Cell	Weight (g)	IR (Ohms)	OCV(V)
1	A123	A01	493	0.8	3.428
2	A123	A02	493	0.88	3.435
3	A123	A09	494	0.9	3.289
4	A123	A11	493	0.86	3.288
5	A123	A13	493	0.88	3.288
6	A123	A15	495	0.87	3.287
7	A123	A16	493	0.9	3.288
8	A123	A17	494	0.86	3.288
9	A123	A19	493	0.86	3.288
10	A123	A21	493	0.89	3.289
11	A123	A22	493	0.84	3.289
12	A123	A23	492	0.84	3.288
13	A123	A24	494	0.82	3.288
14	A123	A25	494	0.86	3.288
15	A123	A26	495	0.85	3.288
16	A123	A30	495	0.84	3.289
17	A123	A31	495	0.85	3.289
18	A123	A32	495	0.85	3.289
19	A123	A33	495	0.85	3.289
20	A123	A34	495	0.85	3.288

Note: Highlighted cells were picked for use in the experiment

Appendix C. Power Cycler Schedules

Sample Code LGC CP

Standard Settings | Professional Settings

ID	Step name	StepTime(hh:mm:ss)	Rate(C)	Volt.(V)	Cur.(A)	Cap.(Ah)	Power(W)	R(Ω)
1	Rest	00:00:30						
2	CC_Chg			4.2000	16.0000			
3	Rest	1000:00:00						
	IF		AuxTMax	<	30.000000	Goto:4		
4	Cycle	Begin ID: 3	Times: 1					
5	CP_Dchg	00:42:00					60.0000	
6	Rest	00:18:00						
7	Rest	1000:00:00						
	IF		AuxTMax	<	30.000000	Goto:8		
8	CP_Chg			4.2000			60.0000	
9	Rest	1000:00:00						
	IF		ChgPlusRestTime	>=	3750.000000	Goto:10		
10	Rest	1000:00:00						
	IF		AuxTMax	<	30.000000	Goto:11		
11	Cycle	Begin ID: 5	Times: 252					
12	End							

Step Name Para

Range

Record Condition
- Time 15 sec
- Volt. V
- Cur. A

Delay Protect
- Step sec
- Continue sec
- Main Aux sec

Safety Limit
- Volt.Lower 2.4500 V
- Volt.Upper 4.2500 V
- Cur.Lower -25.0000 A
- Cur.Upper 25.0000 A
- Cap.Upper Ah
- Delay Time sec

Aux Safety Limit
- Volt.Lower V
- Volt.Upper V
- Temp.Lower 10.0 ℃
- Temp.Upper 45.0 ℃
- Diff Volt. V

Temp.Continue
- Min ℃
- Max ℃

Ratio
- Material mg
- Spec.Cap mAh/g

Loop Impedance
- Impedance Ω
- Aux Diff Volt. V
- Diff Main Aux V

Start StepID 3

Remarks
- Creator Elliott
- P/N
- Remarks: LGC_HEV-P1.5_A1x_Fix_CP_Dis1-60W-42m_Rest-18m_Chg1-60W-4.2VPC_Rest-CplusR-62.5m_252Cy_1S

BFGS Protect Condition
- BFGS Rate
- Detection Time sec
- Volt. V

Plat Volt.
- Plat1 V
- Plat2 V
- Plat3 V

Aux Record Condition
- Time 15 sec
- Volt. V
- Temp. ℃

Apply to all pending steps

Apply to all current steps

Sample Code LGC FR

Standard Settings | Professional Settings

ID	Step name	StepTime(hh:mm:ss)	Rate(C)	Volt.(V)	Cur.(A)	Cap.(Ah)	) Rate	p Cur	g(W	V(mV	Power(W)	R(Ω)
2	Rest	1000:00:00										
	IF		add expression	<=	30.000000	Goto:3						
3	CC_Chg			4.2000	16.0000							
	IF		StepTime	>=	7200sec	chnl. protect						
4	CCCV_Chg			4.2000	10.0000			0000				
	IF		StepTime	>=	1800sec	Goto:5						
5	CC_Dchg				16.0000	7.0000						
	IF		StepTime	>=	3600sec	chnl. protect						
6	Rest	00:00:01										
7	Cycle	Begin ID: 6	Times: 2									
8	SIM	File path	Wh_Lines-43200.txt	Power mode	iplicator: 1							
9	CC_Chg				16.0000							
	IF		CycleAhD	>=	0.000000	Goto:10						
	IF		StepTime	>=	1800sec	chnl. protect						
10	Rest	1000:00:00										
	IF		ChgPlusRestTime	>=	1800.000000	Goto:11						
11	Rest	1000:00:00										
	IF		AuxTMax	<=	30.000000	Goto:12						
12	Cycle	Begin ID: 8	Times: 3									
13	Rest	00:00:01										
14	Cycle	Begin ID: 13	Times: 2									
15	Cycle	Begin ID: 3	Times: 7									
16	CC_Chg			4.2000	16.0000							
	IF		StepTime	>=	3600sec	chnl. protect						
17	Rest	00:00:30										
18	End											

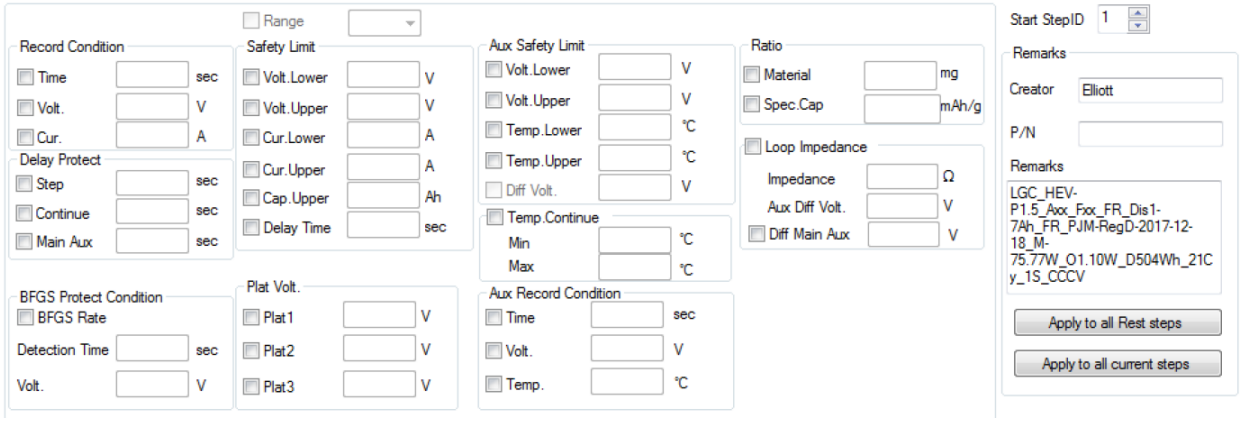

Sample Code LGC RPT

Standard Settings | Professional Settings

ID	Step name	StepTime(hh:mm:ss)	Rate(C)	Volt.(V)	Cur.(A)	Cap.(Ah)	) Rate	Stop Cur.(A)		g(W	V(m	Power(W)
1	Rest	00:00:01										
	Set	User30	CC-CCCV (1 h)									
2	Rest	00:00:30										
3	Rest	1000:00:00										
	IF		AuxTMax	<	100.000000	Goto:4						
4	Cycle	Begin ID: 3	Times: 1									
5	CC_Dchg			2.5000	16.0000							
	IF		StepTime	>=	5400sec	chnl. protect						
6	Rest	1000:00:00										
	IF		LS_PS_Time	>=	4500.000000	Goto:8						
7	Rest	1000:00:00										
	IF		AuxTMax	<	100.000000	Goto:8						
8	CC_Chg			4.2000	16.0000							
	IF		StepTime	>=	5400sec	chnl. protect						
	Set	User1	CC_Step_Time									
9	CCCV_Chg			4.2000	16.0000			0.2500				
	Set	User2	CCCV_Step_Time									
10	Rest	1000:00:00										
	IF		U1_U2_PS_Time	>=	6000.000000	Goto:12						
11	Rest	1000:00:00										
	IF		AuxTMax	<	100.000000	Goto:12						
12	Cycle	Begin ID: 5	Times: 3									
	Set	User30	CP-CPCV (1 h)									
13	Rest	00:00:30										
14	Rest	1000:00:00										
	IF		AuxTMax	<	100.000000	Goto:15						

15	Cycle	Begin ID: 14	Times: 2									
16	CP_Dchg			2.5000								60.0000
	IF		StepTime	>=	5400sec	chnl. protect						
17	Rest	1000:00:00										
	IF		LS_PS_Time	>=	4500.000000	Goto:19						
18	Rest	1000:00:00										
	IF		AuxTMax	<	100.000000	Goto:19						
19	CP_Chg			4.2000								60.0000
	IF		StepTime	>=	5400sec	chnl. protect						
	Set	User1	CP_Step_Time									
20	CCCV_Chg			4.2000	14.2800			0.2500				
	Set	User2	CPCV_Step_Time									
21	Rest	1000:00:00										
	IF		U1_U2_PS_Time	>=	6000.000000	Goto:23						
22	Rest	1000:00:00										
	IF		AuxTMax	<	100.000000	Goto:23						
23	Cycle	Begin ID: 16	Times: 3									
24	Rest	00:00:30										
25	Rest	1000:00:00										
	IF		AuxTMax	<	100.000000	Goto:26						
26	Cycle	Begin ID: 25	Times: 2									
	Set	User30	PULSE									
27	SIM	File path	m-30s_Lines-53.txt	Cur mode	iplicator: 8							
	IF		Volt.	<	2.5000V	Goto:28						
	IF		StepTime	>=	7800sec	chnl. protect						
28	Rest	1000:00:00										

	IF		LS_PS_Time	>=	9000.000000	Goto:30						
29	Rest	1000:00:00										
	IF		AuxTMax	<	100.000000	Goto:30						
30	SIM	File path	m-30s_Lines-53.txt	Cur mode	iplicator: 8							
	IF		Volt.	>	4.2000V	Goto:31						
	IF		StepTime	>=	7800sec	chnl. protect						
	Set	User1	SimChgTime									
31	CCCV_Chg			4.2000	8.0000			0.2500				
	Set	User2	CCCV_Step_Time									
32	Rest	1000:00:00										
	IF		U1_U2_PS_Time	>=	9000.000000	Goto:34						
33	Rest	1000:00:00										
	IF		AuxTMax	<	100.000000	Goto:34						
34	Cycle	Begin ID: 33	Times: 2									
	Set	User30	dVdQ									
35	CC_Dchg			2.5000	0.6670							
	IF		StepTime	>=	108000sec	chnl. protect						
36	Rest	1000:00:00										
	IF		AuxTMax	<	100.000000	Goto:37						
37	Cycle	Begin ID: 36	Times: 2									
38	CC_Chg			4.2000	0.6670							
	IF		StepTime	>=	108000sec	chnl. protect						
39	Rest	1000:00:00										
	IF		AuxTMax	<	100.000000	Goto:40						
40	Cycle	Begin ID: 39	Times: 2									

41	CC_Dchg			2.5000	0.6670							
	IF		StepTime	>=	108000sec	chnl. protect						
42	Rest	1000:00:00										
	IF		AuxTMax	<	100.000000	Goto:43						
43	Cycle	Begin ID: 42	Times: 2									
44	CC_Dchg	00:10:00		2.5000	16.0000							
45	CC_Chg			4.2000	16.0000							
	IF		StepTime	>=	5500sec	chnl. protect						
46	End											

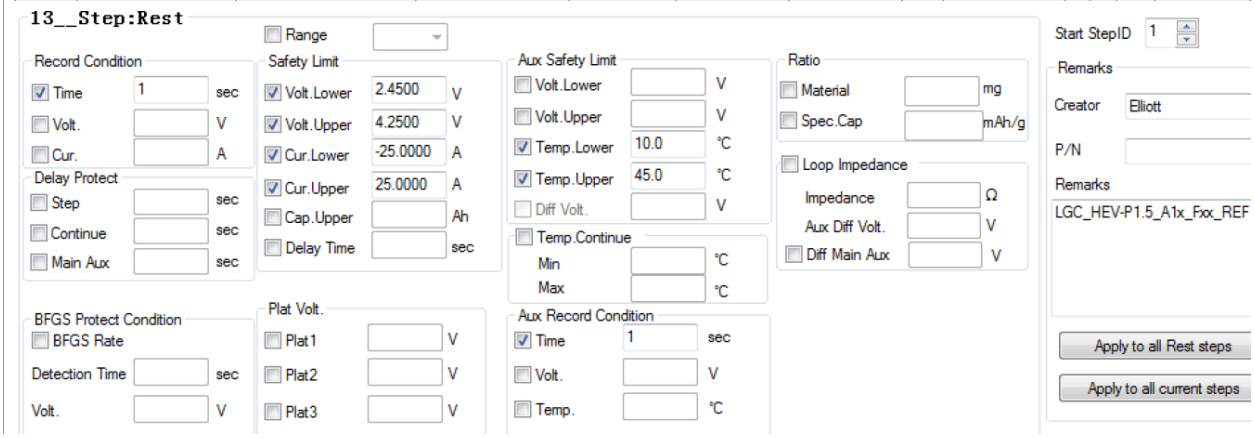

Appendix D. Analysis Code

MATLAB Extraction Code

```
% %Pulls cycle data from excel files and makes a copy and paste table
%
% %Read Data, copy all file paths from Neware xls first to an excel table
% %then to the filepath string array so that "" are not copied
% % The final product is the Table "CopyPaste". Copy this into your master

%STEP 1: You must copy below to command window first before running
% filepath="";
%Step 2: Copy all file paths from Neware xls first to an excel table
% %then to the filepath string array so that "" are not copied.
%Step 3: Click Run and copyandpaste final product
filepath=strrep(filepath(:,1),'"','');
x=array2table(filepath);
y=height(x);
warning('OFF', 'MATLAB:table:ModifiedAndSavedVarnames');
for i=1:y
   if i==1
      Cycledata = readtable(filepath(i,1), 'Sheet', 4,'Range','A:I');
      n(i,1)=height(Cycledata);
   end
   if i>1
      Cycledata_new=readtable(filepath(i,1), 'Sheet', 4,'Range','A:I');
      Cycledata=[Cycledata; Cycledata_new];
      n(i,1)=height(Cycledata_new);
      k(i,1)=height(Cycledata);
   end

end
% m=1;
% j=1;

for j= 1:y
   file=filepath(j,1);
    cellID=strfind(file,'A_A');
   if ~isempty(cellID)
      cellID = extractBetween(file,cellID+2,cellID+4);
   else
      cellID=strfind(file, '5_A');
      cellID = extractBetween(file,cellID+2,cellID+4);
   end
   fileID=strfind(file,'_F1');
   fileID = extractBetween(file,fileID+1,fileID+3);
   typeID=strfind(file,'A123');
   if ~isempty(typeID)
      typeID = extractBetween(file,typeID+0,typeID+3);
   else
      typeID=strfind(file,'LGC');
```

```
    typeID = extractBetween(file,typeID+0,typeID+2);
end
modeID=1;
if typeID=='LGC'
  chemID='NMC+LMO';
  brandID= 'LGCHEM';
elseif typeID=='A123'
  chemID='LFP';
  brandID= 'A123';
end
  filterdata_single(j,1:5)=[brandID,modeID,cellID,fileID,chemID];
for i=1:n(j,1)
    filterdata_new(i,:)=filterdata_single(j,:);
end
if j==1
  filterdata=[filterdata_new(1:i,:)];
elseif j>1
    filterdata=[filterdata; filterdata_new(1:i,:)];
end
if j==1
   for p= 1:n
      if Cycledata{p,1}==1
         filterdata(p,2)='1h_CCCV';
      elseif Cycledata{p,1}==2
         filterdata(p,2)='1h_CCCV';
      elseif Cycledata{p,1}==3
         filterdata(p,2)='1h_CCCV';
      elseif Cycledata{p,1}==4
         filterdata(p,2)='1h_CPCV';
      elseif Cycledata{p,1}==5
         filterdata(p,2)='1h_CPCV';
      elseif Cycledata{p,1}==6
         filterdata(p,2)='1h_CPCV';
      elseif Cycledata{p,1}==7
         filterdata(p,2)='Final Top-up
      end
   m=n(j,1);
   end
elseif j>1
   for p= (m+1):n(j,1)+m
      if Cycledata{p,1}==1
         filterdata(p,2)='1h_CCCV';
      elseif Cycledata{p,1}==2
         filterdata(p,2)='1h_CCCV';
      elseif Cycledata{p,1}==3
         filterdata(p,2)='1h_CCCV';
      elseif Cycledata{p,1}==4
         filterdata(p,2)='1h_CPCV';
      elseif Cycledata{p,1}==5
         filterdata(p,2)='1h_CPCV';
      elseif Cycledata{p,1}==6
         filterdata(p,2)='1h_CPCV';
      elseif Cycledata{p,1}==7
```

```
            filterdata(p,2)='Final Top-up';

          end
        end
        m=m+n(j,1);
    end
end
filterdata=array2table(filterdata);
filterdata.Properties.VariableNames = {'Manufacturer' 'Mode' 'Cell' 'File' 'Chemistry'};

%Step 4: FINAL PRODUCT copy and paste table to master sheet
FinalProduct=[filterdata Cycledata];
%Step 5: If you want to run this again, you must delete entire workspace
```

Sample VBA Code dVdQ /dQdV Plotting

```
Sub LoopAllExcelFiles()
'PURPOSE: To loop through all Excel files in a user specified folder and perform a set task on them
Dim wb As Workbook
Dim myPath As String
Dim myFile As String
Dim myExtension As String
Dim FldrPicker As FileDialog

'Optimize Macro Speed
 Application.ScreenUpdating = False
 Application.EnableEvents = False
 Application.Calculation = xlCalculationManual

'Retrieve Target Folder Path From User
 Set FldrPicker = Application.FileDialog(msoFileDialogFolderPicker)

   With FldrPicker
    .Title = "C:\Users\Mark\Dropbox (RESL)\NEST Repurposing Batts, BT LS\EA vs FR\dvdq"
    .AllowMultiSelect = False
     If .Show <> -1 Then GoTo NextCode
     myPath = .SelectedItems(1) & "\"
   End With

'In Case of Cancel
NextCode:
 myPath = myPath
 If myPath = "" Then GoTo ResetSettings

'Target File Extension (must include wildcard "*")
 myExtension = "*.xls*"

'Target Path with Ending Extention
 myFile = Dir(myPath & myExtension)
```

```
'Loop through each Excel file in folder
   For Z = 0 To 500
 Do While myFile <> ""
   'Set variable equal to opened workbook
    Set wb = Workbooks.Open(Filename:=myPath & myFile)
   'Ensure Workbook has opened before moving on to next line of code
    DoEvents

      'copy name of workbook
       wb.Worksheets(1).Range("A1").Copy Destination:=Sheets("dVdQ").Range("A1").Offset(0, 6 * Z)
       Sheets("dVdQ").Range("A2").Offset(0, 6 * Z) = "Chg"
       Sheets("dVdQ").Range("G2").Offset(0, 6 * Z) = "Dis"
       Sheets("dVdQ").Range("A3").Offset(0, 6 * Z) = "Voltage"
       Sheets("dVdQ").Range("B3").Offset(0, 6 * Z) = "Ah"
       Sheets("dVdQ").Range("C3").Offset(0, 6 * Z) = "dV"
       Sheets("dVdQ").Range("D3").Offset(0, 6 * Z) = "dQ"
       Sheets("dVdQ").Range("E3").Offset(0, 6 * Z) = "dV/dQ"
       Sheets("dVdQ").Range("F3").Offset(0, 6 * Z) = "dQ/dV"
       Sheets("dVdQ").Range("G3").Offset(0, 6 * Z) = "Voltage"
       Sheets("dVdQ").Range("H3").Offset(0, 6 * Z) = "Ah"
       Sheets("dVdQ").Range("I3").Offset(0, 6 * Z) = "dV"
       Sheets("dVdQ").Range("J3").Offset(0, 6 * Z) = "dQ"
       Sheets("dVdQ").Range("K3").Offset(0, 6 * Z) = "dV/dQ"
       Sheets("dVdQ").Range("L3").Offset(0, 6 * Z) = "dQ/dV"

'copy data 8 is the cycle number for the dVdQ cycle
    Dim K As Long
   Dim LastRow As Long
   LastRow = wb.Worksheets(6).Range("D" & Rows.Count).End(xlUp).Row
   For K = 4 To LastRow - 1
   'For K = 20000 To 20050
   If wb.Worksheets(6).Range("A" & K) = "8" And wb.Worksheets(6).Range("G" & K) > 0 Then 'For charge
```

```
   cRow = Sheets("dVdQ").Range("A10000").Offset(0, 6 * Z).End(xlUp).Row 'cRow is the row that has any value in it, so cRow + 1 copies it into the row below

   wb.Worksheets(6).Range("F" & K).Copy Destination:=Sheets("dVdQ").Range("A" & cRow + 1).Offset(0, 6 * Z)

   wb.Worksheets(6).Range("J" & K).Copy Destination:=Sheets("dVdQ").Range("B" & cRow + 1).Offset(0, 6 * Z)

   End If

   If wb.Worksheets(6).Range("A" & K) = "8" And wb.Worksheets(6).Range("G" & K) < 0 Then ' For discharge

   cRow = Sheets("dVdQ").Range("G10000").Offset(0, 6 * Z).End(xlUp).Row 'cRow is the row that has any value in it, so cRow + 1 copies it into the row below

   wb.Worksheets(6).Range("F" & K).Copy Destination:=Sheets("dVdQ").Range("G" & cRow + 1).Offset(0, 6 * Z)

   wb.Worksheets(6).Range("K" & K).Copy Destination:=Sheets("dVdQ").Range("H" & cRow + 1).Offset(0, 6 * Z)

   End If

   Next

   Z = Z + 2

'Save and Close Workbook

     wb.Close SaveChanges:=True

'Ensure Workbook has closed before moving on to next line of code

     DoEvents

'Get next file name

     myFile = Dir

  Loop

Next

'Message Box when tasks are completed

  MsgBox "Task Complete!"

ResetSettings:

  'Reset Macro Optimization Settings

   Application.EnableEvents = True

   Application.Calculation = xlCalculationAutomatic

   Application.ScreenUpdating = True

End Sub


Sub Differentiate()

   P = Sheets("Graph").Range("C1") 'Averager in dVdQ

  ' Dim LastCol As Long

   'LastCol = Sheets("dVdQ").Cells(1, Columns.Count).End(xlToLeft).Column

'For Z = 0 To LastCol
```

```
For Z = 0 To 100

   Dim LastRow As Long

   LastRow = Sheets("dVdQ").Range("A" & Rows.Count).Offset(0, 6 * Z).End(xlUp).Row

For K = 4 To LastRow

If Sheets("dVdQ").Range("A" & K + P).Offset(0, 6 * Z) - Sheets("dVdQ").Range("A" & K).Offset(0, 6 * Z) = 0 Or
Sheets("dVdQ").Range("B" & K + P).Offset(0, 6 * Z) - Sheets("dVdQ").Range("B" & K).Offset(0, 6 * Z) = 0 Then

K = K + 1

Else

  Sheets("dVdQ").Range("C" & K).Offset(0, 6 * Z) = Sheets("dVdQ").Range("A" & K + P).Offset(0, 6 * Z) -
Sheets("dVdQ").Range("A" & K).Offset(0, 6 * Z) 'dV

  Sheets("dVdQ").Range("D" & K).Offset(0, 6 * Z) = Sheets("dVdQ").Range("B" & K + P).Offset(0, 6 * Z) -
Sheets("dVdQ").Range("B" & K).Offset(0, 6 * Z) 'dQ

  Sheets("dVdQ").Range("E" & K).Offset(0, 6 * Z) = Sheets("dVdQ").Range("C" & K).Offset(0, 6 * Z) / Sheets("dVdQ").Range("D"
& K).Offset(0, 6 * Z) 'dV/dQ

  Sheets("dVdQ").Range("F" & K).Offset(0, 6 * Z) = Sheets("dVdQ").Range("D" & K).Offset(0, 6 * Z) / Sheets("dVdQ").Range("C"
& K).Offset(0, 6 * Z) 'dQ/dV


 End If

Next


Next

End Sub


Sub Graph()


Sheets("Graph").Select

Dim cht As Chart


   If Cells(1, 1) = "dVdQ" And Cells(2, 1) = "Dis" And Cells(3, 1) = "LGC" Then


      Set cht = ActiveSheet.ChartObjects("Chart 1").Chart

      'Adjust y-axis Scale

       cht.Axes(xlValue).MinimumScale = -0.1

       cht.Axes(xlValue).MaximumScale = -0.02


      'Adjust x-axis Scale
```

```
        cht.Axes(xlCategory).MinimumScale = 0
        cht.Axes(xlCategory).MaximumScale = 12

'Chart Name
cht.HasTitle = True
cht.ChartTitle.Characters.Text = "NMC + LMO dVdQ Discharge"

'X axis name
cht.Axes(xlCategory, xlPrimary).HasTitle = True
cht.Axes(xlCategory, xlPrimary).AxisTitle.Characters.Text = "Discharge Capacity (Ah)"
'y-axis name
cht.Axes(xlValue, xlPrimary).HasTitle = True
cht.Axes(xlValue, xlPrimary).AxisTitle.Characters.Text = "dV/dQ (V/Ah)"

  ElseIf Cells(1, 1) = "dVdQ" And Cells(2, 1) = "Chg" And Cells(3, 1) = "LGC" Then

      Set cht = ActiveSheet.ChartObjects("Chart 1").Chart
      'Adjust y-axis Scale
        cht.Axes(xlValue).MinimumScale = 0.01
        cht.Axes(xlValue).MaximumScale = 0.08

      'Adjust x-axis Scale
        cht.Axes(xlCategory).MinimumScale = 2
        cht.Axes(xlCategory).MaximumScale = 12

'Chart Name
cht.HasTitle = True
cht.ChartTitle.Characters.Text = "NMC + LMO dVdQ Charge"

'X axis name
cht.Axes(xlCategory, xlPrimary).HasTitle = True
cht.Axes(xlCategory, xlPrimary).AxisTitle.Characters.Text = "Charge Capacity (Ah)"
'y-axis name
cht.Axes(xlValue, xlPrimary).HasTitle = True
```

```
cht.Axes(xlValue, xlPrimary).AxisTitle.Characters.Text = "dV/dQ (V/Ah)"
'End Wit
   ElseIf Cells(1, 1) = "dQdV" And Cells(2, 1) = "Dis" And Cells(3, 1) = "LGC" Then

      Set cht = ActiveSheet.ChartObjects("Chart 1").Chart
      'Adjust y-axis Scale
        cht.Axes(xlValue).MinimumScale = -40
        cht.Axes(xlValue).MaximumScale = 0
      'Adjust x-axis Scale
        cht.Axes(xlCategory).MinimumScale = 3.4
        cht.Axes(xlCategory).MaximumScale = 4.1
              'With ActiveChart
'chart name
cht.HasTitle = True
cht.ChartTitle.Characters.Text = "NMC + LMO dQdV Discharge"
'X axis name
cht.Axes(xlCategory, xlPrimary).HasTitle = True
cht.Axes(xlCategory, xlPrimary).AxisTitle.Characters.Text = "Voltage (V)"
'y-axis name
cht.Axes(xlValue, xlPrimary).HasTitle = True
cht.Axes(xlValue, xlPrimary).AxisTitle.Characters.Text = "dQ/dV (Ah/V)"

 ElseIf Cells(1, 1) = "dQdV" And Cells(2, 1) = "Chg" And Cells(3, 1) = "LGC" Then

      Set cht = ActiveSheet.ChartObjects("Chart 1").Chart
      'Adjust y-axis Scale
        cht.Axes(xlValue).MinimumScale = 10
        cht.Axes(xlValue).MaximumScale = 40
      'Adjust x-axis Scale
        cht.Axes(xlCategory).MinimumScale = 3.5
        cht.Axes(xlCategory).MaximumScale = 4.1
              'With ActiveChart
'chart name
cht.HasTitle = True
```

```
cht.ChartTitle.Characters.Text = "NMC + LMO dQdV Charge"
'X axis name
cht.Axes(xlCategory, xlPrimary).HasTitle = True
cht.Axes(xlCategory, xlPrimary).AxisTitle.Characters.Text = "Voltage (V)"
'y-axis name
cht.Axes(xlValue, xlPrimary).HasTitle = True
cht.Axes(xlValue, xlPrimary).AxisTitle.Characters.Text = "dQ/dV (Ah/V)"
'**********For LFP**********

 ElseIf Cells(1, 1) = "dVdQ" And Cells(2, 1) = "Dis" And Cells(3, 1) = "A123" Then

      Set cht = ActiveSheet.ChartObjects("Chart 1").Chart
      'Adjust y-axis Scale
        cht.Axes(xlValue).MinimumScale = -0.06
        cht.Axes(xlValue).MaximumScale = 0

      'Adjust x-axis Scale
        cht.Axes(xlCategory).MinimumScale = 0
        cht.Axes(xlCategory).MaximumScale = 20

'Chart Name
cht.HasTitle = True
cht.ChartTitle.Characters.Text = "LFP dVdQ Discharge"

'X axis name
cht.Axes(xlCategory, xlPrimary).HasTitle = True
cht.Axes(xlCategory, xlPrimary).AxisTitle.Characters.Text = "Discharge Capacity (Ah)"
'y-axis name
cht.Axes(xlValue, xlPrimary).HasTitle = True
cht.Axes(xlValue, xlPrimary).AxisTitle.Characters.Text = "dV/dQ (V/Ah)"

  ElseIf Cells(1, 1) = "dVdQ" And Cells(2, 1) = "Chg" And Cells(3, 1) = "A123" Then

      Set cht = ActiveSheet.ChartObjects("Chart 1").Chart
```

```
        'Adjust y-axis Scale
          cht.Axes(xlValue).MinimumScale = 0
          cht.Axes(xlValue).MaximumScale = 0.04

        'Adjust x-axis Scale
          cht.Axes(xlCategory).MinimumScale = 2
          cht.Axes(xlCategory).MaximumScale = 20



'Chart Name
cht.HasTitle = True
cht.ChartTitle.Characters.Text = "LFP dVdQ Charge"

'X axis name
cht.Axes(xlCategory, xlPrimary).HasTitle = True
cht.Axes(xlCategory, xlPrimary).AxisTitle.Characters.Text = "Charge Capacity (Ah)"
'y-axis name
cht.Axes(xlValue, xlPrimary).HasTitle = True
cht.Axes(xlValue, xlPrimary).AxisTitle.Characters.Text = "dV/dQ (V/Ah)"
'End With

  ElseIf Cells(1, 1) = "dQdV" And Cells(2, 1) = "Dis" And Cells(3, 1) = "A123" Then

        Set cht = ActiveSheet.ChartObjects("Chart 1").Chart
        'Adjust y-axis Scale
          cht.Axes(xlValue).MinimumScale = -800
          cht.Axes(xlValue).MaximumScale = 0
        'Adjust x-axis Scale
          cht.Axes(xlCategory).MinimumScale = 3.2
          cht.Axes(xlCategory).MaximumScale = 3.4
                'With ActiveChart
'chart name
cht.HasTitle = True
cht.ChartTitle.Characters.Text = "LFP dQdV Discharge"
```

```
'X axis name
cht.Axes(xlCategory, xlPrimary).HasTitle = True
cht.Axes(xlCategory, xlPrimary).AxisTitle.Characters.Text = "Voltage (V)"
'y-axis name
cht.Axes(xlValue, xlPrimary).HasTitle = True
cht.Axes(xlValue, xlPrimary).AxisTitle.Characters.Text = "dQ/dV (Ah/V)"

 ElseIf Cells(1, 1) = "dQdV" And Cells(2, 1) = "Chg" And Cells(3, 1) = "A123" Then

       Set cht = ActiveSheet.ChartObjects("Chart 1").Chart
       'Adjust y-axis Scale
         cht.Axes(xlValue).MinimumScale = 0
         cht.Axes(xlValue).MaximumScale = 600

       'Adjust x-axis Scale
         cht.Axes(xlCategory).MinimumScale = 3.2
         cht.Axes(xlCategory).MaximumScale = 3.4
               'With ActiveChart
'chart name
cht.HasTitle = True
cht.ChartTitle.Characters.Text = "LFP dQdV Charge"
'X axis name
cht.Axes(xlCategory, xlPrimary).HasTitle = True
cht.Axes(xlCategory, xlPrimary).AxisTitle.Characters.Text = "Voltage (V)"
'y-axis name
cht.Axes(xlValue, xlPrimary).HasTitle = True
cht.Axes(xlValue, xlPrimary).AxisTitle.Characters.Text = "dQ/dV (Ah/V)"
    End If
 Call plot
End Sub
Sub plot()
Sheets("dVdQ").Select
Dim lCol As Long
'Dim LastRow As Long
```

```
lCol = Cells(4, Columns.Count).End(xlToLeft).Column
'Sheets("RAW").Range("j1") = lCol
For P = 0 To (lCol / 12) - 1 Step 1
'LastRow = Sheets("dVdQ").Range("A" & Rows.Count).Offset(0, P).End(xlUp).Row
'For Z = 0 To LastRow

Sheets("Graph").Select
    ActiveSheet.ChartObjects("Chart 1").Activate
    Application.CutCopyMode = False
    Application.CutCopyMode = False
    Application.CutCopyMode = False

    ActiveChart.SeriesCollection.NewSeries
    ActiveChart.FullSeriesCollection(P + 1).Name = Sheets("dVdQ").Range("A1").Offset(0, 12 * P)

If Range("A2") = "Chg" And Range("A1") = "dVdQ" Then 'plotting dVdQ Charge

    ActiveChart.FullSeriesCollection(P + 1).XValues = Sheets("dVdQ").Range("B4:B10000").Offset(0, 12 * P)
    ActiveChart.FullSeriesCollection(P + 1).Values = Sheets("dVdQ").Range("E4:E10000").Offset(0, 12 * P)

ElseIf Range("A2") = "Dis" And Range("A1") = "dVdQ" Then 'plotting dVdQ Discharge

    ActiveChart.FullSeriesCollection(P + 1).XValues = Sheets("dVdQ").Range("H4:H10000").Offset(0, 12 * P)
    ActiveChart.FullSeriesCollection(P + 1).Values = Sheets("dVdQ").Range("K4:K10000").Offset(0, 12 * P)

ElseIf Range("A2") = "Chg" And Range("A1") = "dQdV" Then 'plotting dQdV Charge

    ActiveChart.FullSeriesCollection(P + 1).XValues = Sheets("dVdQ").Range("A4:A10000").Offset(0, 12 * P)
    ActiveChart.FullSeriesCollection(P + 1).Values = Sheets("dVdQ").Range("F4:F10000").Offset(0, 12 * P)

 ElseIf Range("A2") = "Dis" And Range("A1") = "dQdV" Then 'plotting dQdV Discharge

    ActiveChart.FullSeriesCollection(P + 1).XValues = Sheets("dVdQ").Range("G4:G10000").Offset(0, 12 * P)
```

```
    ActiveChart.FullSeriesCollection(P + 1).Values = Sheets("dVdQ").Range("L4:L10000").Offset(0, 12 * P)

End If
 Next
End Sub

Sub DeleteGraph()
ActiveSheet.ChartObjects("Chart 1").Activate
ActiveChart.FullSeriesCollection(1).Delete
End Sub

Sub AverageValues()
For Z = 0 To 100
For P = 0 To 3
Dim LastRow As Long
LastRow = Sheets("dVdQ").Range("A" & Rows.Count).Offset(0, 6 * Z).End(xlUp).Row
For K = 4 To LastRow
Sheets("FIN").Range("A" & K).Offset(0, 6 * Z) = Sheets("dVdQ").Range("A" & K).Offset(0, 18 * Z)

End Sub
End Thesis
```

Appendix E. Degradation Results from Preliminary Testing

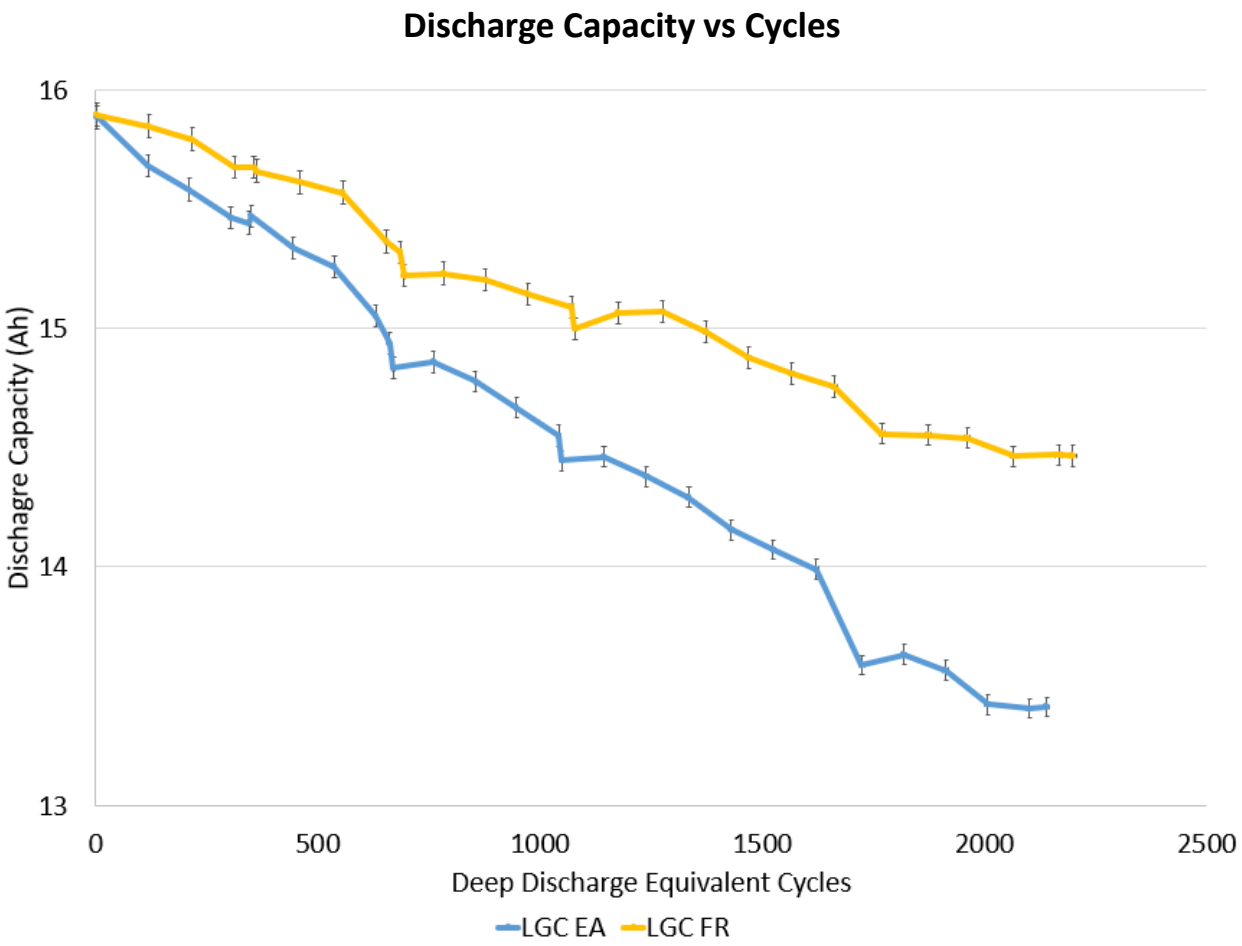

Discharge Energy Capacity and Energy Efficiency vs Cumulative Discharge Energy